

**COMPUTER-ASSISTED APPROACHES TO  
INTRAFASCICULAR MULTIELECTRODE  
STIMULATION**

by

Andrew M. Wilder

A dissertation submitted to the faculty of  
The University of Utah  
in partial fulfillment of the requirements for the degree of

Doctor of Philosophy

in

Computer Science

School of Computing

The University of Utah

May 2014

Copyright © Andrew M. Wilder 2014

All Rights Reserved



## ABSTRACT

Medical intervention to restore motor function lost due to injury, stroke, or disease is increasingly common. Recent research in this field, known as functional electrical stimulation (FES), has produced a new generation of electrode devices that greatly enhance selectivity of access to neural populations, enabling—for the first time—restoration of motor function approaching what healthy humans enjoy. Research with these devices, however, has been severely hampered by the lack of a stimulation platform and control algorithms capable of exploring their full potential.

The following dissertation presents the results of research aimed at addressing this problem. A major theme of this work is the use of software algorithms and analysis principles to facilitate both investigation and control of the motor system. Though many of the algorithms are well known in computer science, their application to the field of motor restoration is novel. Associated with use of these algorithms are important methodological considerations such as speed of execution, convergence, and optimality.

The first phase of the research involved development of a hardware and software platform designed to support a wide range of closed-loop response mapping and control routines. Software routines to automate three time-consuming tasks—mapping stimulus thresholds, mapping stimulus-response recruitment curves, and mapping electrode pair excitation overlap—were implemented and validated in a cat model. Computer control, combined with the use of an efficient binary search algorithm, reduced the time need to complete required implant mapping tasks by a factor of 4 or more (compared to manual mapping), making feasible—for the first time—acute experiments investigating multi-array, multijoint experimental limb control.

The second phase of the research involved investigating the influence of stimulus timing, within multielectrode trains, on the smoothness of evoked muscle responses. A model for predicting responses was developed and used, in conjunction with function optimization techniques, to identify stimulus timings that minimize response variation (ripple). In-vivo validation demonstrated that low-ripple timings can be identified, and that the influence of timing on ripple depends largely on the response kinetics of the motor unit pools recruited

by constituent electrodes.

The final phase of the research involved using the response prediction model to simulate the behavior of a feedback-based, stimulus-timing adjustment algorithm. Multiple simulations were executed to assess the influence of three algorithm parameters—filter bandwidth, error sampling delay, and timing adjustment gain—on two performance metrics—convergence time and percent reduction in ripple. Results show that all parameters have an influence on algorithm performance. Convergence speed is the metric most affected by parameter adjustment, improving by a factor of more than 3 (13 cycles to approximately 4 cycles). Ripple reduction is also affected—exhibiting a 17% reduction with appropriate selection of error sampling delay. These results demonstrate the value of using this simulation approach for parameter tuning.

To all who have come before—whose hard work has laid the mighty foundation on which  
we stand.

# CONTENTS

|  |            |
|--|------------|
| <b>ABSTRACT</b> .....  | <b>iii</b> |
| <b>LIST OF FIGURES</b> .....   | <b>ix</b>  |
| <b>LIST OF TABLES</b> .....  | <b>xi</b>  |
| <b>ACKNOWLEDGMENTS</b> .....   | <b>xii</b> |
| <b>CHAPTERS</b>  |            |
| <b>1. INTRODUCTION</b> .....   | <b>1</b>   |
| 1.1 A Chapter in the Human Story .....                                     | 1          |
| 1.2 The Human Motor System and Its Pathologies .....                       | 2          |
| 1.3 The Peripheral Nervous System and Neuromuscular Function .....         | 3          |
| 1.4 Motor Function and the Impact of Disease and Injury .....              | 4          |
| 1.5 Motor Deficit Prevalence and Medical Interventions .....               | 5          |
| 1.6 Biology of Electrical Stimulation .....                                | 6          |
| 1.7 Clinical Application of Electrical Stimulation .....                   | 7          |
| 1.8 Emerging Technologies in Electrical Stimulation .....                  | 9          |
| 1.8.1 The High-Channel-Count Microelectrode Array .....                    | 9          |
| 1.8.2 Functional Response Mapping on a New Scale .....                     | 10         |
| 1.8.3 Interleaved Intrafascicular Multielectrode Stimulation (IIFMS) ..... | 12         |
| 1.8.4 Challenges Associated with IIFMS .....                               | 13         |
| 1.8.5 Computer-Aided Approaches to IIFMS .....                             | 14         |
| 1.8.6 Organizatin of This Dissertation .....                               | 16         |
| <b>2. EXPERIMENTAL METHODS</b> .....                                       | <b>17</b>  |
| 2.1 Animal Model .....   | 17         |
| 2.2 Electrode Array Implantation .....                                     | 17         |
| 2.3 Methods Pertaining to Chapters 4-6 .....                               | 18         |
| 2.4 Methods Pertaining to Chapters 7-8 .....                               | 18         |
| <b>3. A PLATFORM FOR MULTIELECTRODE FES RESEARCH</b> .....                 | <b>21</b>  |
| 3.1 Design Considerations .....  | 21         |
| 3.2 System Architecture .....  | 22         |

|           |   |           |
|-----------|---|-----------|
| 3.2.1     | Control Module . . . . .  | 23        |
| 3.2.2     | Stimulation Module . . . . .  | 25        |
| 3.2.3     | Biometric Device Array . . . . .  | 25        |
| 3.2.4     | Data Acquisition Module . . . . .   | 25        |
| 3.3       | Development and Testing . . . . .   | 26        |
| <b>4.</b> | <b>PERITHRESHOLD MAPPING . . . . .</b>  | <b>28</b> |
| 4.1       | Motivation . . . . .  | 28        |
| 4.2       | Design . . . . .  | 28        |
| 4.3       | Results . . . . .   | 30        |
| 4.4       | Discussion . . . . .  | 30        |
| <b>5.</b> | <b>RECRUITMENT MAPPING . . . . .</b>  | <b>34</b> |
| 5.1       | Motivation . . . . .  | 34        |
| 5.2       | Design . . . . .  | 34        |
| 5.3       | Results . . . . .   | 35        |
| 5.4       | Discussion . . . . .  | 37        |
| <b>6.</b> | <b>EXCITATION OVERLAP MAPPING . . . . .</b>   | <b>40</b> |
| 6.1       | Motivation . . . . .  | 40        |
| 6.2       | Design . . . . .  | 41        |
| 6.2.1     | Novel Methods . . . . .   | 42        |
| 6.3       | Results . . . . .   | 43        |
| 6.4       | Discussion . . . . .  | 43        |
| <b>7.</b> | <b>RIPPLE REDUCTION VIA<br/>FEEDFORWARD TIMING<br/>ADJUSTMENT . . . . .</b>                                   | <b>46</b> |
| 7.1       | Motivation . . . . .  | 46        |
| 7.2       | Methods . . . . .   | 48        |
| 7.2.1     | Data Collection . . . . .   | 48        |
| 7.2.2     | Data Analysis . . . . .   | 51        |
| 7.3       | Results . . . . .   | 53        |
| 7.3.1     | Data Summary . . . . .  | 53        |
| 7.3.2     | Model Accuracy . . . . .  | 53        |
| 7.3.3     | Stimulus Level . . . . .  | 55        |
| 7.3.4     | Mean Interpulse Interval . . . . .  | 55        |
| 7.3.5     | Stimulus Timing . . . . .   | 56        |
| 7.3.6     | The Effectiveness of Timing Adjustment Arises from Compensation for<br>Dissimilar Response Kinetics . . . . . | 58        |
| 7.4       | Discussion . . . . .  | 62        |
| 7.4.1     | Relevance of Other Timing Optimization Methods . . . . .  | 63        |
| 7.4.2     | Impact of Response Kinetics on Ripple Reduction . . . . .   | 63        |
| <b>8.</b> | <b>OPTIMIZING A FEEDBACK-BASED TIMING ADJUSTMENT<br/>ALGORITHM . . . . .</b>                                  | <b>65</b> |
| 8.1       | Motivation . . . . .  | 65        |
| 8.2       | Methods . . . . .   | 66        |
| 8.2.1     | IIFMS Response Modeling . . . . .   | 67        |
| 8.2.2     | Ripple-Reduction Algorithm . . . . .  | 67        |

|                   |  |           |
|-------------------|--|-----------|
| 8.2.3             | Simulating Algorithm Behavior .....    | 68        |
| 8.2.4             | Optimizing Algorithm Performance ..... | 69        |
| 8.3               | Results .....                          | 69        |
| 8.4               | Discussion .....                       | 69        |
| <b>9.</b>         | <b>DISCUSSION .....</b>                | <b>72</b> |
| 9.1               | Summary .....                          | 72        |
| 9.2               | Impact .....                           | 73        |
| 9.3               | Shortcomings .....                     | 74        |
| 9.4               | Future Challenges in IIFMS .....       | 75        |
| <b>REFERENCES</b> | <b>.....</b>                           | <b>78</b> |

## LIST OF FIGURES

|     |   |    |
|-----|---|----|
| 1.1 | Multilevel structure of the peripheral nerve . . . . .  | 4  |
| 1.2 | Scanning electron microscope image of a 4 mm x 4 mm, 100-Electrode Utah Slanted Electrode Array . . . . .   | 10 |
| 1.3 | Diagram of the cross-sectional coverage of a nerve trunk by an implanted 100-Electrode USEA . . . . .   | 10 |
| 1.4 | Schematic illustrating the asynchronous activation of four independent populations of motor axons within a single muscle, with an interleaved, four-electrode train . . . . .       | 14 |
| 1.5 | Ripple in a response evoked by IIFMS with untuned parameters is higher than ripple in a response evoked by single-electrode stimulation with the same composite frequency . . . . . | 14 |
| 1.6 | Schematic representation of an asynchronous, IIFMS train with n electrodes . . . . .  | 15 |
| 2.1 | 100-Electrode USEA implanted into the sciatic nerve of a cat . . . . .  | 19 |
| 2.2 | Overview of the closed-loop stimulation and recording experimental setup used for gathering data presented in Chapters 7 and 8 . . . . .  | 20 |
| 3.1 | Detailed overview of the four main components of the closed-loop high-channel-count FES platform . . . . .  | 24 |
| 4.1 | Representative series of stimuli sent and responses recorded during execution of the perithreshold search routine . . . . .   | 31 |
| 4.2 | Results of the automated perithreshold mapping routine after mapping an implanted 100-electrode USEA . . . . .  | 32 |
| 4.3 | Representative results from the automated threshold mapping of a 100-electrode USEA implanted into a cat sciatic nerve . . . . .  | 33 |
| 5.1 | Representative torque and EMG recruitment curves generated by the recruitment mapping routine . . . . .   | 38 |
| 5.2 | The set of stimulus-response curves for the same 100-channel USEA implant referenced in Figure 4.3 and Figure 5.1 . . . . .   | 39 |
| 6.1 | Matrix containing all pair-wise overlap values (in %) for a set of 10 electrodes (45 pairs) . . . . .   | 44 |
| 6.2 | Plot representative of output from excitation overlap routine using the 3 force components of a 6-axis load cell . . . . .  | 45 |
| 7.1 | The IIFMS response prediction model . . . . .   | 47 |
| 7.2 | Ripple calculation for a representative response to an IIFMS train . . . . .  | 50 |

|      |   |    |
|------|---|----|
| 7.3  | A simple, linear summation model accurately predicts response waveforms. Example of an actual IIFMS-evoked response overlaid on top of the response predicted by the linear summation model . . . . . | 52 |
| 7.4  | IIFMS response prediction model is highly accurate; group data . . . . .  | 54 |
| 7.5  | Matching forces on individual electrodes does not necessarily yield minimal ripple in IIFMS responses . . . . .   | 56 |
| 7.6  | Ripple in IIFMS-evoked responses is not correlated with variations among forces evoked by individual electrodes . . . . .   | 57 |
| 7.7  | Decreasing IPI generally reduces ripple for IIFMS trains with optimized timings   | 57 |
| 7.8  | Optimization of stimulus timing effectively reduces ripple (group data) . . . . .   | 59 |
| 7.9  | Optimization of stimulus timing reduces power in a low-frequency range (single, representative PEI) . . . . .   | 59 |
| 7.10 | Optimization of stimulus timing reduces power in the low-frequency range (group data) . . . . .   | 60 |
| 7.11 | Timing optimization produces a greater ripple reduction when responses evoked by individual electrodes have dissimilar kinetics . . . . .   | 60 |
| 7.12 | Mean timing shift necessary to minimize ripple correlates with waveform dissimilarity . . . . .   | 61 |
| 7.13 | Distributions of best result for various numbers of executions of the function minimization routine with differing, randomly selected starting points . . . . .                                       | 62 |
| 8.1  | Diagram of the iterative stimulus timing adjustment algorithm (ISTAA) . . . . .   | 68 |
| 8.2  | Five example iterations of the timing-adjustment algorithm . . . . .  | 70 |
| 8.3  | Performance of the ISTAA algorithm for various parameter values . . . . .   | 71 |

## LIST OF TABLES

|  |    |
|--|----|
| 4.1 Threshold Mapping Pseudo Code. . . . .             | 29 |
| 5.1 Recruitment Routine - Asymptote Detection. . . . . | 36 |
| 5.2 Recruitment Routine - Curve Filling. . . . .       | 37 |
| 7.1 Stimulation Parameters for All PEIs . . . . .      | 54 |

## **ACKNOWLEDGMENTS**

This research was made possible by National Institutes of Health grants R01-NS039677 and R01-NS064318-01A1, and the Defense Advanced Research Projects Agency grant N66001-06-C-8005. Additionally, many of the results herein described would not have been obtained but for the incredibly collaborative effort of my advisors in the lab, Greg Clark and Dick Normann, and my fellow graduate students, including Brett Dowden, Scott Hiatt, Mitch Frankel, Noah Ledbetter, Dave Warren, and many others. Thank you all for contributing to such a supportive team environment.

# CHAPTER 1

## INTRODUCTION

Before thought, there was movement. The human brain, pinnacle of evolution, began with the simple need to move—towards light and away from dark, towards food and away from foe. The exquisite precision with which we humans navigate our worlds, both physical and mental, is the result of a long evolutionary progression towards ever greater control over the appendages inherited from our genetic forefathers.

Though our minds have developed to be unlike any in the history of evolution, we share, with our mammalian brethren, much the same means of moving our bodies. Over time, evolution has arrived at a mammalian motor control system that is complex and multifaceted, yet at the same time remarkably robust. It incorporates strategies both centralized and distributed—relying on control systems that range from deliberate, conscious planning to the instantaneous, dynamical properties of tendons and muscles. An internally stored, implicitly represented library of musculo-skeletal dynamics is continuously plumbed to generate best-guess motor commands. At the same time, adjustments are readily made on the fly, as feedback informs the body of deviations from intent. For humans, this system enables the repertoire of movements that define, at a fundamental level, who we are as individuals and, in many ways, how we relate to our fellow humans. Though this system is robust, it is not immune to injury.

### 1.1 A Chapter in the Human Story

The story of the human race is a story of our species' ever advancing ability to shape and control our world—including our own bodies. A central theme of this story is our desire to understand and combat the deleterious effects of age, injury, and disease. Over the past 100 years especially—the approximate span of modern medicine—we have gained tremendous insight into the complex mechanisms operating within our bodies. Over the same period, other advances in science and technology have given us the ability to interact with and manipulate many of these mechanisms. The dissertation contained herein is a

continuation of this human story. It is a tale of the author and colleagues' pursuit of a platform and techniques for interacting with the human nervous system—of developing an improved understanding of how electrical stimulation can be used to provide surrogate motor function for individuals who have lost the ability to control their own bodies.

A major theme of the work presented in this dissertation is the use of software algorithms and analysis principles to facilitate both investigation and control of the motor system. Though many of the algorithms are well known in computer science, their application to the field of surrogate motor restoration is novel. One simple example is the use of a binary search strategy to efficiently identify the electrical input level necessary to produce a desired muscle output (the characteristic muscle force input-output function is monotonically increasing, hence a binary search is optimal). Another example is the development of a multi-input/output muscle response model and the application of function minimization techniques to search model space for outputs with desirable characteristics. Associated with all of these techniques are important methodological considerations such as speed of execution, convergence, and optimality.

An important product of the research described in the following pages is a software and hardware system that enables simultaneous, closed-loop interaction with hundreds of discrete elements of the human neuromuscular system. The research has also produced control algorithms capable of orchestrating activation across groups of these neuromuscular elements to evoke smooth, fatigue-resistant forces in individual muscles. Ultimately, the platform and algorithms were used together to achieve surrogate, bi-lateral sit-to-stance limb movements in a cat model (a feat requiring simultaneous, coordinated control of the many muscles needed to generate such movements). This work, combined with other ongoing investigations in the field of motor function restoration, points to a bright and hopeful future for individuals with paralysis and other motor deficits—and a new chapter in the story of human existence.

## 1.2 The Human Motor System and Its Pathologies

Broadly speaking, the human motor system consists of three main components: 1) the musculo-skeletal system; 2) afferent and efferent elements of the peripheral nervous system (PNS); and 3) various sensory, planning, motor-control, and reflex-circuit regions of the central nervous system (CNS) [1]. Each of these systems is susceptible to various types of disease and injury. For example, musculo-skeletal function can be affected by occupation-related overuse, trauma, and degenerative diseases (such as muscle dystrophy

and osteoarthritis). Common causes of loss of peripheral nervous system function include nerve palsy, trauma such as spinal chord injury (SCI), and various neuropathies such as amyotrophic lateral sclerosis (ALS) and multiple sclerosis (MS). Motor function elements of the central nervous system can be affected by traumatic brain injury (TBI), stroke, and degenerative diseases such as Parkinson's and ALS. To varying degrees, medical intervention can help restore or offset losses in motor function resulting from these various pathologies. The work presented in this dissertation focuses on one such intervention—using electrical stimulation of the peripheral nervous system to provide surrogate motor function for patients with damage to upper motor neurons and (in the case of SCI) spinal interneurons.

### 1.3 The Peripheral Nervous System and Neuromuscular Function

The somatic peripheral nervous system begins in the spinal chord where axons from peripheral sensory neurons synapse on CNS sensory neurons and spinal interneurons, and dendrites of motor neurons receive inputs from descending CNS motor neurons and spinal interneuron circuits. On each side of the vertebral column, motor axon bundles exit from the ventral side and, along with sensory nerve bundles from the dorsal side, coalesce into large nerve trunks that extend distally to various innervation targets. In the human lower limb, for example, neurons providing sensory and motor function are grouped in three main nerve trunks (femoral, sciatic, and muscular branch of the sciatic) and a collection of smaller bundles. Nerve structure is complex, consisting of an outer layer called the epineurium which contains blood vessels and one or more subgroupings of neurons called fascicles. Each fascicle consists of a membrane called the perineurium which, in turn, contains a set of nerve fibers. For a detailed depiction of nerve organization see Figure 1.1.

As each main nerve trunk runs distally, groups of sensory and motor fibers branch off towards their innervation targets. Each motor axon synapses, at its distal end, with at least one muscle fiber, and often many. A motor axon, together with the set of muscle fibers it innervates, forms what is called a motor unit . Individual muscles typically contain tens to hundreds of motor units. Mammalian limbs, which are controlled by many muscles, can contain many thousands of motor units. The human leg, for example, contains the tens of thousands of motor units [2].

When a motor axon fires, it releases a neurotransmitter (acetylcholine) at every point at which it synapses with a muscle fiber (neuromuscular junction). This action triggers a chemical/electrical cascade (muscle action potential) in the muscle fiber that, mediated by various scaffold-like protein elements within the cell, leads to shortening of the fiber. Unlike

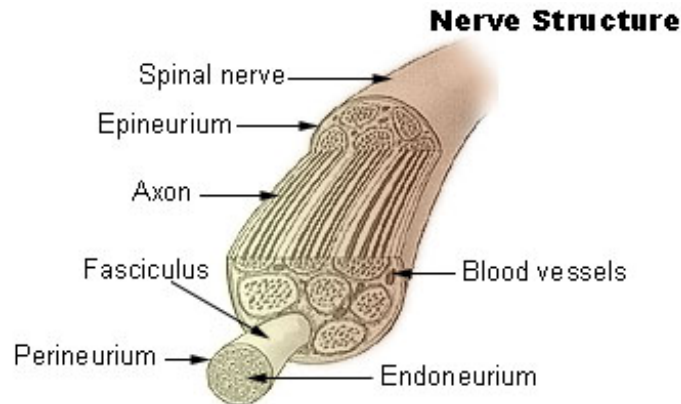


**Figure 1.1:** Multilevel structure of the peripheral nerve. Groups of individual axons are enclosed in perineurium to form fascicles, which are, along with blood vessels, enclosed by epineurium to form the nerve body. (Gray’s Anatomy, public domain)

typical synapses, where axonal neurotransmitter release may or may not trigger an action potential in the downstream neuron, firing of a motor axon always triggers a muscle action potential. From the point in time at which the muscle action potential begins, the process of muscle cell shortening reaches its peak effect in tens of milliseconds—depending on fiber type. In the absence of additional action potentials, a muscle fiber will relengthen to its passive resting length within one hundred to several hundred milliseconds—again depending primarily on fiber type. If enough muscle fibers shorten, all within a window of a few tens of milliseconds, the muscle body will shorten enough to pull on the tendons that connect it to the musculo-skeletal system—typically to a bone. As the tendon transmits an increasing level of force from the muscle to the skeletal frame, the result result is a change in skeletal geometry that, to the outside world, appears as limb movement.

## 1.4 Motor Function and the Impact of Disease and Injury

Voluntary limb movement is the result of a complex interplay of multiple factors including musculo-skeletal dynamics, external loads, and intrinsic forces produced by the mass action of many motor unit contractions. In the context of a specific person and a given movement goal, external loads and musculo-skeletal dynamics are, by definition, fixed (though by no means constant). Control of limb movement, therefore, is achieved by the modulation of motor unit behavior, and thus, ultimately, motor neuron firing patterns. At its proximal end in the spinal chord, a motor neuron receives inputs to its dendritic arbor from two sources, primary motor neurons descending from the cortex (and other higher regions), and interneurons from various spinal circuits. Spinal circuits include

reflex pathways and pattern generators, and serve to mediate various highly-stereotyped movement patterns, such as withdrawing from a noxious stimulus or the sequential and cyclical components of walking. Descending motor inputs serve to activate, suppress, or modulate spinal circuit behavior, and, in some cases, directly control PNS motor axon output.

Motor deficits resulting from stroke, trauma, and disease are commonly the result of the death or permanent disabling of populations of upper motor neurons, and, in the case of SCI, lesioning of spinal interneurons, and PNS motor axon cell bodies at the site of injury. Lesions associated with SCI can extend through the entire cross section of the spinal chord, though more often, they are "incomplete," leaving some of the neural elements intact. In any case, there are a variety of motor deficits associated with these various pathologies. Stroke typically results in varying degrees of weakness and lack of coordination of the limbs on the affected side of the body. Disease, such as MS, typically results in progressive weakening and eventual loss of volitional control of all skeletal muscle function. Motor deficits from SCI are often highly patient-specific, depending on the location and severity of the lesion. In many cases, volitional control of lower limb and bladder and bowel function is impaired or lost. For SCI in high cervical regions, upper limb and respiratory function can also be lost. An important aspect of these various disease and injury modes is that, though control signals from higher motor control centers are lost, spinal interneurons and lower motor neuron cell bodies often remain fully functional. A negative consequence of this state is that without descending inputs, which are in many cases inhibitory, spinal circuits often become hyperactive, leading to involuntary muscle spasticity. On the positive side, the presence of intact spinal and PNS elements provides an avenue in which to pursue medical interventions for restoring lost function.

## **1.5 Motor Deficit Prevalence and Medical Interventions**

In the United States, approximately 10 million individuals live with long-term motor deficits resulting from various forms of injury and disease. The major categories (as mentioned above) include stroke (6,243,000), TBI (3,170,000), SCI (273,000), and MS (211,000) [3-7].

There are various approaches, currently in clinical use, to treating and managing the symptoms associated with loss of upper motor neuron and spinal interneuron function. For example: Drugs are administered immediately post injury to minimize lesion extent, as well as chronically, to reduce muscle spasticity. Surgery is used to ablate or alter residual neural

circuitry in order to reduce spasticity and enhance or diminish reflex pathways. Surgery is also used, in some cases, to alter musculo-tendon geometry to replace paralyzed muscles with those still under volitional control. Rehabilitation techniques, including various forms of physical therapy, are employed to help patients develop strategies for using their residual volitional motor function to achieve movement goals. Wheelchairs and various orthoses (and in cases of high cervical lesion, ventilators) are employed to provide function that cannot be achieved through rehabilitation training alone. Finally, in a small number of patients, surrogate activation of lower motor neurons via extrinsic electrical stimulation has been used to restore, to a limited extent, lost motor function.

Although many of these approaches substantially improve the lives of individuals with motor deficits, none restores the full range of function that healthy people enjoy. Truly treating these various pathologies will, ultimately, require the ability to repair, regenerate, and reintegrate lost neural elements at the site(s) of lesion. Until that goal has been achieved, however, the treatment approach with the most potential for advancement in improving the functional abilities of such patients is extrinsic electrical stimulation.

## 1.6 Biology of Electrical Stimulation

Extrinsic electrical activation of a PNS motor neuron can be achieved by the application of a relatively short-duration (10-1000 ms) voltage gradient along the length of its axon. If the gradient is sufficient to depolarize beyond “threshold,” a portion of the axonal membrane—typically in the region nearest the cathode—a set of voltage-gated sodium ion channels are activated triggering a large and rapid depolarization (i.e., an action potential) at that point in the membrane. Once induced, the action potential propagates along successive nodes of ranvier in a myelinated motor axon, as would an endogenous action potential, though an electrically induced action potential travels in both directions from the site of stimulation [8].

Electrical stimulation applications employ a variety of electrode geometries and positioning to achieve the requisite motor-axon-triggering voltage gradients. Electrode locations used in clinical and research applications include the skin surface, muscle surface (epimysial), muscle belly (intramuscular), nerve surface (epineural), and nerved interior (intrafascicular). Typical electrode geometries include disk, wire, cuff, and needle. Electrode geometry is to a large extent dictated by electrode location. For example, surface and epimysial electrodes often have a disc geometry, whereas intrafascicular electrodes typically have either a wire or needle geometry. In addition to differences in geometry and position, FES systems also

employ greater or fewer numbers of electrodes, depending on the application. The more selective is the access each individual electrode provides to the target neural population, the larger is the number of electrodes that can be effectively used. Given the large number of motor units present in the PNS, an FES system intended to restore natural limb movement would, ideally, employ a very large number of highly-selective electrodes.

## 1.7 Clinical Application of Electrical Stimulation

Across the clinical and research arenas, restoration of muscle function via electrical stimulation of nervous tissue is referred to by various names, including electrical stimulation (E-Stim), transcutaneous electrical nerve stimulation (TENS), functional neuromuscular stimulation (FNS), and functional electrical stimulation (FES). Coined in 1967 to describe electrical stimulation of the peripheral nervous system as an aid in rehabilitation treatment after stroke [9], FES has become the term most commonly used today. However, its modern usage has expanded to include pathologies beyond stroke and applications other than limb movement.

Electrical stimulation of the nervous system is currently used in several highly effective and commercially successful medical interventions, including the cochlear prosthesis and the cardiac pacemaker. Numerous other FES applications have received FDA clearance and been employed in clinical research settings, to varying degrees of success. Phrenic nerve stimulators have been used to restore diaphragm function for breathing (e.g., NeuRx DPS Diaphragm Pacing System™). A sacral nerve stimulator, known as Finetech-Brindley bladder control system, has been used to restore bladder voiding function. Peroneal nerve stimulation systems (e.g., ODFS® Odstock Dropped Foot Stimulator) restore ankle dorsiflexion to correct “foot-drop” resulting from stroke, palsy, or incomplete SCI [10]. There are even multielectrode systems that provide limited restoration of lower and upper limb and hand function (Sigmedics Inc. Parastep® I System, and the NeuroControl Freehand System) [11].

Though these clinical research uses of FES have proven beneficial to patients, FES is still not considered a mature technology by patients, researchers, or the medical establishment. Quoting from a medical coverage policy [12] published in 2013 by Humana Inc. (a health insurance company):

Humana members may NOT be eligible under the Plan for the use of FES for any indications other than those listed above. This technology is considered experimental/investigational as it is not identified as widely used and generally accepted for the proposed use as reported in nationally recognized peer-reviewed medical literature published in the English language.

For FES systems to gain widespread acceptance, in the medical community and target patient population, as a mature technology, they must first improve in a range of areas. Chief among these are cost, usability, functionality, durability, social acceptability, and, for implanted systems, ease of surgical procedure.

The performance of currently available FES systems, in these categories, is strongly linked to the function(s) targeted for restoration. Implanted FES systems targeting functions that are highly stereotyped—where volitional involvement is unnecessary, or limited to simple on/off control—are often able to restore a level of function close to normal, and hence score much higher in the usability and functionality categories—the canonical example being the cardiac pacemaker. It is likely that less established systems in this category, such as phrenic pacing and bladder/bowel voiding, will gain increasing use and acceptance in the medical community as issues of cost reimbursement and durability are addressed. Systems targeting control of hand and limb movement (i.e., for reaching, grasping, standing, and walking), however, score low in the functionality, usability, and ease of surgical implantation categories. This is primarily because the motor patterns enabled by these systems are typically preprogrammed, and what aspects are under volitional control, are unintuitive. For example, such systems typically require patients to use some unrelated motor signal (i.e., contralateral shoulder position) to select from a limited number of preprogrammed motor patterns. To attain widespread patient acceptance, these systems must provide access to a greater range of movements in a much more intuitive manner.

The performance of an FES system, in these categories, is also determined, to a large extent, by the choice of electrode and electrode location. For example, surface electrodes are inexpensive, easily replaceable, and do not require surgery. However, they do require daily donning, doffing, and mapping/calibration procedures that can be impractical for unassisted users. Additionally, such system do not always provide selective access, or in some cases any access, to muscles necessary for the targeted function. Implanted epimysial or intramuscular wire systems do provide selective access to individual muscles, but implanting them requires expensive and invasive surgical procedures. Such systems are also vulnerable to lead breakage, though recent studies of such systems have demonstrated increased lead longevity [11]. Ultimately, none of the electrode technologies presently used in clinical research systems provides a specificity of access to the neuromuscular system anywhere near what the human nervous system provides. This fundamentally limits their ability to restore natural movement, and hence their ability to achieve widespread acceptance.

## 1.8 Emerging Technologies in Electrical Stimulation

In both clinical and academic communities, researchers are actively investigating new methods to improve on the shortcomings of current FES systems. In the area of volitional control of limb movement, much work has been done on decoding intent using electrodes placed in the motor cortex. One group has even used decoded motor commands, computed in real time, to control intramuscular electrical stimulation to produce grasping motion in a primate model [13]. Several groups are investigating techniques for using epidural and intraspinal stimulation to activate or facilitate activation of existing spinal circuits that generate and modulate various coordinated limb movements, such as standing and walking [14,15]. Encouragingly, in some patients with complete loss of motor function below a spinal chord injury, this approach has been associated with reemergence—to varying degrees—of *volitional* control of lost function. Yet other groups are investigating whether feedback information from endogenous, biological limb-position and muscle-force sensors can be reliably acquired from neural sensory pathways and used to enable closed-loop control of movement; the goal being to obviate the need for extrinsic sensors, which have historically exhibited low durability in the field, and, for cosmetic reasons, tend to decrease patient acceptance [16]. Yet other groups have developed new electrode technologies that provide more selective access to the peripheral nervous system [17–20], with the added benefit of reduced surgical complexity. The ability to selectively activate small populations of motor axons within a nerve trunk, provided (to a greater or lesser extent) by various incarnations of this new class of electrodes, has enabled new approaches to functional electrical stimulation [21]. The work presented in this dissertation focuses on various aspects of using one of these new electrode technologies, the high channel count penetrating microelectrode array, to achieve functionally useful, multimuscle limb movement.

### 1.8.1 The High-Channel-Count Microelectrode Array

The three-dimensional penetrating microelectrode array, also known as the Utah Slanted Electrode Array (USEA), was developed in collaboration at the University of Utah [19]. It has a square (or rectangular) geometry, and consists of an array of electrically independent silicon microelectrodes with thin ( $50\ \mu\text{m}$ ), insulated shafts of varying length (.5-1.5 mm), each with a small metalized tip (Figure 1.2).

When an appropriately sized USEA is implanted into a peripheral nerve trunk, the three-dimensional geometry of the array provides coverage for a large portion of the cross-

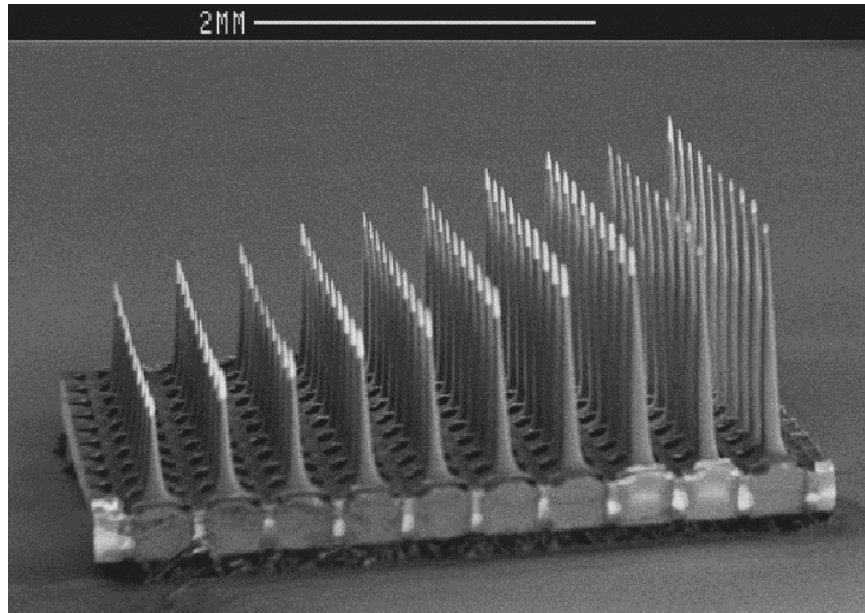


**Figure 1.2:** Scanning electron microscope image of a 4 mm x 4 mm, 100-Electrode Utah Slanted Electrode Array. (Reproduced with permission from Branner and colleagues [22])

sectional area of the nerve (Figure 1.3). This spatial arrangement of electrode tips enables selective excitation of multiple, independent groups of motor units. Getting to the point where this level of access can be effectively employed, however, requires a nontrivial effort.

### 1.8.2 Functional Response Mapping on a New Scale

With traditional electrode technologies (e.g., surface, epimysial, and intramuscular), electrodes are placed in or near the target muscles. In such situations, it is clearly evident which muscle is activated by which electrode. All that remains, then, is mapping, for each electrode, how the target muscle response changes as the stimulus level changes. Given that

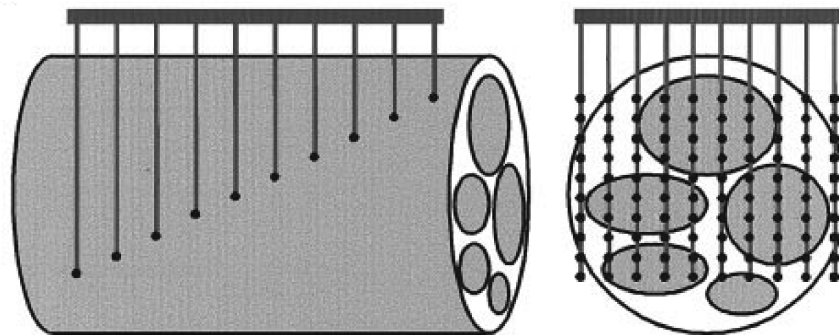


**Figure 1.3:** Diagram of the cross-sectional coverage of a nerve trunk by an implanted 100-Electrode USEA. (Reproduced with permission from Branner and colleagues [22])

clinical FES systems employ at most a dozen or two electrodes (and often many fewer), this task can be managed relatively quickly. In the case of an implanted USEA, however, it is not evident which electrodes activate which populations of motor axons (i.e., which muscle or set of muscles). Like traditional electrodes, is it also unknown how the set of activated motor axons (i.e., the functional response) changes as the charge delivered by each electrode is increased or decreased. Unlike traditional electrodes, however, populations of motor axons activated by various USEA electrodes can overlap (i.e., because of the physical proximity of electrodes, electrical fields from different electrodes can excite the same axon). Thus, effectively mapping the response characteristics of a USEA requires the additional step of measuring how axonal excitation overlap between pairs of electrodes changes as stimulus levels change.

Multiple researchers (including Branner, McDonnall, Dowden, and Frankel) have, in collaboration with others, reported detailed investigations of the various functional responses that can be achieved with the USEA [19, 21–28]. For every USEA implant, in each of these investigations, a preliminary step of mapping various, simple response characteristics of individual electrodes and pairs of electrodes was necessary before investigation of more complex stimulation patterns could be accomplished. For the research that preceded the work presented in this dissertation, USEA implant mapping was carried out manually in a process that proved long and painstaking. For Branner et al., this was more or less the point of the experiments. For McDonnall et al., however, even though mapping simple response characteristics was not the main focus of the study—they were investigating multielectrode stimulation strategies—it consumed the lion’s share of the overall experiment duration. In light of the experience garnered by this team, it was clear that manual response mapping posed an impediment to conducting further research with the USEA in an expedient manner.

Though response mapping is necessary for any experiment involving stimulation with the USEA, there is no obvious reason that it must be done manually. For some tasks, such as distinguishing between various voices in a crowded and noisy environment, computers (i.e., software algorithms) are not yet able to replicate human performance. Automating the task of response mapping with software algorithms, however, is an entirely approachable problem (though the implementation details are not obvious). The main prerequisite for implementing such algorithms is a software and hardware platform that provides closed-loop, programatic, access to the stimulus-response cycle. That is, for software automation of mapping to be possible, the algorithm must have control of stimulation and access to response metrics. The manual limb palpation technique used by Branner et al. to

detect muscle twitches is (obviously) not appropriate for mapping automation; however, the digitized, single-axis force signals used by McDonnall et al. are perfectly sufficient.

### 1.8.3 Interleaved Intrafascicular Multielectrode Stimulation (IIFMS)

It was initially thought that the proximity of various USEA electrode tips to individual motor axons might provide selective access to slow-twitch motor units, and hence enable stimulation strategies that mimicked natural recruitment order. Ultimately, this proved not to be the case. However, experiments did demonstrate that when implanted in a main nerve trunk (for example the sciatic nerve of cat), the USEA typically provides a half dozen or more electrodes, per each of the major muscles targeted by the nerve, that, at low stimulus levels, selectively activate independent motor axon populations in those muscles [22]. This level of access enabled the development of stimulation strategies that mimic the asynchronous activation of motor units seen in the intact motor system [21].

In the intact human body, motor units are activated asynchronously at low frequencies (8-24 Hz—with occasional high-rate bursts to achieve maximal force output) [29,30]. The lower the activation rate, the longer the metabolic mechanisms of the muscle fibers are able to keep up with energy demands. At low, physiological rates, each activated motor unit produces an unfused contraction (as described previously in this chapter). However, because muscles have many motor units, and because the intact motor system activates these motor units asynchronously with respect to one another, overall muscle force output at the tendon is smooth—and thus, functionally useful.

In contrast, because electrical stimulation with surface, epimysial, and wire electrodes is typically achieved with a single electrode per muscle, motor units within a muscle are, of necessity, activated synchronously. Thus, much higher, aphysiologic rates of motor unit activation are needed to achieve smooth forces. Higher rates of stimulation lead more rapidly to muscle fatigue, and hence limit the duration of evoked movements [31,32]. Furthermore, with a single electrode, recruitment order is always the same, leading preferentially to fatigue of units recruited first.

Beginning with Rack and Westbury in 1969, several research groups have investigated the possibility of producing smooth, long-lasting muscle forces by artificially activating muscles in a biomimetic manner. The approach employed involves asynchronous activation of independent motor-unit groups (Figure 1.4), with each group firing at a low rate [33,34]. Results of these studies proved very encouraging; however, the techniques used to isolate independent populations of motor neurons required invasive surgical exposure of ventral

nerve roots—an approach not well suited for clinical application. More recently, several groups have explored the possibility of achieving asynchronous motor-unit activation with less invasive, multielectrode intrafascicular interfaces (such as the 100-electrode USEA and others) [21] [35–37]. These studies have shown that it is possible to achieve fatigue-resistant muscle activation in a manner suited for human clinical application. This approach has come to be known as interleaved intrafascicular multielectrode stimulation (IIFMS).

#### 1.8.4 Challenges Associated with IIFMS

An important practical issue these studies encountered is the complexity of selecting stimulation parameters for IIFMS trains, (as compared with selecting parameters for single-electrode trains). These complexities are particularly evident when the issue of intraperiod variation (ripple) in evoked force is considered. Ripple must be low for muscle forces to be functionally useful—this is clearly evident when observing how ripple in the motor output of Parkinson’s patients (called tremor in that patient population) dramatically impedes the usefulness of movements. In FES applications, responses to single electrode stimulus trains tend to be low-ripple, whereas IIFMS trains tend to elicit responses with high levels of ripple—even when the composite frequency is such that, delivered on a single electrode, it would evoke a low-ripple response (Figure 1.5). Achieving low-ripple responses with single-electrode trains is simply a matter of increasing stimulus frequency until ripple falls below the target level. In contrast, multielectrode trains have a much larger parameter set, including electrode count, stimulus strength for each electrode, stimulus rate for each electrode, and timing of stimuli across electrodes within a single period (Figure 1.6). The interactions among these parameters—especially with respect to how they influence ripple—are substantially more complex than those for single-electrode trains. Selecting from among all possible stimulation parameter combinations in a way that consistently achieves smooth muscle responses is a nontrivial task. This is especially true when faced with the constraint of keeping stimulus rates low to delay the onset of muscle fatigue.

In IIFMS studies conducted by McDonnall, identifying stimulus parameters that achieved low-ripple forces at a target level was a tedious trial-and-error process—conducted entirely by hand—that often took many hours. McDonnall’s approach focused on searching for stimulus levels that matched the force evoked by each electrode. While this worked in many instances, achieving low-ripple responses by adjusting only stimulus strength was not always possible.

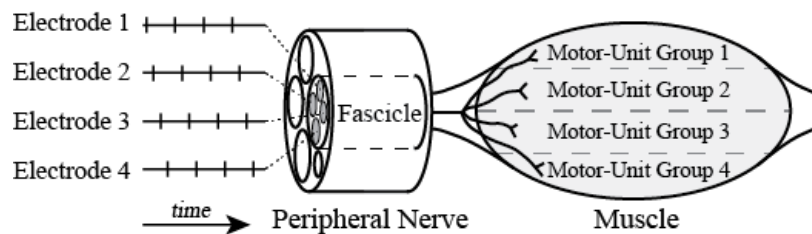


**Figure 1.4:** Schematic illustrating the asynchronous activation of four independent populations of motor axons within a single muscle, with an interleaved, four-electrode train.

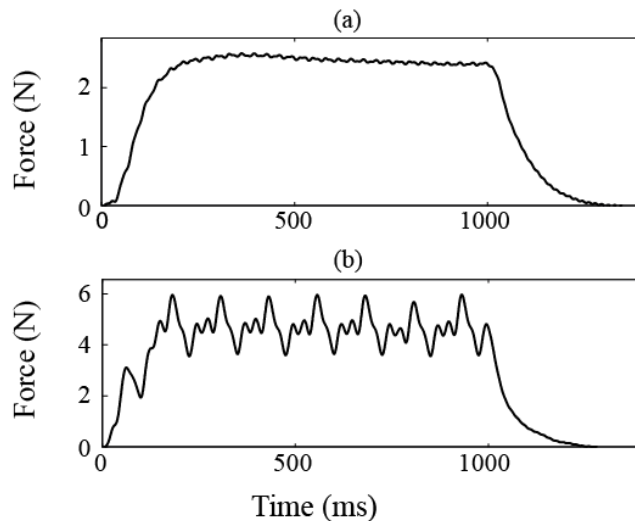


**Figure 1.5:** Ripple in a response evoked by IIFMS with untuned parameters is higher than ripple in a response evoked by single-electrode stimulation with the same composite frequency. (a) Muscle response produced by stimulation at 32 Hz on a single electrode. (b) Response produced by asynchronous stimulation on 4 electrodes, each electrode firing at 8 Hz, yielding a composite stimulation frequency of 32 Hz. For this particular asynchronous stimulation case, no special effort was made to optimize parameters. Even though the composite stimulation rates are identical, the response to IIFMS (bottom trace) has a much higher level of ripple than does the response to single-electrode stimulation (top trace).

### 1.8.5 Computer-Aided Approaches to IIFMS

Clearly, a manual approach to selecting and controlling IIFMS parameters, which is, at best, time-intensive and error-prone, poses a major impediment to further research exploring the application of IIFMS to larger FES goals, such as coordinated limb movement. As is the case for functional response mapping, what is needed for IIFMS is a hardware and software platform and additional software control programs for assisting or automating exploration of the parameter space and control of individual parameters.

Significant progress has been made towards this goal, though it has yet to be fully realized. Most notably, work accomplished (in conjunction with the work presented in

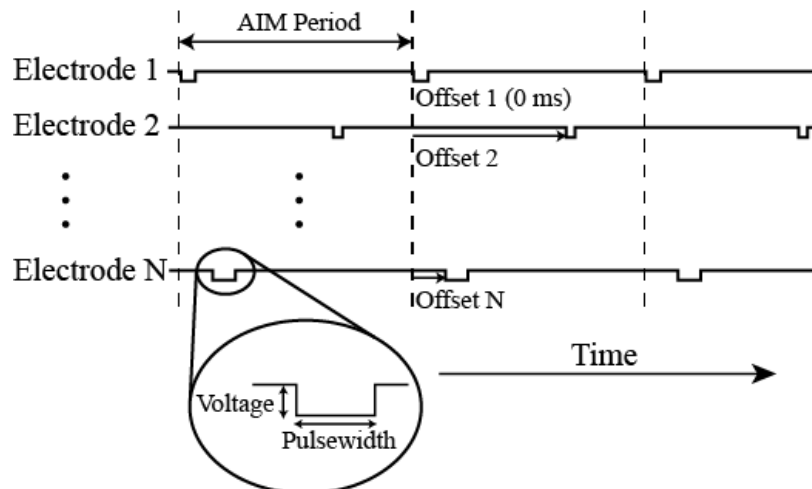


**Figure 1.6:** Schematic representation of an asynchronous, IIFMS train with  $n$  electrodes. For this particular train, the stimulus rate is the same on each electrode; however, the stimuli are phased asynchronously across the  $n$ -electrode IIFMS cycle.

this dissertation) by Frankel et al. has demonstrated (and validated in-vivo) an approach to controlling *stimulus levels* on individual electrode in an IIFMS train, to achieve target isometric and time-varying forces and torques (Frankel et al.) [28, 38, 39]. Frankel’s work, however, does not fully address the challenge of adjusting the relative *timing* of individual stimuli within an IIFMS train. Use of IIFMS in clinical practice will, likely, require a system capable of controlling both of these parameters, in real time, to achieve targeted functional tasks.

The work presented in this dissertation directly addresses the challenge of adjusting stimulus timing in IIFMS trains, as well as the burden of mapping stimulus-responses relationships for the hundreds of electrodes present in a multi-array experiment. With regard to the latter point, the work, described here, includes the development and in-vivo testing and validation of a hardware and software platform that provides programmatic, concurrent control of stimulation on hundreds of electrodes, coupled with an ability to monitor dozens of response metrics, such as muscle electrical activity, muscle forces, limb torques, and limb end-point forces. The closed-loop platform developed in this work is the first of its kind in motor-function restoration research. Importantly, the programmatic access to response information that it provides enables stimulus-response mapping to be automated—i.e., controlled completely by software. To demonstrate this capability, three specific stimulus-response mapping programs were implemented and executed (using the platform) in an in-vivo animal model. At a prosaic level, these programs are valuable because they relieve the experimenter/clinician of the arduous task of mapping electrodes

manually. More importantly, however, they greatly *reduce* the time needed to complete the requisite mapping tasks, making it feasible (for the first time) to pursue multi-array experiments investigating control of complex, multijoint limb movements.

The second part of the dissertation describes novel work in the area of optimizing and controlling interelectrode stimulus timing in IIFMS trains. The first part of this section presents a feed-forward algorithm for adjusting stimulus timings to minimize ripple in isometric muscle contractions. The algorithm employs the use of known single-electrode responses (measured in-vivo) combined with an IIFMS response prediction model to make optimized timing predictions. This work represents the first published method for feed-forward IIFMS timing adjustment. The algorithm was implemented in software and validated in an in-vivo animal model using the closed-loop stimulation platform (described above). The second part of this work, on interelectrode stimulus timing control, focuses on optimizing a preexisting algorithm for feed-back based adjustment of this parameter. In this part of the work, the response-modeling approach employed in the feed-forward algorithm (described above) was used in a novel way to simulate the effect, on response ripple, of timing adjustments made over successive cycles of a continuous, free-running IIFMS train. Building on this novel ability to simulate the timing-adjustment algorithm behavior, the impact of various values of the algorithm parameters was explored and optimized values identified.

All told, the platform and algorithms presented in this dissertation provide the researcher and clinician with extremely useful set of tools for exploring IIFMS-based motor-restoration. A concrete demonstration of this point is the successful use of these tools to achieve 6-joint bipedal stance in an experimental cat model [52].

### 1.8.6 Organizatin of This Dissertation

The work described above is organized in the body of this dissertation, in the following manner. Chapter 2 describes the methods employed for all in-vivo animal experiments. Chapter 3 describes the design of the closed-loop FES platform used to execute response mapping and IIFMS control algorithms. Chapters 4 through 6 describe the design and in-vivo validation of the three automated response mapping programs. Chapter 7 presents results of experiments measuring performance of the feed-forward IIFMS timing-adjustment algorithm. Chapter 8 describes the results of work to simulate and optimize the feed-back based IIFMS timing-adjustment algorithm. Finally, Chapter 9 discusses the importance and shortcomings of all the work presented in this dissertation and identifies several remaining hurdles hindering the wide-spread adoption of the IIFMS approach in clinical practice.

## CHAPTER 2

### EXPERIMENTAL METHODS

#### 2.1 Animal Model

The work presented in this dissertation relies on data collected over the course of multiple neuromuscular electrophysiology experiments involving adult cats. In many ways, the adult cat provides an ideal model for investigating electrical stimulation of the neuromuscular system. The morphology of the cat musculoskeletal and peripheral nervous systems is highly consistent across specimens, thus reducing many potential sources of interexperiment variability. Surgical access to lower-limb nerves trunks and musculature is expedient, allowing for easy implantation of stimulating and recording electrodes, and other response acquisition instrumentation. Additionally, cat neurophysiologic (and overall physiologic) function is very tolerant of extended periods of anesthesia, allowing for complex, long-running experiments. Finally, the cat model has been used extensively in motor-physiology and neuromuscular stimulation research, thus it brings with it a rich context of previous work in which our results can be rigorously analyzed and compared.

All work involving animals was done in accordance with procedures approved by the University of Utah Institutional Animal Care and Use Committee. In all experiments, animals were induced with telazol (10 mg/kg IM), intubated, and then mechanically ventilated. General anesthesia was maintained with isoflurane (1.5-2.5%). Vital signs, including electrocardiogram, heart rate, expired CO<sub>2</sub>, blood pressure, and body temperature, were monitored every 15 minutes. Fluid and blood sugar levels were maintained with an IV drip of lactated ringer solution (15 ml/hr). All experiments were acute, and at the end of experiments, animals were euthanized with an IV injection of potassium chloride (KCl).

#### 2.2 Electrode Array Implantation

All results reported in this dissertation were achieved with the use of the Utah Slanted Electrode Array (USEA) (described in Chapter 1). The USEA provides a means to selectively excite multiple, independent groups of motor units belonging to individual muscles.

Given this level of selective access to the peripheral nervous system, the USEA serves as an ideal electrode interface for neuromuscular stimulation research. For the experiments discussed in this dissertation, one or more 10x10 (100-electrode) USEAs were implanted into lower limb nerve trunks including the main branch of the sciatic nerve, the muscular branch of the sciatic nerve, and the femoral branch of the sciatic nerve. (At most one USEA was implanted in any one trunk. See [40] for a complete description.) In every case, the USEA was implanted into an exposed nerve with a pneumatic inserter, as described in [41]. Once implanted, the USEA was secured in place by suturing the wire bundle to the epineurium. Additionally, in many cases, the USEA was enclosed (along with the nerve) in a thin silicon cuff to isolate it from movement of the overlying muscle (Figure 2.1) .

### **2.3 Methods Pertaining to Chapters 4-6**

The close-loop stimulation platform introduced in the previous chapter (and described in detail in Chapter 3) was created to provide programmable access to arbitrary sets of independent stimulating electrodes and multiple varieties of electrical and biomechanical response metrics. Chapters 4-6 describe the design and validation of various automated routines that use the closed-loop platform to map, for each implanted electrode, a variety of response metrics to a range of stimulus parameters. These routines were designed, implemented, and tested in an iterative manner, sometimes spanning several experiments. By design, specific methods differed from experiment to experiment, but all involved implantation of one or more USEAs into hind-limb peripheral nerves of cat, and instrumentation of the hind limb with fine-wire EMG electrodes and torsional or axial load cells. Once surgical preparation was complete, the implant was allowed a 30-minute period for neurologic function to stabilize. Finally, the automated routines were executed at least once, and often multiple times.

### **2.4 Methods Pertaining to Chapters 7-8**

The work described in Chapters 7 and 8 presents data collected over the course of two neurophysiology experiments. In both experiments, the animal was placed in a prone position on a small raised platform on the surgery table. A skin incision was made on the posterior aspect of the right leg from mid-femur to the calcaneus. The skin was then removed from both the medial and lateral aspects of the leg musculature. Plantar flexors—triceps surae (medial gastrocnemius, lateral gastrocnemius, and soleus) plus plantaris—were freed of surrounding connective tissue and muscles. The proximal tip of the calcaneus was removed from the foot with tendons still attached. A hole was then drilled through the

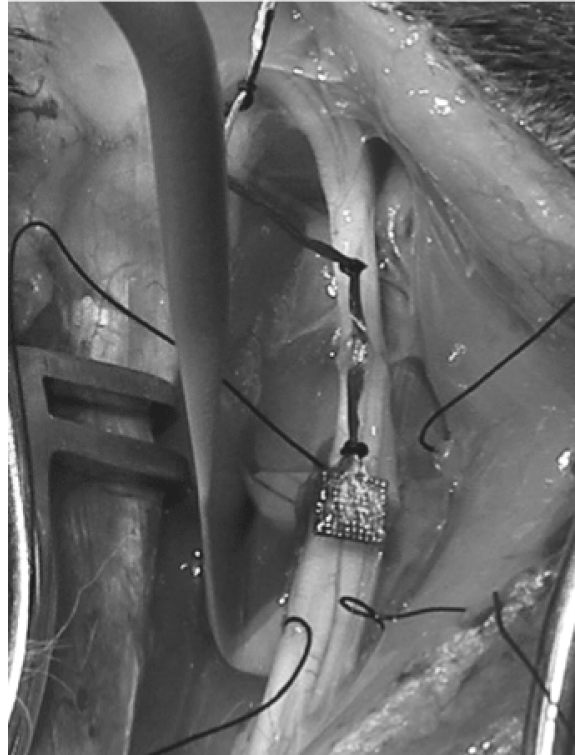


**Figure 2.1:** 100-Electrode USEA implanted into the sciatic nerve of a cat.

calcaneus chip, allowing it to be connected (via high-strength steel cable) to a linear force transducer (Model 31 - Honeywell Inc., Columbus, OH), mounted to the table, for subsequent measurements of isometric forces evoked by nerve stimulation. Next, a skin incision was made on the lateral aspect of the right thigh from iliac crest to knee. The biceps femoris muscle was exposed and reflected to access the sciatic nerve. Bone pins were inserted into the proximal and distal ends of the femur and rigidly attached to the surgery table with the femur at an approximately 45 degree angle with respect to the plane of the table. The sciatic nerve was then freed of surrounding connective tissue. Finally, a 10x10 USEA (median electrode impedance 150 k Ohms) was pneumatically inserted into the sciatic nerve at mid-femur [41]. The lateral thigh incision was sutured closed over the implanted USEA to preserve normal physiologic conditions for the nerve. A diagram of the experimental setup can be seen in Figure 2.2. Following array implantation, the preparation was left undisturbed for a period of approximately 30 minutes to allow for stabilization of physiologic function. Subsequently, perithreshold, recruitment, and overlap routines were executed to identify sets of 4 to 8 of low-overlap electrodes capable of evoking contraction in the target muscles—the triceps surae. Finally, the main focus of the experiment—multiple executions of the IIFMS parameter exploration software routine—was carried out.

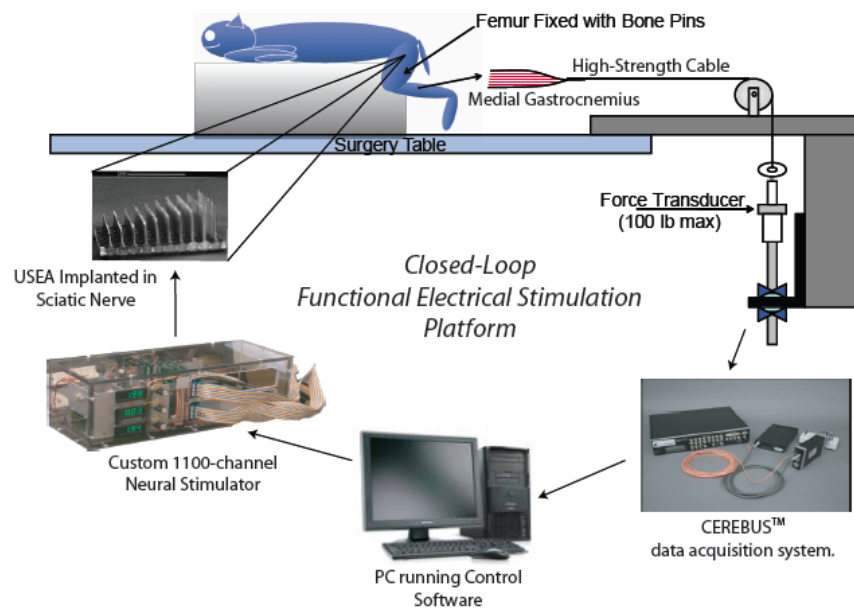


**Figure 2.2:** Overview of the closed-loop stimulation and recording experimental setup used for gathering data presented in Chapters 7 and 8.

# CHAPTER 3

## A PLATFORM FOR MULTIELECTRODE FES RESEARCH

### 3.1 Design Considerations

As described in Chapter 1, natural human movements and sensory perceptions result from complex activity patterns distributed over large populations of neurons. For many FES applications, eliciting truly natural movements or sensations via these large neural populations will require neural interfaces with channel counts one or two orders of magnitude greater than those used in clinical applications today [42]. The need for increased selectivity of access to neural populations is being addressed by a new generation of high-channel-count neural interface devices for stimulation and recording [43–47]. High-channel-count devices (such as the USEA, described in Chapter 1) offer significant advantages over traditional devices with regard to the breadth of sensory perceptions and motor responses that can be elicited via a single implanted device [21, 22]. However, conducting neuromuscular electrophysiology research with such devices—with the eventual goal of employing them in clinical FES applications—poses a host of new challenges.

Before a neural interface device can be effectively used, the response characteristics of individual stimulation electrodes must be mapped. In present research, and clinical applications, this is typically done manually [45, 48–50]. Mapping stimulus-response characteristics of an neural interface electrode manually is a tedious and time-intensive process; it is barely manageable for devices with channel counts of a few tens. For channel counts in the hundreds, or potentially thousands, manual electrode mapping is not feasible in practice. Thus, to make use of high-channel-count devices practicable, automating the task of mapping the physiological response characteristics of individual electrodes is necessary. Given the complexities of IIFMS trains, it is also necessary to have a system that is able to control the large number of parameters associated with multielectrode stimulation patterns. Indeed, the collective experience of the author and collaborators, using high-channel-count devices in many neurophysiology experiments, confirms this assessment. Having spent hundreds

of hours manually mapping implanted devices and tweaking parameters for multielectrode stimulation trains, it has become clear that a system able to automate the process of response mapping, and tune or control IIFMS train parameters, is critical to any attempt at building a sophisticated, high-electrode-count prosthesis.

Providing automated response-mapping, and programatic IIFMS parameter control, can be distilled to three system requirements. First, it is necessary to have stimulation hardware capable of independently, and simultaneously, addressing hundreds of electrodes (potentially across multiple implanted devices) [42]. Second, it is necessary to have the ability to record a wide range of functional responses to stimulation. Third, the system must provide programatic control of stimulation and access to response data.

The closed-loop FES platform presented in this chapter, and used to acquire the results presented in this dissertation, was designed and built specifically to address these requirements. It is capable of generating complex sequences of electrical stimuli on hundreds of channels while simultaneously measuring the corresponding physiologic responses—all in a completely programmable manner. With the ability to both stimulate and record, the platform can be programmed to perform a wide range of stimulus-response mapping and multielectrode stimulation routines.

## 3.2 System Architecture

The closed-loop FES platform consists of four main components: 1) a control module, 2) a stimulation module, 3) a set of biometric devices, and 4) a data acquisition module (see Figure 3.1). The control module is responsible for coordinating activity of the entire system. It manages the stimulation module and the data acquisition module, analyzes response data, and provides an interface through which users can configure, initiate, and visualize results for response-mapping and multichannel stimulation routines. It consists of custom software running on a desktop PC. The stimulation module consists of a custom designed and built stimulation device capable of generating constant-voltage, biphasic stimulation pulses on up to 1100 independent channels [51]. The stimulation hardware is operated via a high-speed digital I/O card which is, in turn, controlled by custom software running on a PC. The array of biometric devices consists of the set of analog or digital devices necessary to measure physiologic responses relevant to stimulation. The data acquisition module records output from the biometric device array. For this component, we used a commercial data acquisition system.

At a fundamental level, the FES platform is designed to function as a closed, stimulus-response feedback loop (see Figure 3.1). Information flows around the loop, starting with a stimulation command from the control module, continuing through each component, and returning to the control module in the form of a response measurement. The following sections present each component in detail, focusing on its design, its role in the feedback-loop, and the means by which it communicates with other components.

### 3.2.1 Control Module

The control module consists of custom software running on a PC. The software is a command-line-driven application written in C++ (compiled in Visual Studio 2005), designed to run on any Windows™ PC with an ethernet adapter, a serial port (RS-232), an appropriate processor (Intel P4 or later), and disk storage capacity of tens of gigabytes or greater. The software provides the user with an interface for configuring the stimulation and recording modules and selecting, configuring, and running routines for stimulus response-mapping (algorithms described in Chapters 4, 5, and 6), exploring the influence of various IIFMS parameters (algorithms described in 8), or executing sequences of multielectrode stimulation patterns in an open loop manner—for example, for eliciting coordinated limb movements [52]. Response mapping and IIFMS parameter exploration routines are implemented in the control module software and are executed an iterative series of stimulus-response loops. After each loop, stimulation parameters are modified based on an algorithmic analysis of previous responses. Loops are repeated until the specific aim of the routine is achieved. The control software starts each stimulus-response iteration by sending a digital output pulse to the data acquisition module instructing it to begin recording response data to disk. The controller then sends, via the serial port, a stimulation command, consisting of stimulus parameters specified in a high-level ASCII-based format, to the stimulation module. Communication with the stimulation module is primarily unidirectional, but can flow in the opposite direction in the case of error conditions. When the stimulation is complete, the controller triggers the data acquisition system to stop recording. The controller then copies the recorded data file from the data acquisition system to a local drive, opens the file, and analyzes the response data. As a mapping or multielectrode stimulation routine progresses, stimulus parameters and response metrics are recorded to a delimited text file for later analysis. Additionally, during a routine, the results of each stimulus-response iteration are plotted to the screen using Matlab® (called from c++). When applicable, Matlab® plots are saved to file for later review.

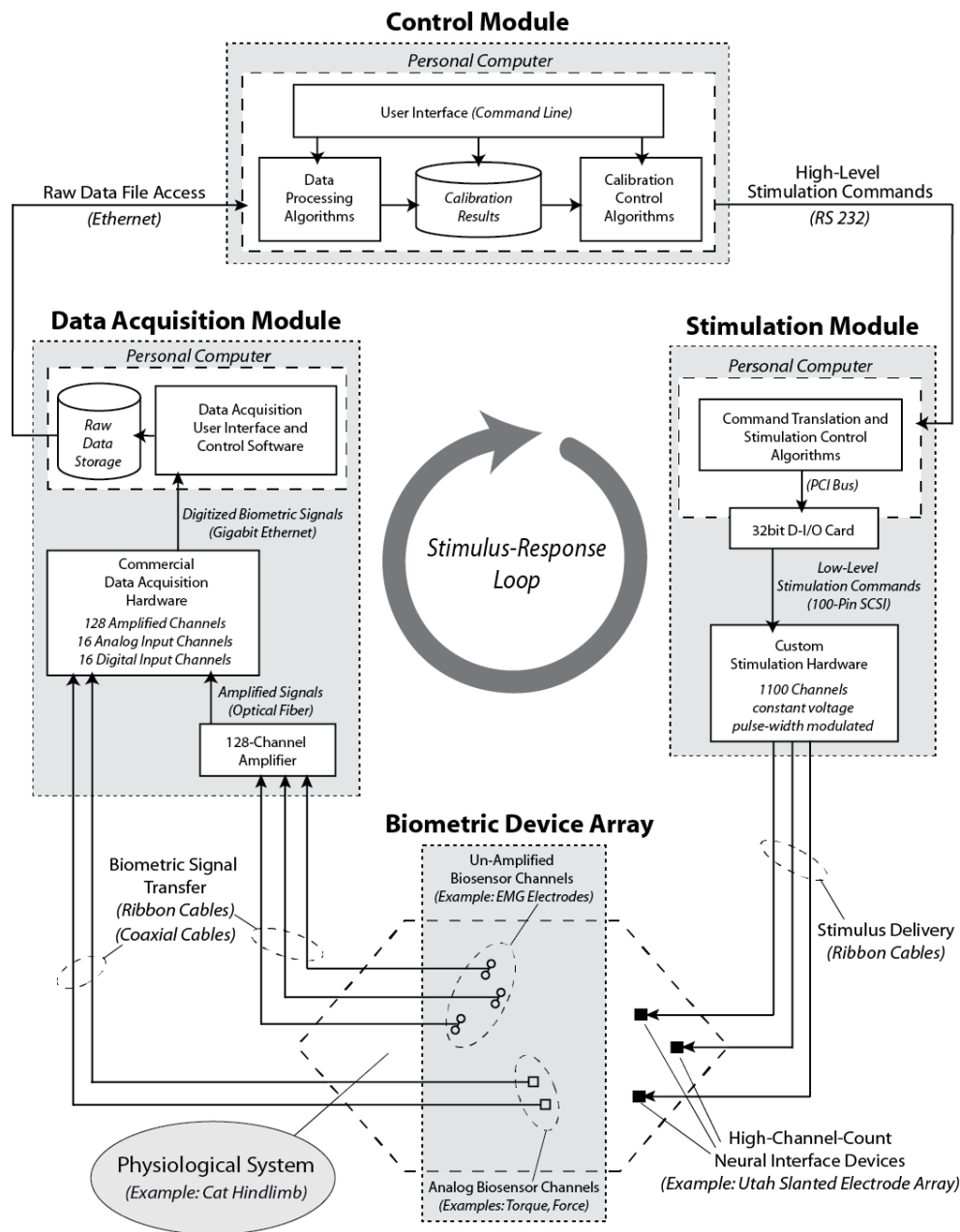


**Figure 3.1:** Detailed overview of the four main components of the closed-loop high-channel-count FES platform. Stimulation commands and response information flow in a clockwise direction, originating and terminating at the Control Module.

### 3.2.2 Stimulation Module

The stimulation module consists of several subcomponents: a custom control program, a high-speed digital I/O card (Adlink Technologies Inc.), a PC, and a custom, 1100-channel stimulation device [51]. The stimulation module was designed to function as part of the closed-loop FES platform, but can also function in a stand-alone, open-loop mode.

When operating as part of the closed-loop FES platform, the stimulation control program first initializes the digital I/O card and then executes a continuous loop in which it waits for high-level commands from the control module (or a keyboard command to terminate). When a high-level command is received, the program translates it into low-level instruction words and sends these to the stimulation hardware bus via the high-speed digital I/O card. The stimulation hardware is designed in a modular way that allows it to operate with as few as 100 stimulation channels installed. Stimulation channels (circuits are implemented with discrete components on a custom-designed printed circuit board (PCB). Each PCB (or “card”) provides 50 stimulation channels and can be interfaced via 2 26-pin connectors. As output-channel requirements for a given FES application increase, more stimulation cards (up to 60) can be added to the hardware. Any high-channel-count electrode array with a compatible connector or connector adapter can be used with the stimulation hardware. Experiments conducted for this dissertation primarily involved one or more 100-channel 10x10 USEA wired to “paddle-board” connectors (consisting of a PCB mounted with 4 IDC-26 connectors). Simple ribbon cables can be used to connect stimulation card outputs to high-channel-count device connectors.

### 3.2.3 Biometric Device Array

The role of the biometric device array is to measure physiologic responses of interest for the given FES application. Hence, this component will often consist of a heterogeneous set of biosensors. With respect to system architecture, any device that produces a signal compatible with the data acquisition module can be used. Additionally, the total number of sensors is configurable up to the input channel capacity of the data acquisition module. Typical biometric devices used in neuromuscular electrophysiology experiments conducted for this dissertation include: fine-wire EMG electrodes, single-axis, and multi-axis force load cells, torsion load cells, and goniometers.

### 3.2.4 Data Acquisition Module

The role of the data acquisition module is to record all signals produced by the biometric device array. Hence, the main design/selection criterion for this component is that it be

capable of recording the full range of outputs from the biosensors employed in the intended FES application. Additionally, the data acquisition system must be able to handle the number of response signals required for the particular application. For example, stimulus-response mapping of a high-channel-count array implanted in a peripheral nerve trunk may require simultaneous measurement of EMG signals from tens of muscles. Equally important, the system must be able to sample response signals at rates appropriate to the frequency bands of interest within those signals. For example, muscle action potentials have a time course of a few milliseconds and relevant frequencies in the low kHz, necessitating sample rates of approximately 10 k/sec. Finally, the system must be capable of recording signals and exposing them to client applications via some persistent, off-line (i.e., hard disk), or buffered, real-time (i.e., dedicated RAM) interface.

To meet these needs, we selected a Cerebus<sup>TM</sup> data acquisition system (Blackrock<sup>®</sup> Microsystems, Salt Lake City, UT). The Cerebus<sup>TM</sup> is capable of recording 128 channels with input in the 1  $\mu$ V to 8.9 mV range, 16 analog channels in 1 mV to 5V range, and 16 channels of digital TTL-compliant input. Additionally, it can record continuously at sample rates up to 30 thousand samples per second (sufficient for frequencies associated with muscle action potentials and motor responses, such as muscle EMG, muscle force, and joint torque). Initiation and termination of recording on the Cerebus<sup>TM</sup> can be controlled by a digital input signal. Recorded data are stored in a binary file format (NEV/NSx2.1) on the hard drive [53].

### 3.3 Development and Testing

The closed-loop FES platform described above was developed and tested over the course of a series of many neuromuscular electrophysiology experiments, all aimed at the long-term goal of using multiple 100-electrode USEAs, implanted in lower limb nerve trunks, to elicit coordinated stance behavior in an adult cat model. The first mapping routine to be implemented employed a binary search strategy to identify the perithreshold stimulation level (i.e., the minimum stimulus for consistently evoking a small motor response). The second routine added the ability to identify response asymptote and to map the full stimulus-response curve (from perithreshold to asymptote) for each electrode. The third routine automated the task of measuring excitation overlap for stimulation on pairs of electrodes. The fourth routine was implemented to test the accuracy of using single-electrode train responses to optimize various multielectrode train parameters, and to assess the influence, for IIFMS trains, of intraperiod stimulus timing on intraperiod response variation (ripple).

An additional routine for executing complex multielectrode stimulation patterns for the purpose of eliciting coordinated multijoint limb movements was also implemented, and used extensively, though details are not discussed in this dissertation (see [52]). After the initial algorithm development stage, each mapping routine was validated over the course of hundreds of executions, in-vivo. The remainder of this dissertation describes, in detail, the design and performance of these routines.

## CHAPTER 4

### PERITHRESHOLD MAPPING

#### 4.1 Motivation

In the field of FES, mapping perithreshold stimulus levels of neural interface electrodes serves as a standard first metric for assessing overall implant viability and muscle-activation specificity [18, 20, 22]. For a given electrode-type (e.g., intraneural electrodes such as the LIFE and USEA) a lower perithreshold stimulus level indicates closer proximity of stimulating electrode to excited axonal populations—which typically enables higher muscle-activation specificity. In previous studies, by the author’s group and others in the field, [17, 22] threshold mapping was typically accomplished using manual palpitation, or force measurements (i.e., from a load cell), as the response metric. Selectivity of muscle activation was either determined via palpitation, or inferred from other indirect techniques, such as measurement of excitation overlap (described in Chapter 6). To enable our group’s long-term goal of using the closed-loop FES platform, together with high-channel-count implants, to elicit functional, multijoint stance behavior (with the cat model), we needed an approach to mapping that could assess both threshold and muscle specificity in an automated manner, in both an isolated preparation and an intact neuromuscular system.

#### 4.2 Design

To satisfy these requirements, the perithreshold mapping algorithm was designed in a generic way to be capable of operating with a variety of different response types and with one or multiple response channels. For example, the mapping routine was implemented to be capable of using electromyographic (EMG) signals from multiple muscles (each instrumented with a bipolar pair of fine-wire electrodes). In the case of EMG responses, the mapping routine identifies, for a given stimulating electrode, the minimum stimulus level for which perithreshold activation is detected by a single EMG sensor. Given a USEA implanted in sciatic nerve trunk, the mapping routine identifies and reports which of the lower limb muscles each electrode preferentially activates, and the minimum single-pulse stimulus level

(in the case of the closed-loop FES platform, controlled by pulse-width) required to elicit a perithreshold response. Perithreshold stimulus has been defined in different ways by various groups. For our purposes, we define it as the stimulus level which consistently evokes a specific, small but measurable response (i.e., 50  $\mu\text{V}$  of EMG). Although the mapping routine was designed to handle multiple response channels, it can operate with only a single response channel (for example, from a force or torque load cell), or, for that matter, any biopotential that exhibits a positive, monotonic relationship to stimulus level. To locate the perithreshold stimulus level, the mapping routine employs a binary search algorithm, outlined in Table 4.1.

The threshold mapping routine can be configured to use the threshold stimulus level for the previously mapped electrode as the starting point for locating the threshold on the next stimulation channel. This improves search efficiency by taking advantage of the tendency for thresholds to cluster—due to somatotopy at the site of device implantation, similarity in electrode impedance, and/or other factors.

**Table 4.1:** Threshold Mapping Pseudo Code.

| <b>Initialization</b> |  |
|-----------------------|--|
| <b>1</b>              | pulse_width = (set by operator)          |
| <b>2</b>              | pulse_width_limit = (set by operator)    |
| <b>3</b>              | accuracy = (set by operator)             |
| <b>4</b>              | low_bound = 0                            |
| <b>5</b>              | high_bound = pulse_width_limit           |
| <b>6</b>              | threshold_found = false                  |
| <b>Loop</b>           |  |
| <b>7</b>              | stimulate at pulse_width                 |
| <b>8</b>              | measure response                         |
| <b>9</b>              | if (response < threshold)                |
| <b>10</b>             | low_bound = pulse_width                  |
| <b>11</b>             | pulse_width *= 2                         |
| <b>12</b>             | else                                     |
| <b>13</b>             | high_bound = pulse_width                 |
| <b>14</b>             | pulse_width = (high_bound - low_bound)/2 |
| <b>15</b>             | if ((high_bound - low_bound) < accuracy) |
| <b>16</b>             | threshold = high_bound                   |
| <b>17</b>             | threshold_found = true                   |
| <b>18</b>             | break                                    |
| <b>19</b>             | if (low_bound >= pulse_width_limit)      |
| <b>20</b>             | break                                    |

### 4.3 Results

To date, the automated calibration tool has been used to generate hundreds (possibly thousands) of threshold maps. Figure 4.1 shows the sequence of single-pulse stimuli (and the resulting EMG responses) generated by the mapping routine during perithreshold search on a single electrode in an implanted 100-electrode USEA. Figure 4.2 shows stimuli sequences generated during perithreshold mapping of an entire 100-electrode USEA. Figure 4.3 shows the perithreshold stimulus levels, grouped by muscle, for a 100-electrode USEA implanted into sciatic nerve (at mid-thigh) of a cat. For this implanted USEA, active electrode yield was approximately 64%. (Note: for our purposes, “active” electrodes are those able to evoke a perithreshold response in one of the instrumented muscles at a stimulus level at or below the stimulus limit set, for safety, by the user.) On average, the automated routine maps active electrodes in 16.4 seconds ( $n = 3200$ ) and inactive electrodes in 3.6 seconds ( $n = 1800$ ). Extrapolating to a prosthesis involving 600 stimulation channels (for example six 100-electrode USEAs), and an active electrode yield of 70%, the automated system would complete perithreshold mapping for all arrays in around 126 minutes (2.1 hours). By comparison, manually mapping perithreshold levels for a 100-electrode USEA takes approximately 90 minutes (or 9 hours for 6 arrays). Thus by using the automated system, time required for perithreshold mapping is reduced by 77%.

### 4.4 Discussion

There are several areas where improvements could be made to the perithreshold mapping routine. Chief among them is execution speed. The speed of the routine is governed by two factors: time required to complete an iteration of the stimulus-response loop, and number of loops (stimuli) required, per electrode, to determine the perithreshold stimulus level.

The duration of the stimulus-response loop is governed by software-imposed delays, set specifically to limit the frequency of muscle activation. Activation at frequencies of 2 Hz and above have been shown to induce fatigue in skeletal muscle [54]. Thus, loop-completion time has been set to a minimum of 0.5 seconds. However, for the typical high-channel-count implant, not all electrodes activate the same muscle (indeed this is the whole point of such implants). Thus, it might be possible, by carefully selecting electrodes which activate different muscles, to reduce stimulation-response loop time, by mapping several stimulation channels in an interleaved manner, without risking the possibility of muscle fatigue. Given that EMG potentials dissipate rather quickly (on the order of milliseconds), it would, in theory, be possible to stimulate on successive electrodes after only a few 10s of ms without

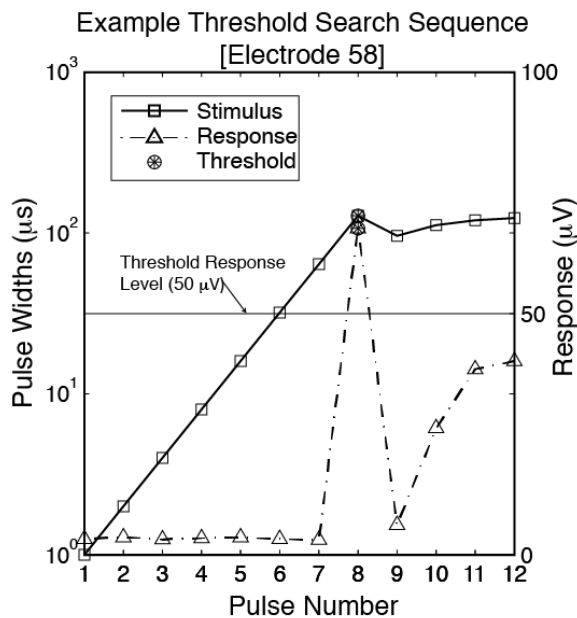


**Figure 4.1:** Representative series of stimuli sent and responses recorded during execution of the perithreshold search routine. The ordinate scale on the left-hand side of the figure denotes the pulse-width of the stimuli in microseconds. Stimuli pulse-width values are represented by squares. The ordinate scale on the right-hand side of the figure denotes the recorded response in microvolts. Response values are represented by triangles. In total, the search algorithm sent 12 stimuli of varying pulse-widths. It identified the eighth stimulus (circled asterisks), with pulse-width 128  $\mu\text{s}$ , as the smallest stimulus capable of evoking a response above the predefined perithreshold activity level (50  $\mu\text{V}$ ).

risking response signal contamination. (This would clearly *not* be possible in the case of force or torque responses where responses require 10s to 100s of milliseconds to dissipate).

The number of stimuli required to map an electrode reflects the efficiency of the threshold search algorithm. The mapping routine currently uses a binary-search algorithm, which is optimal over the general set of monotonic functions. However, it may be possible to take advantage of the characteristically sigmoidal shape of muscle response recruitment curves (discussed in Chapter 5), for example, by iteratively fitting collected responses to a sigmoid and then using the sigmoid to inform the selection of the successive stimulus level—ideally enabling the algorithm to pick a level that is closer to threshold stimulus.

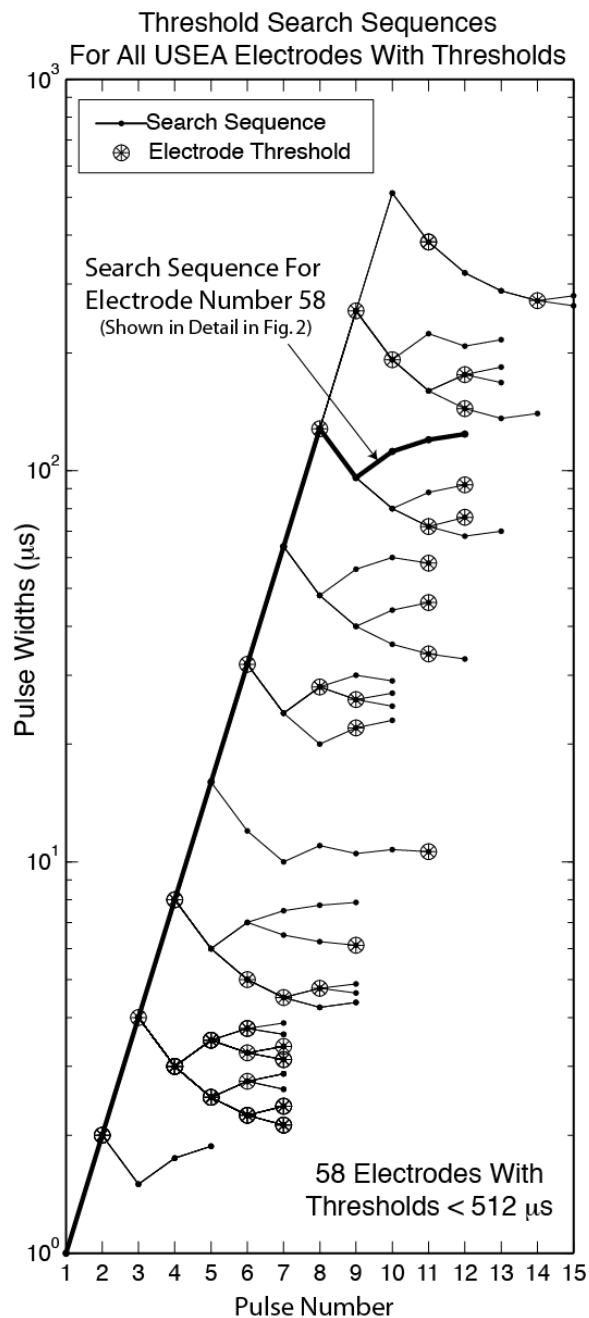


**Figure 4.2:** Results of the automated perithreshold mapping routine after mapping an implanted 100-electrode USEA. Shown in the figure are search sequences for which a perithreshold response in an instrumented muscle was evoked with a stimulus pulse-width less than 512  $\mu\text{s}$ . Each line represents the search sequence for a single electrode. For this USEA implant the automated perithreshold mapping routine was able to evoke a perithreshold response via 58 of the 100 electrodes. Circled asterisks indicate perithreshold stimuli. (Note: several groups of electrodes share the same threshold pulse-width value).

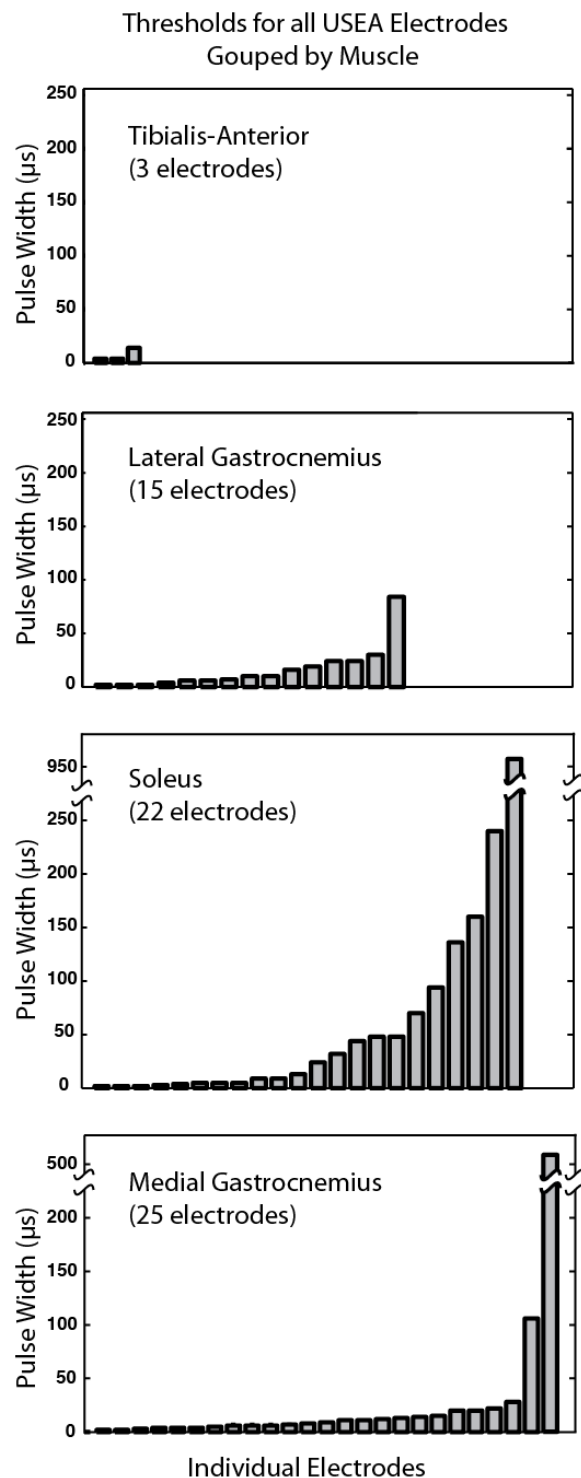


**Figure 4.3:** Representative results from the automated threshold mapping of a 100-electrode USEA implanted into a cat sciatic nerve. Each bar represents the mapping result for a single electrode. Height of a bar indicates the pulse-width required to elicit muscle activity greater than the perithreshold criterion. The bars/electrodes are grouped by the muscle in which the activity is observed [Tibialis Anterior (3 electrodes), Lateral Gastrocnemius (15 electrodes), Soleus (22 electrodes), Medial Gastrocnemius (25 electrodes)]. Thirty-five electrodes did not elicit responses above the perithreshold criterion in any of the four instrumented muscles (for pulse-widths less than  $1024 \mu\text{s}$ ). Total time to complete map was 36 minutes.

## CHAPTER 5

### RECRUITMENT MAPPING

#### 5.1 Motivation

Recruitment curves are another standard metric for assessing neural implant efficacy [18, 20, 22]. Employing a neural implant for FES research applications requires, at a minimum, knowledge of the full range of responses that can be elicited (recruited) by each electrode. Of particular interest is whether individual electrodes can selectively elicit a useful functional response from a single muscle or agonist group without also activating spurious or opposing responses (i.e., from an antagonist). The steepness of an electrode’s recruitment curve indicates how practicable it will be to achieve “graded” responses with that electrodes during functional stimulation. Electrodes for which the response range maps to a wide range of stimulus levels are more useful because targeted response levels can be more reliably achieved. As argued in Chapters 1 and 3, automation of the recruitment mapping process is a practical necessity for neural implants with electrode counts in the 10s and 100s. Indeed, automated recruitment mapping has proven to be an essential prerequisite to the author and colleagues’ over-arching experimental aim of evoking graceful 3-joint stance with a multiple-USEA-implant cat model.

#### 5.2 Design

Recruitment mapping involves measuring some physiologic response to a set of stimuli of increasing strength (charge). A naive approach to generating a recruitment curve might involve simply delivering a series of stimuli, in which strength is increased by a constant amount from one to the next. However, even assuming knowledge of the perithreshold stimulus level, this approach would require many pulses (and hence time) to ensure adequate coverage of the full response range. In the case of electrodes implanted in peripheral nerves, muscle responses typically exhibit a sigmoidal relationship to linear increases in stimulus strength [55]. Given this predictable pattern, it is possible to greatly improve on the performance of the naive approach. The recruitment mapping algorithm, implemented

for the closed-loop FES system, starts by first locating the stimulus level at which the response reaches periasymptote, and then “fills in” the interior of the response curve with a series of stimuli, starting below the perithreshold level (as determined by the method described in Chapter 4) and continuing to periasymptote. The algorithm is designed to be able to fill in the curve to a user-specified level of accuracy—as may be necessitated by the particular FES application. Locating the periasymptote stimulus level is accomplished using the algorithm outlined in Table 5.1. Filling in the curve is accomplished by a gap-bisection method outlined in Table 5.2. Much like the threshold mapping routine, the recruitment mapping routine is design to map recruitment using any of a variety of response metrics, including force, torque, and EMG.

An additional consideration in recruitment mapping is the functional utility of elicited muscle responses. Given the complex, anisotropic structure of the peripheral nerves, electrodes of implanted USEAs exhibit a wide range of recruitment abilities. Many electrodes lie in intrafascicular regions, in close proximity to motor axons. Some, however, end up in interfascicular space, and others may, depending on the quality of the implant, fall altogether outside of the epineurium. Thus, as a first step, the recruitment mapping routine checks, for each electrode, that the response to a large stimulus exceeds some user-specified threshold. For example, in a map of muscle force recruitment, the algorithm can be configured to first send a  $256 \mu\text{s}$  single-pulse probe stimulus on each USEA electrode. Recruitment curves are then generated only on electrodes for which the probe stimulus elicits a peak twitch response greater than some user-specified level—typically this value represents a minimum bar for functional utility (e.g., 1N). Alternatively, the routine can be configured to only generate recruitment curves for electrodes with perithreshold stimulus levels below some user-specified level (e.g.,  $100 \mu\text{s}$ ).

During the execution of the recruitment routine, algorithm parameters and stimulus and response levels (as well as raw response waveforms) are saved to a series of files for later, offline analysis. Additionally, as the routine is executing, curves are visualized for the user with Matlab™ plotting functions (called from C++), and updated after each new stimulus-response pair is generated.

### 5.3 Results

Figure 5.1 shows the results of the automated recruitment mapping routine for a single electrode. Figure 5.2 presents the recruitment map for an entire 100-electrode USEA. In the context of a high-channel-count electrode array, a recruitment “map” is simply the

**Table 5.1:** Recruitment Routine - Asymptote Detection.

| <b>Initialization</b> |  |
|-----------------------|--|
| 1                     | pulse_width = threshold_pulse_width                      |
| 2                     | pulse_width_limit = (same as used in threshold routine)  |
| 3                     | threshold_response = (same as used in threshold routine) |
| 4                     | growth_factor = 2.0                                      |
| 5                     | stimulus_count = 0                                       |
| 6                     | previous_4_responses = [ 0, 0, 0, 0 ]                    |
| 7                     | asymptote_found = false                                  |
| <b>Loop</b>           |  |
| 8                     | stimulate at pulse_width                                 |
| 9                     | measure response   |
| 10                    | previous_4_responses[mod(stimulus_count, 4)] = response  |
| 11                    | stimulus_count++   |
| 12                    | if ((response < previous_response*1.1)                   |
| 13                    | && (response > threshold_response*5))                    |
| 14                    | growth_factor = 1.1                                      |
| 15                    | if (max_deviation(previous_4_responses) <                |
| 16                    | mean(previous_4_responses)*0.05)                         |
| 17                    | asymptote_found = true                                   |
| 18                    | break  |
| 19                    | else   |
| 20                    | pulse_width *= growth_factor                             |
| 21                    | if (pulse_width > pulse_width_limit)                     |
| 22                    | break  |

collection of recruitment curves for all of the active electrodes. For the map depicted in Figure 5.2, recruitment curves were generated for the 55 electrodes with perithreshold stimulus pulse-widths below 100  $\mu$ s. The map was generated in 45 minutes. Averaging over a set of 155 curves (selected at random from a series of in-vivo experiments) it takes the routine 11 stimulus-response iterations to identify response asymptote. Each iteration takes approximately 0.87 seconds to complete. Thus, asymptote identification requires roughly 9.6 seconds. Given this performance, a 15-point recruitment curve (sufficient to give a reasonable picture of recruitment behavior) would take approximately 23 seconds to complete (10 s for asymptote + 15 x 0.87 s for the curve). Assuming 50% of implanted electrodes are capable of eliciting large enough responses to warrant stimulus-response mapping, it would take approximately 115 minutes (1.9 hours) to generate the recruitment map for a 600-channel prosthesis.

**Table 5.2:** Recruitment Routine - Curve Filling.

| <b>Initialization</b> |   |
|-----------------------|---|
| <b>1</b>              | threshold_pulse_width = (determined in threshold routine) |
| <b>2</b>              | threshold_response = (determined in threshold routine)    |
| <b>3</b>              | asymptote_pulse_width = (determined in previous step)     |
| <b>4</b>              | asymptote_response = (determined in previous step)        |
| <b>5</b>              | max_response_gap = (set by operator)                      |
| <b>6</b>              | pulse_width = (asymptote_pw - threshold_pw)/2             |
| <b>7</b>              | all_pulse_widths = [ . . . ]                              |
| <b>8</b>              | all_responses = [ . . . ]                                 |
| <b>Loop</b>           |   |
| <b>9</b>              | stimulate at pulse_width                                  |
| <b>10</b>             | measure response  |
| <b>11</b>             | all_pulse_widths.insert(pulse_width)                      |
| <b>12</b>             | all_responses.insert(response)                            |
| <b>13</b>             | if ((response - next_lesser_response) > max_response_gap) |
| <b>14</b>             | pulse_width = (pulse_width - next_lesser_pw)/2            |
| <b>15</b>             | else  |
| <b>16</b>             | while ((next_larger_response - response) <                |
| <b>17</b>             | max_response_gap)   |
| <b>18</b>             | if (no larger response exists)                            |
| <b>19</b>             | break:Loop  |
| <b>20</b>             | else  |
| <b>21</b>             | response = next_larger_response                           |
| <b>22</b>             | next_larger_response = second_larger_response             |
| <b>23</b>             | pulse_width = (next_larger_pw - pulse_width)/2            |

## 5.4 Discussion

The recruitment mapping routine has been used in-vivo many hundreds of (possibly over a thousand) times and has proven to be a truly invaluable tool for high-channel-count research. An obvious potential improvement would be to integrate it with the perithreshold mapping routine. Given that often a few super-threshold stimuli are delivered while mapping and electrode's threshold, it makes sense to incorporate the responses to these stimuli directly into the recruitment curve. This would reduce the total number of stimulus-response iterations required to fully map an electrode (i.e., threshold and recruitment). To illustrate the importance of improved mapping efficiency, a reduction in average number of pulses required to calibrate an electrode—from 65 (9 perithreshold, 56 stimulus-response) to 55 (7 perithreshold, 48 stimulus-response)—would yield an overall time savings of 15%. This savings would be substantial when calibration for multiple devices requires hundreds of minutes.

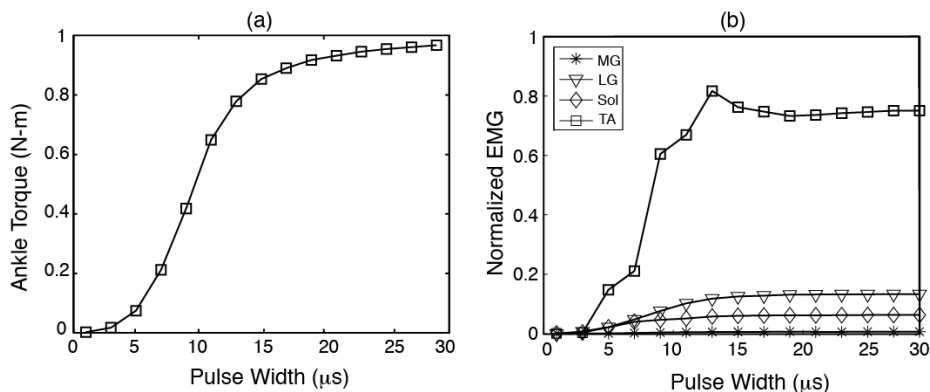


**Figure 5.1:** Representative torque and EMG recruitment curves generated by the recruitment mapping routine. (a) Joint-level responses, as measured by a torsional load cell placed at the left hind-limb ankle, to a series of single-pulse stimuli of increasing pulse width. (b) Individual muscle responses, to the same series of stimuli, as measured by bipolar fine-wire EMG electrodes implanted in the three ankle plantar flexors, lateral gastrocnemius (LG), medial gastrocnemius (MG), soleus (Sol), and the ankle dorsiflexor tibialis anterior (TA). All stimulus pulse widths were selected by the mapping program without operator guidance.

Another area for improvement is enhancing the the curve filling (gap bisection) algorithm, to be able to handle shifts or variability of the muscle recruitment function (resulting from micromovements of the interface device, shifts in response sensors position, and/or actual changes in muscle force capabilities—from fatigue, etc.). The algorithm could be modified to check for unexpected responses (i.e., responses that imply nonmonotonic recruitment behavior) and then decide on an appropriate, corrective course of action such as reconfirming previous, conflicting, points, switching to gap bisection with respect to a best fit sigmoid or, in cases of large shifts, regeneration of the entire curve.

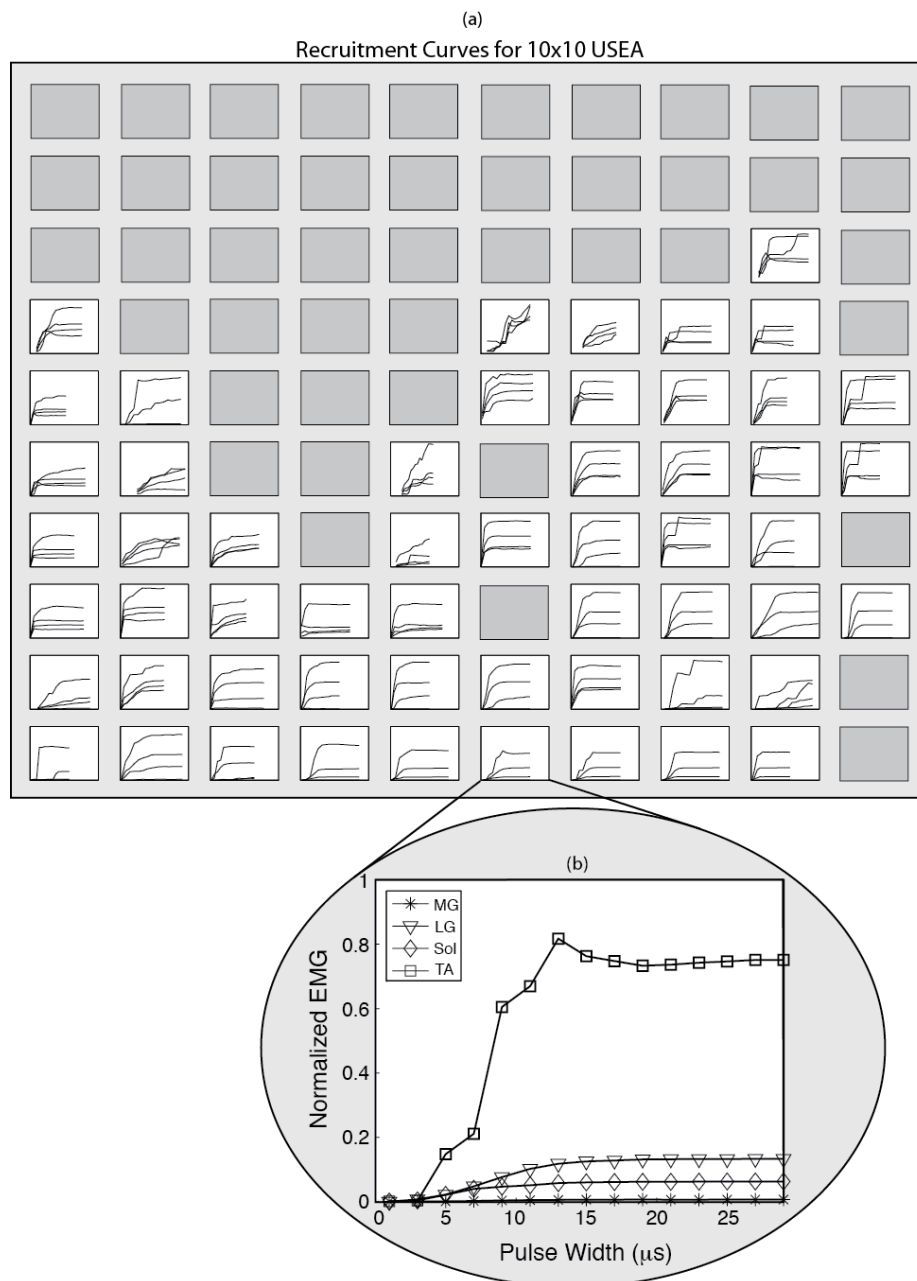


**Figure 5.2:** The set of stimulus-response curves for the same 100-channel USEA implant referenced in Figure 4.3 and Figure 5.1. (a) Each box represents the EMG recruitment curves for a single USEA electrode. (Note: Abscissa scale is not the same for all plots). Plots are displayed in a 10x10 grid representing the layout of the 10x10 USEA. Curves were generated only for the 55 electrodes with perithreshold stimulus levels below 100  $\mu\text{s}$ . This criterion was chosen by the operator before the start of the routine. During the routine, all stimulus pulse widths were selected and delivered by the mapping program without operator guidance. The 55 recruitment curves were generated in approximately 45 minutes. (b) Detailed view of a recruitment curve generated by the system (same as shown in Figure 5.1).

## CHAPTER 6

### EXCITATION OVERLAP MAPPING

#### 6.1 Motivation

As described in Chapter 1, electrical stimulation of peripheral nerve via penetrating microelectrodes is accomplished by creating a voltage gradient between an electrode and the current return path. If the gradient is large enough, it will induce action potentials in a set of motor (and sensory) axons—starting with those near the electrode tip and extending out in a roughly spheroid manner as the current from stimulating electrode to return is increased [17, 56]. In the case of intrafascicular (and epineural) stimulation protocols involving asynchronous activation of multiple electrodes (IIFMS—described in the next chapter) from a multielectrode neural interface, it is important to characterize the interaction between axonal excitation zones of the electrodes involved. Specifically, it is important to quantify, for various stimulation levels (ranging from threshold to asymptote), the percentage of axons excited by more than one electrode. During asynchronous multi-electrode stimulation, motor-units excited by more than one electrode will fire at a higher rate than their peers causing them to fatigue faster. This leads to a decline in overall force output (and an increase in intraperiod variation in force), ultimately defeating the purpose of the multielectrode approach.

Over the past several decades, researchers investigating epineural and intrafascicular multielectrode stimulation have converged on a standard approach to measuring excitation overlap [17, 18, 21, 22]. The technique, which measures overlap between pairs of electrodes, takes advantage of two important properties of the underlying neuromuscular system system. The first is that neurons (in this case motor neurons) have an absolute refractory period ( $\sim 1$  ms) following action potential, during which they cannot fire again [1]. The second is that the force produced by the simultaneous, or nearly coincident ( $\Delta t < 20$ ms), contractions of independent motor units in the same muscle is summed by the muscle tendon. Overlap for a given set of stimuli on two electrodes can be deduced by comparing the sum of the force evoked by each stimulus independently to the force produced by the same stimuli in a

doublet sequence (i.e., in series, offset by a short delay). The offset must be long enough to electrotonic avoid summation of voltage gradients but short enough to lie within the neural refractory period. The greater the overlap between the two excitation zones, the lower will be the doublet response as compared to the sum of the single-stimulus responses.

As is the case for threshold and recruitment mapping, measuring overlap by hand is, at best, a tedious task—even for a single target response level on a single pair of electrodes it can take tens of minutes. Manually measuring pair-wise overlap for a set of 8 electrodes is at the limit of what can be accomplished by hand in an experimental or clinical setting [57]. Measuring overlap at multiple force levels, for many sets of electrodes, across multiple implants is not feasible in practice.

## 6.2 Design

To address this issue, the author implemented a software routine that automates the task of measuring excitation overlap. The routine works as follows. The user enters a set of electrodes and a target single-electrode stimulus response level. The routine then computes all possible pairs of electrodes. A set of 10 electrodes, for example, would have  $\binom{10}{2} = 45$  pairs. For each electrode of each pair, a response-targeting routine (similar to the threshold routine described in Chapter 4) searches, to within a user-specified accuracy, for the stimulus level that elicits the target response. Even though electrodes belong to multiple pairs, the stimulus level is always redetermined before testing each pair because the response to a given stimulus can change over time (due to various factors, including electrode movement and muscle fatigue). Once the appropriate stimulus level for each electrode is identified, the overlap routine is executed as follows. For a pair of electrodes (a,b), first a set of 20 stimuli, consisting of 5 on each electrode and 10 doublets (where the second stimulus is delayed 750  $\mu$ s), are delivered in random order at 1-second intervals (in five of the doublets, electrode a precedes electrode b, and in the other five the order is reversed). Evoked muscle forces are recorded for each stimulus. Overlap is then calculated as follows. Each group of five responses is averaged ( $\bar{f}_a, \bar{f}_b, \bar{f}_{ab}, \bar{f}_{ba}$ ). The sum of the mean singlet responses for the two electrodes ( $\bar{f}_{a+b}$ ) is computed. The mean doublet response ( $\bar{f}_d$ ) is computed. The difference between the singlet response sum and mean doublet response ( $\bar{f}_{a+b} - \bar{f}_d$ ) is computed. Finally, percent overlap is calculated as this difference divided by the mean doublet response. 0% overlap indicates that the two stimuli excite completely independent populations of motor units, whereas 100% overlap indicated that they excite the same population.

When overlap measurement for all pairs is complete, the routine prints out, for various overlap cutoff levels (i.e., 10%, 20%, etc.), the sets of electrodes, for which all pairs in the set have overlap below that cutoff level. The interface also provides the operator an option to enter a specific overlap cutoff for which to generate sets.

$$\bar{f}_{a+b} = \bar{f}_a + \bar{f}_b \quad (6.1)$$

$$\bar{f}_d = \frac{\bar{f}_{ab} + \bar{f}_{ba}}{2} \quad (6.2)$$

$$\%Overlap = 100 * \frac{\bar{f}_{a+b} - \bar{f}_d}{\bar{f}_d} \quad (6.3)$$

### 6.2.1 Novel Methods

Historically, overlap measurement has involved averaging the isometric force responses to many repetitions of the same stimulus (up to 64 [17]), typically with a delay between stimuli of a second or more. An obvious shortcoming of this approach is the time it takes (even when the process is automated) to execute the necessary series of pulses. Another, more serious problem involves the nature of muscle force recruitment. In an acute preparations, force is typically measured by removing the distal muscle tendon from its insertion point and attaching it to a force transducer. When the muscle is instrumented in this way, measured twitch forces represent a combination of the action of the contractile muscle fibers and the elastic properties of the tendon. During a twitch contraction, not all of the contractile action of the activated muscle fibers is translated into force at the transducer; some is “absorbed” by lengthening of the tendon. The effect of tendon elongation, on force, decreases during the course of a tetanus as the tendon lengthens. This phenomenon has the problematic effect of increasing the response to doublets, as compared to singlets, making overlap appear smaller than it actually is. To address this issue we implemented, in the routine, an approach to measuring overlap that employs rapid trains of pulses instead of single pulses. The routine allows the operator to set train parameters—typical values used are 40 Hz for 500 ms or 1 s. By limiting analysis to the force level within the window of response plateau, the effect of tendon stretch on the overlap computation is minimized. An additional benefit of this approach is that overlap can be determined more quickly, as response measurement does not require the execution of multiple trials.

Another problem with the standard method of overlap measurement is that it requires invasive, and irreversibly destructive, surgical intervention to instrument the muscle for force transduction. Such an approach is, by definition, not suitable for actual FES applications

involving intact musculoskeletal systems. To address this practical consideration, we devised a method of measuring overlap that uses a multidimensional force transducer attached to the foot to measure responses. Conceptual aspects of this approach were developed in collaboration [27]. Implementation of the approach, in software, was completed by the author.

### 6.3 Results

The mean time required to measure overlap for a pair of electrodes using the single twitch method is 36.9 s (n=153). For the pulse train method, the average time to measure pairwise overlap is 26.5 s (n=316). For a USEA implant in a cat lower limb nerve trunk, typically between 4 and 12 electrodes are able to selectively activate each major muscle. For this range of electrode set sizes, the corresponding times required to measure pairwise overlap with the twitch method would be 3.7 and 40.6 minutes, per muscle, and from 2.7 to 29.2 minutes for the train method. Figure 6.1 shows a typical matrix of pair-wise overlap values measured by the routine. Figure 6.2 shows a typical plot generated by the routine when using 3-dimensional force responses.

### 6.4 Discussion

Given that measuring overlap for a pair of electrodes manually takes several minutes (at the fastest), the automation of this task saves a tremendous amount of time. In acute experiments, which have a fixed limit on duration, shortening the overlap mapping task by several hours is critical to ensuring sufficient time to accomplish the larger experimental goals. Perhaps more importantly, it frees the experimenter to focus his/her mental energy on experimental aims—overlap mapping is an incredibly tedious and exhausting task that can consume a significant portion of the experimenter’s ultimately finite attention. Currently, a substantial portion of the algorithm execution time is spent reverifying response levels for each electrode before the start of the single-pulse or train overlap stimuli. In the case of a chronic implant, where the electrode interface has stabilized, it may be possible to remove the reverification step from the routine—hence making it more efficient.

A question often raised, regarding overlap assessment, is whether the presence of interaction among sets larger than two electrodes (i.e., triplet and quadruplet overlap) exists and exerts an influence on output of multielectrode trains, and if so, whether these kinds of interactions should also be measured. The answer to the first question is yes—as stimulus levels increase on all electrodes, there will undoubtedly be motor units that are activated by more than two electrodes. If these electrodes and stimulus levels are used in a multielectrode

|                  |    | Electrode Number |      |      |     |       |      |      |      |      |      |
|------------------|----|------------------|------|------|-----|-------|------|------|------|------|------|
|                  |    | 9                | 10   | 41   | 56  | 57    | 58   | 82   | 83   | 84   | 85   |
| Electrode Number | 9  | X                | 21.7 | 21.0 | 6.0 | 10.3  | 5.9  | 10.3 | 11.0 | 9.4  | 15.7 |
|                  | 10 |                  | X    | 17.9 | 4.1 | -10.2 | 5.9  | 11.9 | 12.6 | 5.9  | 12.7 |
|                  | 41 |                  |      | X    | 3.1 | -12.8 | 5.0  | 9.5  | -4.2 | 5.6  | -5.8 |
|                  | 56 |                  |      |      | X   | 24.0  | 19.4 | 12.3 | 35.7 | 19.9 | 9.1  |
|                  | 57 |                  |      |      |     | X     | 26.2 | 20.7 | -4.4 | 19.0 | 93.4 |
|                  | 58 |                  |      |      |     |       | X    | 16.0 | 12.7 | 13.9 | 6.9  |
|                  | 82 |                  |      |      |     |       |      | X    | 25.2 | 30.1 | 3.5  |
|                  | 83 |                  |      |      |     |       |      |      | X    | 32.0 | 16.6 |
|                  | 84 |                  |      |      |     |       |      |      |      | X    | 88.6 |
|                  | 85 |                  |      |      |     |       |      |      |      |      | X    |

**Figure 6.1:** Matrix containing all pair-wise overlap values (in %) for a set of 10 electrodes (45 pairs). This representative data set was collected in 34 minutes.

train, the resulting triple and quadruple activation will cause motor units to fatigue at an even faster rate than those activated by only two electrodes. There are three reasons, however, why the overlap routine described in this chapter does not measure interaction among sets larger than two. The first is that, for biological reasons measuring overlap is technically challenging for sets of three electrodes and impossible for sets of four or more. Given that the refractory period of a motor unit is approximately 1 ms and the electronic decay of a stimulus pulse is approximately 400 microseconds [44], at most three pulses can be delivered that are guaranteed both not to electrically summate and not to activate any axons multiple times (i.e., the prerequisite for overlap measurement). The second reason is that if, as is the goal, all pair-wise overlap measurements are zero, is is logically impossible for there to be any zones of triple, quadruple, etc. overlap; hence, there is no need to measure these interactions. The final reason is that, in practice, if the number of motor units activated by several electrodes in a multielectrode train is small, then neither their initial nonlinear force contributions, nor the subsequent loss of their output (resulting from rapid fatigue) will have a large effect on the overall muscle output.

Overlap: elecA [8] elecB [22] = [17.4643%]

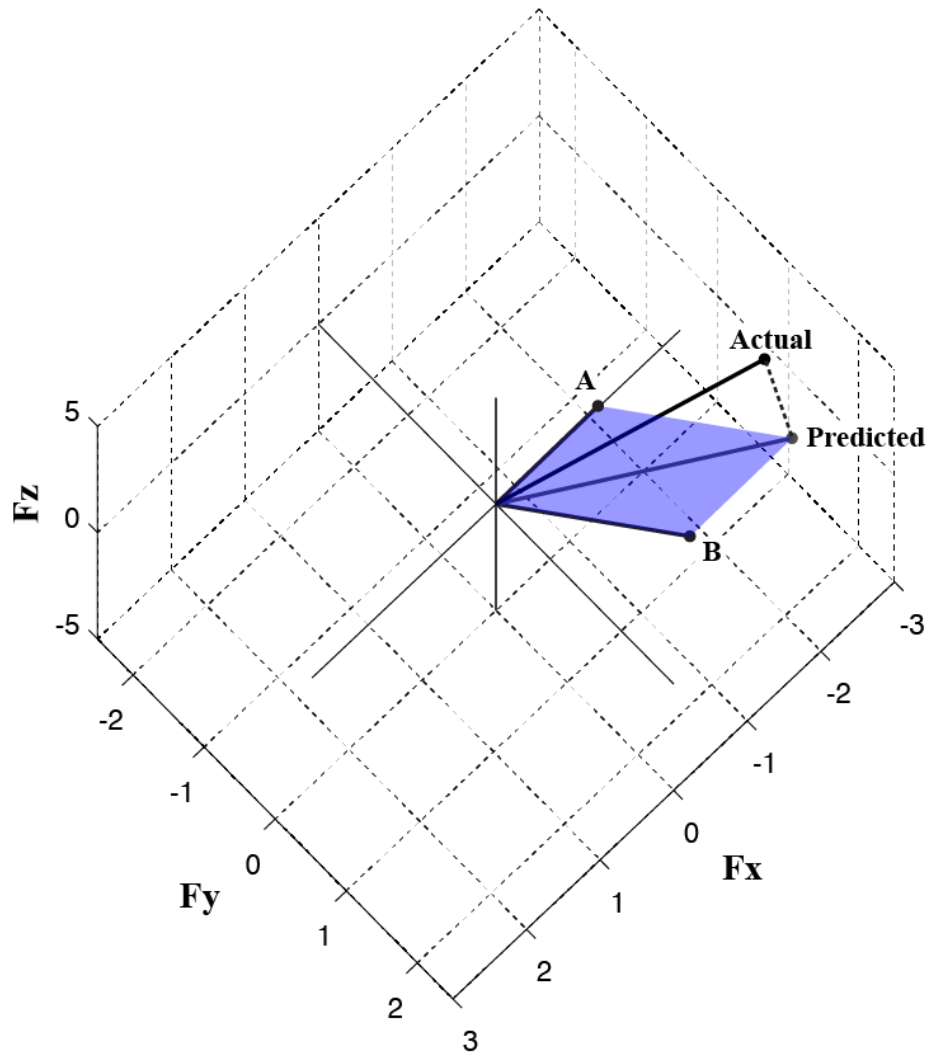


**Figure 6.2:** Plot representative of output from excitation overlap routine using the 3 force components of a 6-axis load cell. (Note: annotated for clarity in black-and-white format).

# CHAPTER 7

## RIPPLE REDUCTION VIA FEEDFORWARD TIMING ADJUSTMENT

### 7.1 Motivation

Chapter 1 introduces the emerging field of IIFMS, and some of the encouraging experimental results that have been achieved by various groups. An important practical issue that has not been fully addressed, however, is the complexity of selecting stimulation parameters for IIFMS trains (as compared with selecting parameters for single-electrode trains). These complexities are particularly evident when the issue of intraperiod variation (ripple) in evoked force is considered. Ripple must be low for muscle forces to be functionally useful; however, IIFMS-evoked responses tend to elicit responses with high levels of ripple (even when their composite frequency would, on a single electrode, evoke a low-ripple response) (Figure 1.5). Achieving low-ripple responses with single-electrode trains is simply a matter of increasing stimulus frequency until ripple falls below the target level. In contrast, multielectrode trains have a much larger parameter set, including electrode count, stimulus strength for each electrode, stimulus rate for each electrode, and timing of stimuli among electrodes (Figure 1.6). The interactions among these parameters—especially with respect to how they influence ripple—are substantially more complex than those for single-electrode trains. Selecting from among all possible stimulation parameter combinations in a way that consistently achieves smooth muscle responses is a nontrivial task. This is especially true when faced with the constraint of keeping stimulus rates low to delay the onset of muscle fatigue.

In early studies involving multielectrode stimulation, the task of selecting parameters to achieve low-ripple forces at a target level was typically accomplished by hand in a trial-and-error manner. Efforts to minimize ripple often focused on searching for stimulus levels that matched the peak force evoked by each electrode. For one group (McDonnall, personal communication) identifying low-ripple stimulus parameters often took

hours. Further, achieving low-ripple responses by adjusting only stimulus strength was not always possible. More recently, Frankel has demonstrated a method for control of stimulus strength, to achieve time-varying force trajectories [28]. Little work, however, has been done investigating the influence intraperiod stimulus timing on response ripple.

This chapter presents the results of studies investigating the relationships between various IIFMS parameters and response ripple. Also presented are results of studies assessing the feasibility of using a simple response-prediction model to identify IIFMS timings that minimize response ripple. The model takes single-electrode responses, measured in-vivo, as inputs and predicts the response to a composite IIFMS train as the linear sum of the single-electrode responses, shifted by the given IIFMS timings (Figure 7.1). Although a linear tendon-force-summation model is not accurate under all conditions, it has been shown to be largely valid for short-duration isometric muscle contractions, specifically during constant-force periods of the response [58].

Given this response prediction model, the effect of a large number of timings can be explored *in silico* rapidly using a small set of actual single-electrode responses, recorded in-vivo in a relatively short time. Function optimization techniques can be used, in conjunction with the model, to methodically search the parameter space for timings that minimize ripple.

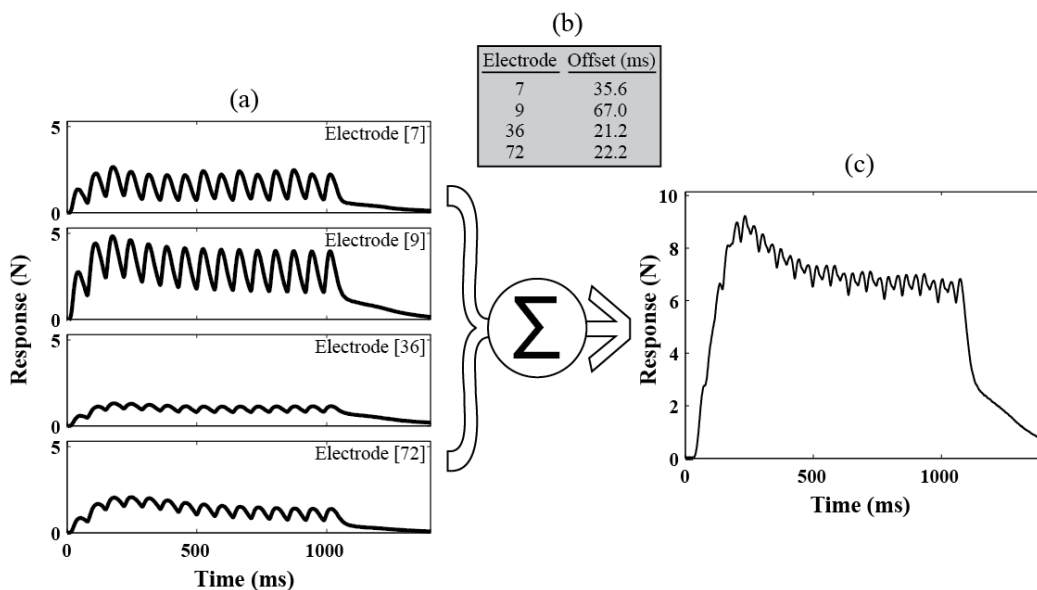


**Figure 7.1:** The IIFMS response prediction model. (a) In-vivo responses to single-electrode trains on each of the four electrodes. (b) Stimulus times for the IIFMS train. (c) Predicted response to the IIFMS train given the times specified in (b). The predicted response is generated by shifting the single-electrode responses by the specified times and summing the shifted waveforms.

Exploring the parameter space *in silico* is several orders of magnitude faster than doing so in-vivo, making this approach to tuning IIFMS timings practical in an experimental settings.

Experiments were conducted in-vivo to explore the effects of IIFMS parameters on response ripple, and to validate the response prediction model and timing-optimization approach. In these experiments, motor axons were stimulated via a 100-electrode (10x10) USEA implanted into the sciatic nerve, and evoked isometric force responses in the isolated plantar flexors were measured with a linear force transducer [22]. Model predictions for IIFMS trains, covering a wide range of stimulus parameters, were compared with actual responses measured in-vivo. Performance of the model-based function-optimization technique, at identifying stimulus timings that reduced response ripple, was assessed. Two supplemental analyses were conducted to quantify other aspects of the stimulus timing optimization method. The first looked at its effect on the power spectral density (PSD) of the muscle response waveform. The second investigated the relationship between dissimilarity in individual electrode evoked-response kinetics and the efficacy of the optimization method.

## 7.2 Methods

The data presented in this chapter were collected in two neuromuscular electrophysiology experiments with an acute cat model. For a detailed description of surgical preparation and electrode implantation, see Chapter 2. After the USEA was implanted in the sciatic nerve, automated stimulus-response mapping routines, as described in Chapters 4, 5 and 6, were executed to identify electrodes that elicited functionally-useful force levels and then to select a subset that exhibited minimally overlapped axonal excitation fields. All experimental manipulations were controlled by the closed-loop stimulation platform described in Chapter 3.

### 7.2.1 Data Collection

A series of trials involving IIFMS parameter exploration and timing optimization were executed with an automated software routine implemented by the author to run on the closed-loop FES platform. The routine accepts three input parameters: a set of low-overlap electrodes, a target single-electrode-train peak response range (e.g., 2-7 N), and a set of one or more IIFMS periods (e.g., 80, 100, 120 ms). The routine first determines, for each (electrode, period) combination, the stimulus levels that elicit the low and high bounds of the target response range. Then, for each IIFMS period, the program executes a series of parameter exploration iterations (PEIs) consisting of the following steps (described in detail in the following sections). First, for each individual electrode, the response to a short train is measured in-vivo. Next, the response to an IIFMS train with even stimulus timing is

measured in-vivo. Then, optimized IIFMS stimulus timings are predicted using the linear response model and function optimization method. Finally, the IIFMS train with optimized timings is executed in-vivo and the response measured.

All results reported here involve stimulus trains that were between 1000 ms and 1500 ms in duration. Single-electrode train response targeting was accomplished with a binary search algorithm similar to the one described in Chapter 4 and [59].

### 7.2.1.1 Single-Electrode Trains

In the first step of each parameter exploration iteration, pulsewidths are selected for each of the  $N$  electrodes randomly from within the pulsewidth range determined in the force targeting step. Then, one single-electrode pulse train is executed for each electrode, with approximately 5 seconds rest between trains. Responses to these single-electrode trains are recorded and saved for use in subsequent steps.

### 7.2.1.2 IIFMS Train with Even Stimulus Timing

In this step, the program constructs an IIFMS train with evenly timed stimuli by combining the single-electrode trains from the previous step, with a time shift between trains of  $1/N$ th of the IIFMS period (see Figure 1.6 for illustration of  $N$ -electrode cycle). The timing of stimuli in the resulting IIFMS train is the same as that produced by the rotary method described in [33] and the interleaved form described in [37] and [21]. An important point to note is that the rate of stimuli on each individual electrode remains the same within the IIFMS train as it was for the single-electrode trains delivered in the previous step. After creating the IIFMS train, the program executes it in-vivo and records the response.

### 7.2.1.3 Ripple Quantification

For responses to single-electrode and IIFMS trains, ripple is measured as follows. The force waveform is first divided into segments corresponding to the length of the IIFMS period (Figure 1.6). Next, for each period, ripple is computed as the range of the response divided by the mean. Finally, the overall response ripple is computed as the mean of the ripple values for all periods within the region of response plateau (Figure 7.2).

### 7.2.1.4 Timing Optimization and In-Vivo Validation

Ripple is measured in the same way, for predicted responses, as it is for actual responses, recorded in-vivo. Thus, given a set of  $N$  single-electrode responses, the effect of a particular

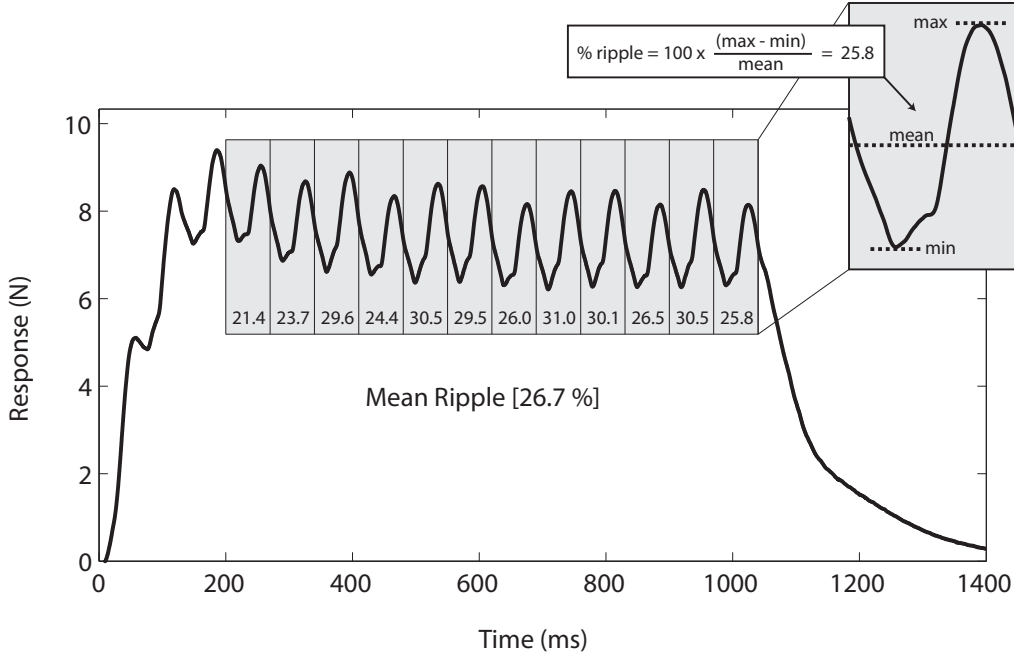


**Figure 7.2:** Ripple calculation for a representative response to an IIFMS train. The response waveform is divided into regions corresponding to the IIFMS period. Inset: ripple for each period is calculated as 100 times the range over the mean. Main figure: ripple for the entire train is computed as the mean of the ripple for each period during the response plateau.

stimulus timing, on ripple, can be predicted by first predicting the IIFMS response waveform (Figure 7.1), and then computing ripple for that waveform. In the context of optimization, the combination of the response prediction step and the ripple computation step can be formulated as an objective function ( $f$ ) that takes a vector of stimulus offsets as input, and returns ripple ( $r$ ) as a scalar output (equation 7.1 and equation 7.2).

$$\bar{o} = (o_1, o_2, o_3, \dots, o_n) \quad (7.1)$$

$$r = f(\bar{o}) \quad (7.2)$$

A function-minimization algorithm can then be applied to this objective-function to search for offsets that minimized response ripple. Typically, function-minimization algorithms evaluate the objective function repeatedly, each time with slightly modified input arguments, eventually honing in on inputs that minimize the function output. This study used the *fminsearch* routine available in Matlab<sup>®</sup>, which employs a simplex search algorithm (described in detail in [60]). As part of each PEI, *fminsearch* is used to identify optimized IIFMS timings for the given set of electrodes and the single-electrode train response waveforms for those electrodes (previously recorded in-vivo). The IIFMS train with optimized

timings is then executed and the response is recorded. The in-vivo IIFMS response is used later to assess the performance of the optimization technique.

## 7.2.2 Data Analysis

The responses from all PEIs across all experiments were combined, and the following analyses were conducted.

### 7.2.2.1 Model Accuracy

Three metrics quantifying the accuracy of the response prediction model were computed: 1) correlation between predicted and actual raw force waveforms (as determined by a sample-by-sample comparison); 2) correlation between predicted and actual force ripple; and 3) correlation between predicted and actual mean force (in the region of response plateau) (Figure 7.3).

### 7.2.2.2 Parameter Influence

The influence, on response ripple, of three different IIFMS parameters, stimulus strength, mean interphase interval (IPI—i.e., composite frequency), and stimulus timing was assessed. To quantify the influence of stimulus strength, correlations between percent ripple in IIFMS train response and two metrics of variance in the set of single-electrode train responses—coefficient of variation (Cv) and relative range (range/mean)—were computed. To evaluate the influence of mean IPI, percent ripple in IIFMS responses were compared to mean IPI. To assess the effect of stimulus timing, the distribution of ripple in the set of responses to trains with evenly-timed stimuli was compared to the distribution of ripple in the corresponding set of responses to trains with optimized timing.

### 7.2.2.3 Supplementary Data Analyses

To better understand the effects of stimulus-timing optimization, we performed two additional analyses. First, we looked at its effect on the power spectrum of the IIFMS train response. Given that the musculotendon system acts as a low *pass* filter, the low frequency components of the ripple waveform are the most problematic (in the context of functional movement). Thus, it is useful to know what effect timing optimization has on the frequency components of the force waveform. Second, we conducted directed analyses to determine whether ripple reduction occurred preferentially when responses evoked by constituent electrodes were kinetically dissimilar.

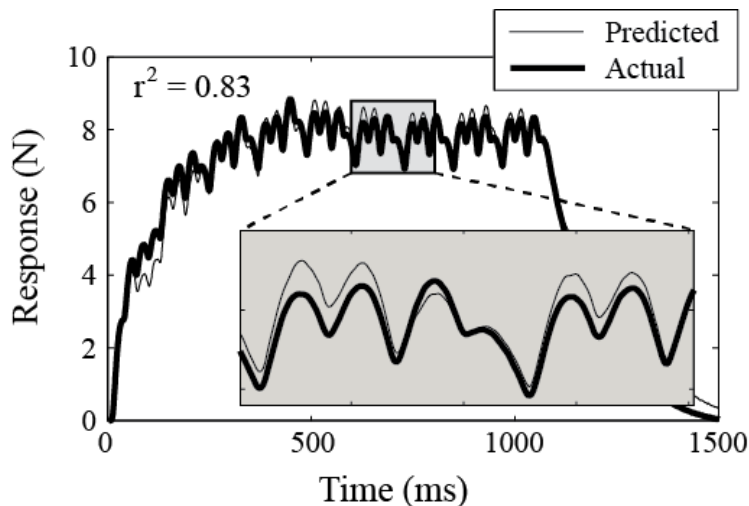


**Figure 7.3:** A simple, linear summation model accurately predicts response waveforms. Example of an actual IIFMS-evoked response overlaid on top of the response predicted by the linear summation model. The high correlation between the two responses (shown in detail in inset) suggests that linear summation of single-electrode responses is a reasonable approach to predicting responses to IIFMS trains.

#### 7.2.2.4 Meta Analysis of Function Minimization Method

As mentioned previously, optimization of the ripple function was achieved with an out-of-the-box function optimization method *fminsearch* supplied by the Matlab<sup>®</sup> analysis environment. The *fminsearch* function uses the Nelder-Mead simplex algorithm to find a local minimum of the objective function around a supplied starting vector [60]. Given that the result is not guaranteed to be a global minimum, it is likely that a single execution of the minimization function with a single starting point will not always identify the best electrode timing values. To address this possibility, a meta analysis was conducted to assess the performance of the minimization method, and determine how many executions of the optimization method are necessary to ensure a near-optimal result. The analysis was conducted as follows. For various-sized sets of actual single-electrode train responses, the minimization method was executed a large number of times, each time with a different random starting point (i.e., a set of stimulus timings randomly selected from 0 to the IIFMS period length). The results were then pooled and subsets of various size (i.e., representing different number of executions of the minimization function) were selected. For each execution set the best result was identified. The distribution of these best values for all execution sets of a given size were plotted. Finally, the distributions for each execution set size were compared.

## 7.3 Results

Results show that, in general, a simple linear summation model accurately predicts IIFMS-evoked responses under isometric and isotonic conditions. Model accuracy is sufficient for the model to be used to search for IIFMS timings that reduce response ripple (compared to similar IIFMS trains with evenly spaced electrode timings). IIFMS timings can be adjusted to reduce ripple even when responses evoked by individual electrodes are kinetically dissimilar to one another. Unexpectedly, we found that optimizing stimulus strengths—by minimizing variance in single-electrode train peak response level—proved to be less effective at reducing IIFMS response ripple than optimizing stimulus timing. Generally, decreasing mean IPI (increasing stimulus frequency) lowered response ripple; however, the effect was not as strong as expected.

### 7.3.1 Data Summary

160 PEIs were completed in which a total of 320 IIFMS trains and 760 single-electrode trains were executed and responses measured. Train duration ranged from 1000 ms to 1500 ms. Electrode group size ranged from 4 to 8. Single-electrode periods ranged from 160 milliseconds to 70 milliseconds (6.2 Hz to 14.3 Hz). Mean interpulse periods for IIFMS trains ranged from 30 ms to 17.5 ms (33.3 Hz to 57.1 Hz) (Table 7.1). Mean response plateau values for single-electrode trains ranged from 0 N to 5.26 N. Mean response plateau values for IIFMS trains ranged from 3.15 N to 25.3 N.

### 7.3.2 Model Accuracy

In many PEIs, predicted waveforms matched actual waveforms extremely well (Figure 7.3), and, overall, the linear-summation model produced accurate predictions of response waveform shape (mean  $r^2$  predicted vs. actual = 0.7,  $n = 360$ ; Figure 7.4). There were also high correlations between ripple in predicted and actual responses ( $r^2 = 0.84$ ), and between predicted and actual mean plateau force ( $r^2 = 0.98$ ; Figure 7.4). We found that predicted ripple and predicted mean force consistently differed slightly from the model-predicted values, suggesting a small nonlinear component to tendon force summation. This observation is consistent with [58].

**Table 7.1:** Stimulation Parameters for All PEIs

| Set Number | Electrode Count | N-Electrode Period (ms) | Mean IPI (ms) | PEI Count |
|------------|-----------------|-------------------------|---------------|-----------|
| 1          | 4               | 70                      | 17.50         | 5         |
| 2          | 4               | 100                     | 25.00         | 10        |
| 3          | 4               | 120                     | 30.00         | 50        |
| 4          | 4               | 100                     | 25.00         | 10        |
| 5          | 4               | 80                      | 20.00         | 10        |
| 6          | 5               | 100                     | 20.00         | 10        |
| 7          | 4               | 100                     | 25.00         | 14        |
| 8          | 4               | 120                     | 30.00         | 15        |
| 9          | 8               | 150                     | 18.75         | 15        |
| 10         | 6               | 120                     | 20.00         | 15        |
| 11         | 8               | 160                     | 20.00         | 5         |

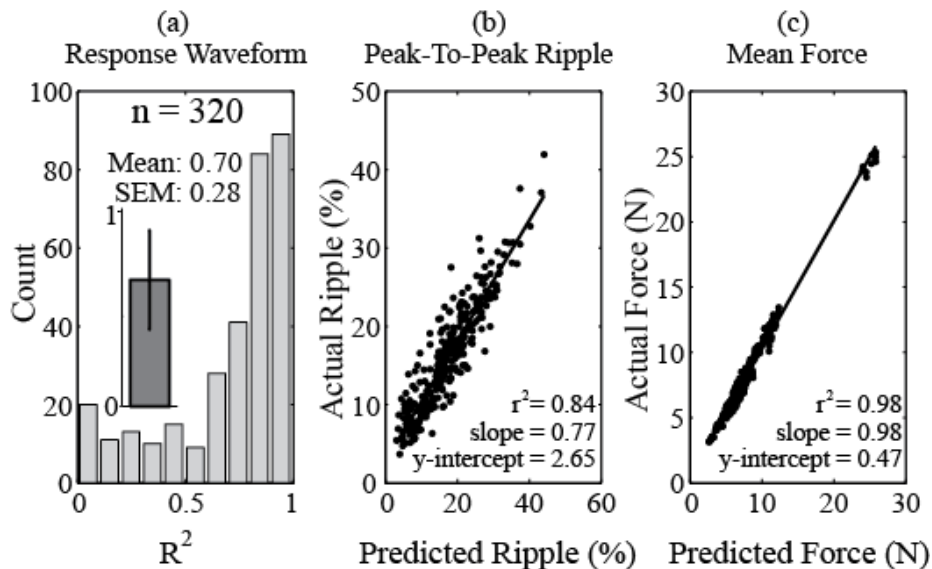


**Figure 7.4:** IIFMS response prediction model is highly accurate; group data. Results computed for a set of 320 predictions. (a) Distribution of correlation values between predicted and actual response waveforms (within the region of response plateau). The inset shows grouped data. The mean of 0.7 indicates that the actual waveform is highly correlated with the prediction, suggesting that the model will be useful in optimization routines. (b) Predicted peak-to-peak ripple versus actual ripple. The high correlation suggests that the model is a good predictor of actual response ripple. (c) Predicted mean response level versus actual level. The correlation between these two data sets is very high, indicating that the linear summation model is a very good predictor of actual response force.

### 7.3.3 Stimulus Level

Counter to our initial expectations, we found that adjusting stimulus strengths to minimize variance in single-electrode-train peak response level (across electrodes in the IIFMS set) did not usually produce the lowest-ripple IIFMS response. Figure 7.5 presents a clear example in which the response to an IIFMS train with matched single-electrode-train response levels has greater ripple than the response to an IIFMS train constructed from single-electrode trains with unmatched responses. To assess the effect of single-electrode response variability on ripple, we plotted IIFMS response ripple against the coefficient of variation (Cv) and relative range of the single-electrode response peaks. Additionally, we computed the associated correlations (Figure 7.6). We found that for the range of single-electrode response levels examined (which included differences between greatest and smallest response of up to a factor of 3.1), neither metric of variance among single-electrode-train responses correlated strongly with ripple. This was true for IIFMS trains with even stimulus timings ( $r^2$  Cv vs. % ripple = 0.00,  $r^2$  relative range vs. % ripple = 0.22), as well as IIFMS trains with optimized stimulus timing (Figure 7.6). This result is contrary to assumptions underlying approaches used in previous multielectrode FES studies, and indicates that, within a broad range of values, adjustment of stimulus strength alone is not a particularly effective approach to achieving low-ripple in IIFMS responses. The factors underlying this apparent mismatch were, subsequently, investigated further, as detailed in a later section.

### 7.3.4 Mean Interpulse Interval

Unexpectedly, over the range of IPIs tested, ripple in IIFMS-evoked responses did not decrease uniformly as a function of IPI (i.e., frequency). For the set of responses to timing-optimized IIFMS trains, ripple was somewhat correlated with IPI (generally increasing as IPI increased). The distribution of means for ripple in all IIFMS train responses was plotted vs. mean IPI. For trains with even electrode timing, the mean ripple ranged from 14.2 to 22.6%. For trains with optimized electrode timing, the mean ripple ranged from 6.4 to 18.1% (Figure 7.7). The likely explanation for this unexpected result is that response kinetics were not well controlled across PEIs. For a stimulus train of a given frequency, motor unit groups with different kinetics will exhibit responses with different levels of ripple. Thus, any variation, across PEIs, in the average response time of activated motor-unit groups, would influence ripple independently from IPI—potentially confounding the correlation between IPI and ripple.

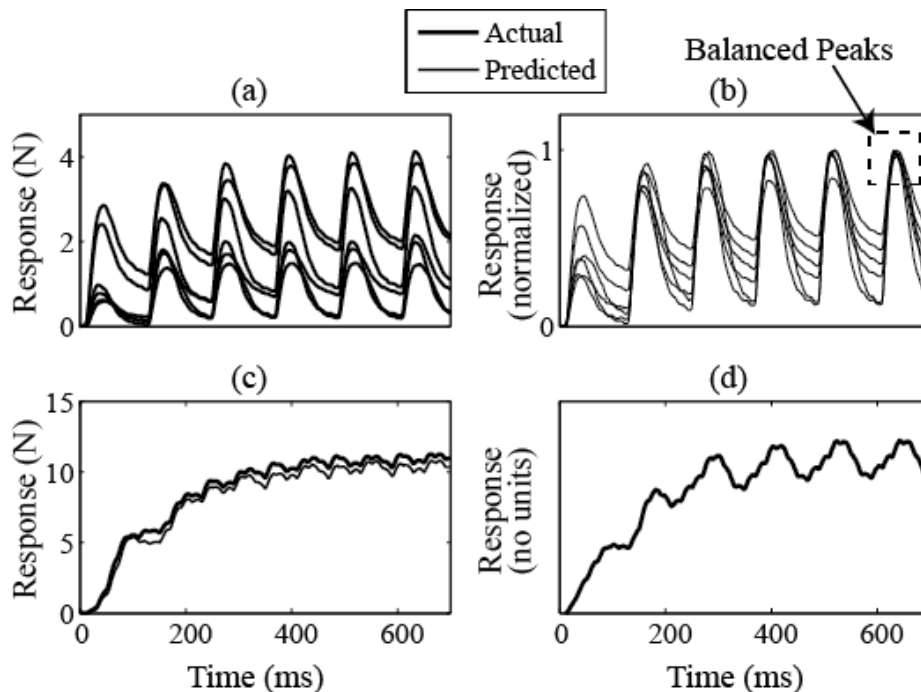


**Figure 7.5:** Matching forces on individual electrodes does not necessarily yield minimal ripple in IIFMS responses. Example of detailed response waveforms recorded during an iteration of the parameter exploration routine. (a) Actual response waveforms for the 6 electrodes used in the IIFMS train. (b) The response waveforms for the same 6 electrodes after they were scaled so that their peak response amplitude is equal. (c) The actual and predicted IIFMS train responses given the unbalanced single-electrode responses shown in (a). (d) The predicted IIFMS train response, given the normalized single-electrode train responses shown in (b). Note higher ripple in (d) compared with (c).

### 7.3.5 Stimulus Timing

In contrast to stimulus strength, stimulus timing proved to have a large influence on IIFMS response ripple. To quantify the effects of optimizing stimulus timing, we plotted the distribution of response ripple for even-timing IIFMS trains and the distribution of ripple for optimized-timing trains, for all 160 PEIs (Figure 7.8). The mean response ripple for the even-timing trains was 19.1%, whereas the mean response ripple for the optimized-timing trains was only 12.9%. The difference in the means of the two distributions was statistically significant ( $P=0.000$ ). We also computed the effect of optimizing stimulus timing on power in the response waveform. This was accomplished by first band-pass filtering the signal (1 Hz to 100 Hz), and then computing the Welch power spectral density estimate. The power reduction ratio (optimized/even) due to stimulus timing optimization was computed for each of the 160 PEIs within a low-frequency band (defined, for our purposes, as 1 Hz to two times the constituent frequency). An example of this computation for a single

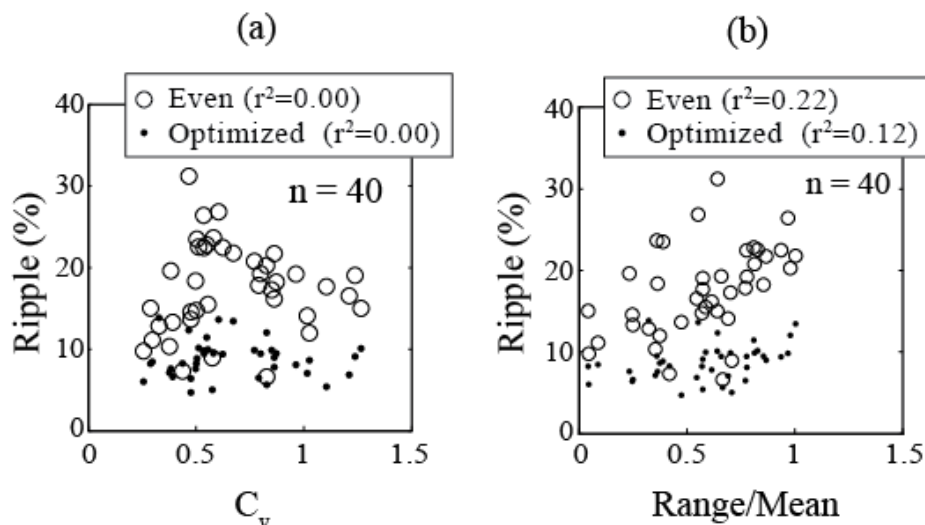


**Figure 7.6:** Ripple in IIFMS-evoked responses is not correlated with variations among forces evoked by individual electrodes. (a) Ripple in responses to IIFMS trains versus coefficient of variation ( $C_v$ ) for the set of single-electrode response peaks (for trains with a mean IPI of 20 ms). (b) Shows ripple values for the same set of trains vs. range/mean for single-electrode response peaks. Both plots show data for trains with even stimulus timings (circles) and trains with optimized stimulus timings (dots). Low variability in single-electrode response peaks (i.e., unmatched peaks) did not correspond to a low-ripple composite response. Quite the opposite, low-ripple responses could be elicited even when single-electrode response peaks were not matched.

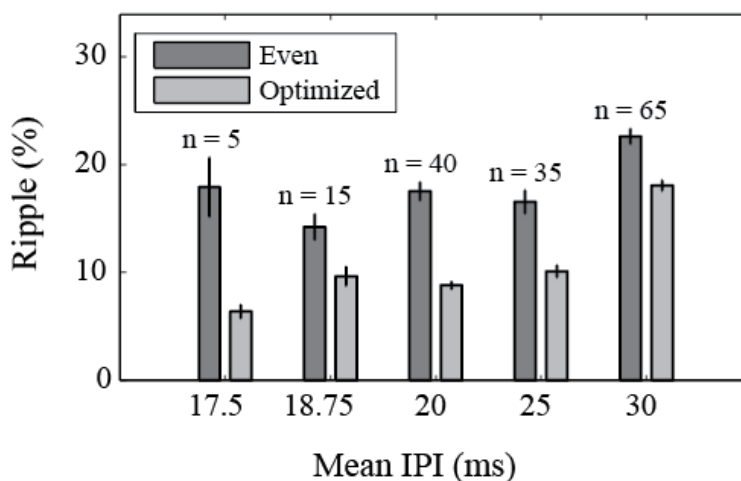


**Figure 7.7:** Decreasing IPI generally reduces ripple for IIFMS trains with optimized timings. Additionally, timing optimization decreases IIFMS ripple across a range of different IPIs. Mean response levels (and standard error of mean whiskers) for sets of  $N$  ( $N = 5, 15, 40, 35, 65$ ) in-vivo responses for IIFMS trains with various mean IPI values. For each IPI, the left bar shows ripple for even-timing trains and the right column shows ripple for optimized-timing trains.

representative PEI is shown in Figure 7.9, and a histogram of the results for all PEIs is plotted in Figure 7.10. As can be seen from these two figures, optimizing stimulus timing substantially reduced power in the low-frequency range (mean reduction=55.8%).

### 7.3.6 The Effectiveness of Timing Adjustment Arises from Compensation for Dissimilar Response Kinetics

As noted above, time shifting the stimuli in an IIFMS train was relatively effective in reducing response ripple, whereas adjusting stimulus strengths to produce matched single-electrode-train response peaks was not. Supplementary analyses were conducted to investigate the factors underlying these effects, and to account for these nonintuitive results.

Observing that response kinetics varied widely across individual electrodes used in the PEIs, we posited that this factor might explain the greater effectiveness of tuning stimulus timing (as compared to stimulus-strength) for reducing IIFMS response ripple. Two subsequent analyses were performed to examine this hypothesis. As a first, quantitative test, the question of whether optimization produced a greater reduction in ripple for responses that had dissimilar kinetics, compared with responses that had similar kinetics was examined. This was indeed the case (Figure 7.11). The 16 PEIs in which single-electrode response peaks had been matched were divided into two equal-sized groups on the basis of their single-electrode response waveform kinetics. One group had relative similar response kinetics, and the other group had relatively dissimilar response kinetics. For responses with similar kinetics, timing optimization did not significantly reduce ripple (6.5% decrease, paired  $t_7 = 0.56$ ,  $p = 0.59$ ), relative to ripple produced with even timing. In contrast, for responses with dissimilar kinetics, timing optimization produced a 33.1% decrease in ripple (paired  $t_7 = 7.89$ ,  $p = 0.000$ ). The difference in ripple reduction between the two groups was significant (unpaired  $t_{14} = 2.33$ ,  $p = 0.036$ ). These results indicate that timing optimization has a greater effect on reducing response ripple in IIFMS trains when constituent electrode response kinetics are dissimilar.

As a second quantitative test, simulations were conducted in which the timing optimization algorithm was employed on sets ( $n=10,000$ ) of single-electrode-train responses, selected randomly from the entire group of responses collected across all PEIs. Responses to even-timing and optimized-timing IIFMS trains were predicted and ripple was computed. Additionally, the kinetic similarity of each set of electrodes was quantified. Group results were analyzed to determine whether the size of the mean timing shift necessary to minimize ripple was positively correlated with the dissimilarity among constituent electrode response kinetics. This was found to be the case (Figure 7.12). As the dissimilarity of waveforms

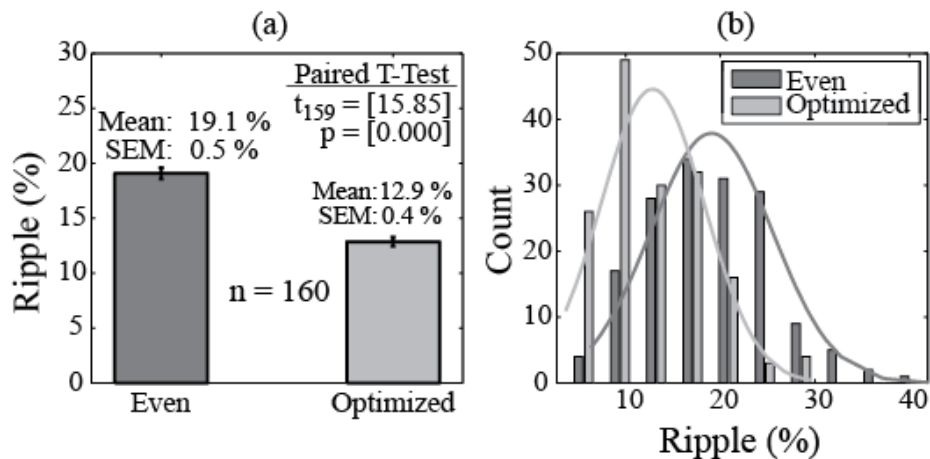


**Figure 7.8:** Optimization of stimulus timing effectively reduces ripple (group data). (a) Summary of data for electrode stimulus timing optimization. (b) Distribution of stimulus timing optimization results with fitted Gaussian curves. Stimulus timing optimization achieved a 32% reduction in ripple for all IIFMS trains.

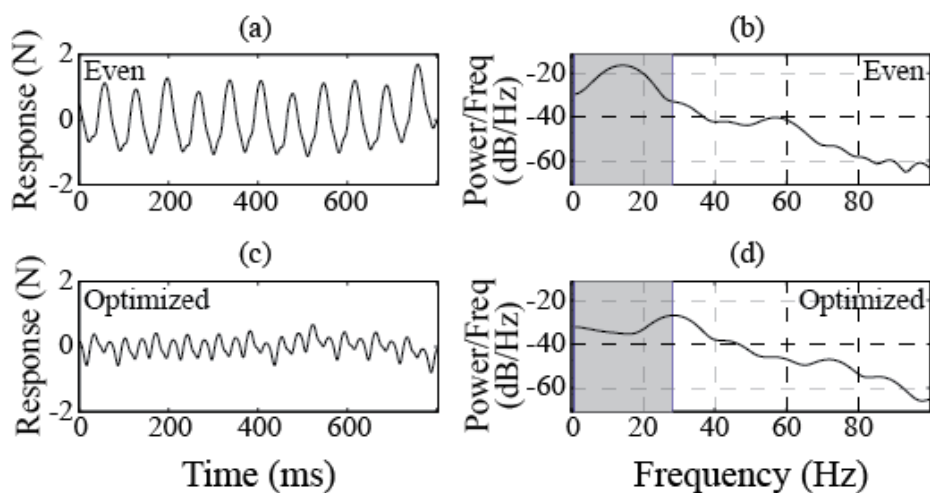


**Figure 7.9:** Optimization of stimulus timing reduces power in a low-frequency range (single, representative PEI). Left column: Filtered, demeaned, 800-ms portion of responses to IIFMS trains with even timings (a) and optimized timings (c). Right-hand column: Welch power spectral density estimates for the corresponding responses shown in the left column.

increased, the mean timing shift necessary to minimize ripple also increased. However, as might have been expected, time shifting was not always necessary for minimizing ripple of kinetically dissimilar electrode sets. One possible explanation for this finding is that serendipitous ordering of kinetically similar pairs of responses (from a set of responses that is, overall, dissimilar) can produce antiphase pairings that result in a low ripple even-timing IIFMS response—in such situations no time shift would be required.

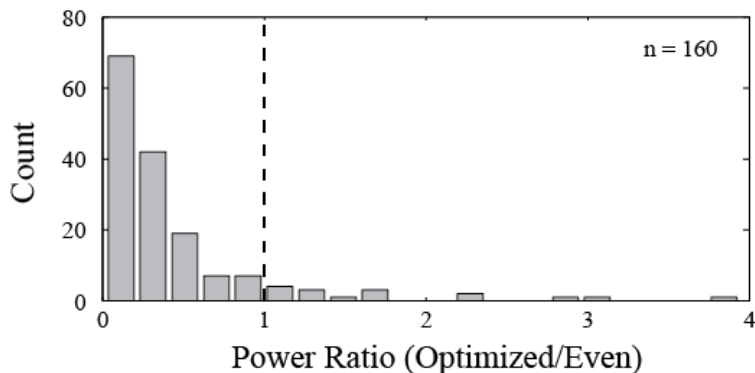


**Figure 7.10:** Optimization of stimulus timing reduces power in the low-frequency range (group data). Summary of power reduction data for all 160 PEIs. Each data point is computed as power in the low-frequency range for the optimized-timing IIFMS-evoked response divided by power in the same range for the even-timing IIFMS-evoked response. The preponderance of power ratios less than one indicates that the power of the low frequencies, corresponding to ripple, was effectively reduced by optimization of stimulus timing.

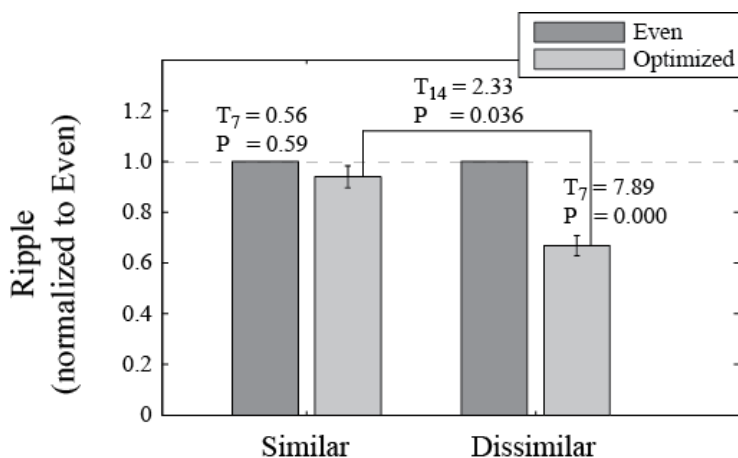


**Figure 7.11:** Timing optimization produces a greater ripple reduction when responses evoked by individual electrodes have dissimilar kinetics. Data shown here are taken from the 16 PEIs in which single-electrode response peaks were matched. The data were further subdivided into two groups based on similarity of single-electrode response waveform kinetics. The left pair of bars shows data for the group with similar single-electrode waveform kinetics, and compares response ripple for IIFMS trains with even-timing with ripple for IIFMS trains with optimized timing. (The data in each even-optimized pair are normalized to the even-timing ripple value.) For responses with similar kinetics, timing optimization did not significantly reduce ripple. The right pair of bars shows the same comparison for the set of PEIs with dissimilar single-electrode waveform kinetics. Timing optimization significantly reduced ripple, and this ripple reduction was greater than that obtained for responses with similar kinetics. These results demonstrate that ripple reduction due to timing optimization is greater for sets of electrodes with dissimilar response kinetics.

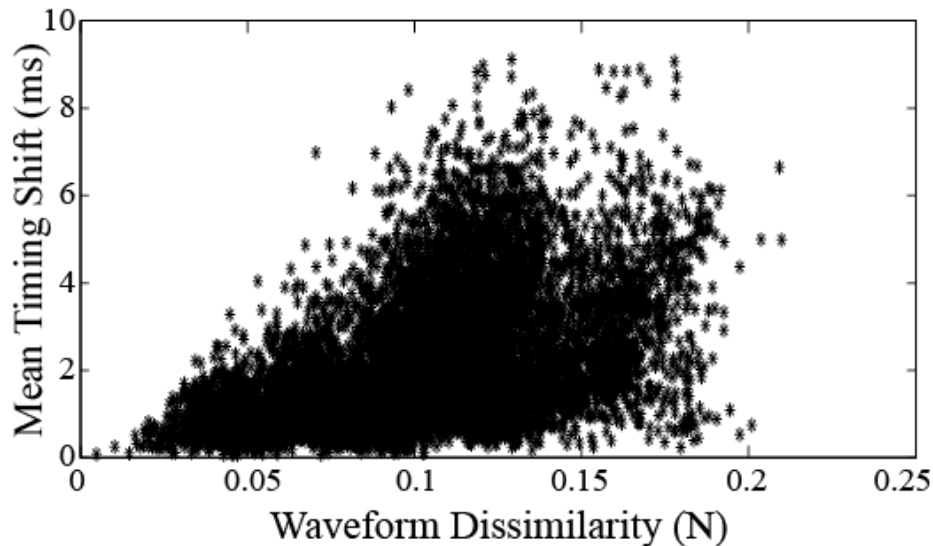


**Figure 7.12:** Mean timing shift necessary to minimize ripple correlates with waveform dissimilarity. Results obtained from 10,000 timing-optimization simulations. For each simulation, optimized timings were computed for a set of 4 normalized single-electrode responses (randomly selected from a set of 40). Dissimilarity between single-electrode waveforms (defined as the mean, over all pairs, of the RMS difference between each pair of responses) was also computed. Mean timing shift was computed as the mean of the absolute value of the differences between optimized timings and even timings. Results indicate that as the dissimilarity of waveforms increased, the time shift that was necessary to minimize ripple also increased.

Taken together, these results demonstrate that time shifting stimuli can effectively reduce response ripple for IIFMS trains, particularly when the responses to stimuli on constituent electrodes have substantially different kinetics.

### 7.3.6.1 Meta Analysis of Function Minimization Method

Results of the meta analysis of the function minimization method are presented in Figure 7.13. As might be expected, the more times the minimization function is called with different, random starting points, the higher is the likelihood of identifying a near-optimal solution. From the figure, it is apparent that the improvement in performance achieved by increasing the number of executions is asymptotic. Given the specific results, it seems that much of the gain in performance is achieved by increasing execution count from 8 to 32. Considering that executions of the *fminsearch* algorithm are relatively time consuming, these meta analysis results suggest that 32 executions represents a reasonable trade off between execution time and optimality.

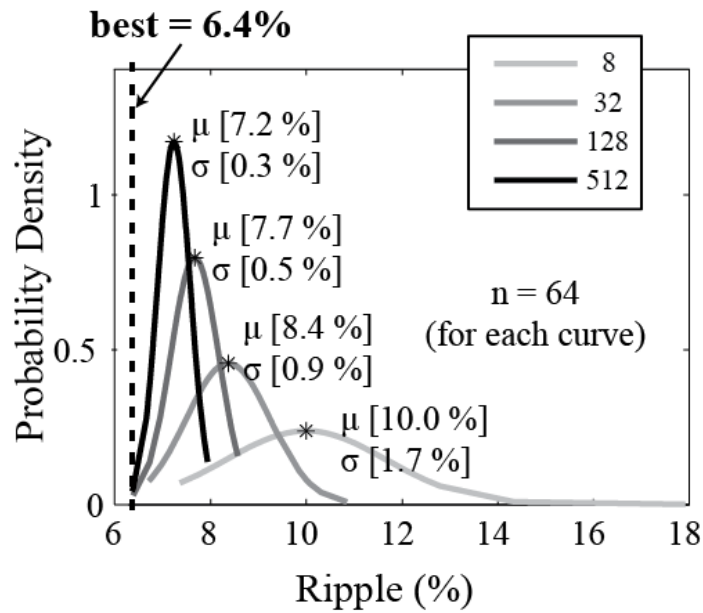


**Figure 7.13:** Distributions of best result for various numbers of executions of the function minimization routine with differing, randomly selected starting points. As the number of executions increases, the best-of-set result improves. Performance improvement appear asymptotic with respect to increase in set size.

## 7.4 Discussion

IIFMS offers several potential advantages over single-electrode FES, chief of which is increasing the fatigue resistance of evoked responses. The work described in this chapter study demonstrates that, under certain conditions, a simple model can accurately predict IIFMS-evoked responses, and thus, could be used to explore and optimize an important part of the large and complex IIFMS parameter space in a timeframe applicable to a research setting. Results indicate that stimulus timing has a much greater influence on response ripple than was previously appreciated. This novel approach to stimulus timing selection was consistently able to achieve a significant reduction in IIFMS train response ripple (compared to standard even-timing IIFMS trains). This was true even when constituent motor unit groups exhibited dissimilar kinetics—a feat not achievable through stimulus strength adjustment alone. The ability to utilize multimuscule, multielectrode activation even when single-electrode responses are kinetically dissimilar extends the range of circumstances under which IIFMS may be usefully employed. Although there are still many challenges to applying IIFMS in a clinical setting, the approach presented here offers a meaningful, and practical contribution to the emerging use of multielectrode FES.

### 7.4.1 Relevance of Other Timing Optimization Methods

At least one other method of optimizing timings has been proposed [61]. This method, which involves using the response waveform from a period of stimulation to derive timing adjustments for stimuli in the next period, is not applicable to short-duration contractions as it requires multiple stimulation periods to converge to a low ripple state (i.e., the contraction might be over before ripple is reduced to a useful level). Given that short-duration muscle contractions are used in an important subset of the human movement repertoire—including sit-to-stance, gait, cycling, and various muscle-strengthening exercises—having a technique that is uniquely applicable to short-duration movements is quite valuable. Also, given that the isometric response measurement conditions employed in this study can be achieved easily in a research and clinical settings, the technique presented here is practical to employ.

### 7.4.2 Impact of Response Kinetics on Ripple Reduction

An interesting yet potentially counter-intuitive result of research presented here is that matching force levels across electrodes does not necessarily lead to an IIFMS train with a minimal-ripple response. One possible reason that this phenomenon has not been reported previously is that the majority of previous studies, unlike the present work, involved combining individual responses that had similar kinetics. For example, several prior studies with multielectrode trains have utilized isolated ventral root stimulation [33, 34]. This experimental approach has allowed researchers to elicit responses with similar size and shape by carefully selecting the population of motor axons activated by each stimulating electrode. Additionally, stimulation was typically super-maximal, and often restricted to activation of a single muscle. In cases where evoked response kinetics are similar across electrodes, even distribution of stimuli across the IIFMS period is likely to be close to optimal—with respect to response ripple. Consequently, the importance of timing may not have been readily apparent.

In contrast, with intrafascicular multielectrode interfaces, such as the USEA, implanted in main nerve trunk, a multielectrode train will typically activate multiple muscles, each with a slightly different fiber-type compositions (and hence response time), all in a sub-maximal manner. In such situations, the effect of variation in response kinetics among electrodes becomes much more evident—as the task of minimizing response ripple can no longer be accomplished solely by matching force peaks. As demonstrated above, adjusting stimulus timing offers a new means of reducing ripple in such situations. The timing optimization process described in this paper, in fact, minimizes ripple from both kinetic and force imbalances at the same time.

The ability to elicit low-ripple responses, despite dissimilar individual electrode response kinetics, might be very useful in a clinical FES setting, because it would enable control of muscles with differing kinetics (such as the four plantar flexors), with the same multielectrode IIFMS train. For a given functional goal, distributing stimulation across multiple muscles would reduce the force requirement on any one, and, hence, provide a means of further delaying the onset of fatigue.

# CHAPTER 8

## OPTIMIZING A FEEDBACK-BASED TIMING ADJUSTMENT ALGORITHM

### 8.1 Motivation

As described in Chapters 1 and 7 interleaved intrafascicular multielectrode stimulation (IIFMS) is a promising approach to fatigue-resistant motor function restoration [21, 33, 37]. A major practical problem associated with IIFMS, however, is that without proper parameter selection, muscle contractions can display high levels of ripple. Chapter 7 discusses the influence of various IIFMS parameters on response ripple, and presents a feedforward technique for selecting IIFMS timings to reduce ripple. Unfortunately, because this technique is based on response characteristics that, while known initially, tend to change in unpredictable ways over the course of long contractions, it is, ultimately, only useful for short-duration muscle contractions. If the value of IIFMS is to be fully explored in research settings, and employed in clinical applications, a feedback-based approach to minimizing ripple during long-duration movements is necessary.

Frankel et al. demonstrated a means of using feedback control to adjust stimulus levels to achieve low-ripple force trajectories over long duration trains [28]. Although this work represents a major contribution to the field of IIFMS, there are several scenarios in which stimulus level adjustment alone may not be sufficient for achieving desired response trajectories, while maintaining low ripple levels. The first is characterized by differential fatigue of the activated motor unit groups. If several groups fatigue to the point where they are not able to produce the requisite contribution to the overall force output, ripple in the response waveform will grow. As stimulus levels are increased on electrodes with fatigued motor units—to compensate for their decline in force recruitment—those electrodes will eventually begin to recruit the same motor units as their nonfatigued neighbors (i.e., activation overlap will increase). Multiple activations of motor units within each cycle of an IIFMS train will lead to rapid fatigue, causing the overall force output to fail. The second

scenario in which feedback control of stimulus level may be insufficient to control ripple is when the recruited motor unit groups have different kinetics (described in detail in the previous chapter).

To address the problem of ripple from force and kinetic imbalance, one group (Wise et al. [61]) has devised an approach to adjusting IIFMS timings in real time. This approach—applicable to trains longer than a few seconds—represents significant progress towards making IIFMS control practical in experimental and clinical environments. As it is presented, however, the specific steps of the approach are not entirely clear. Additionally, no values are given for the various algorithm parameters, and its performance and optimality are not characterized—indeed they are uncharacterizable, except for in an empirical, trial-and-error manner. These shortcomings seriously impair the ultimate utility of the approach.

The work presented in this chapter focuses on enhancing the value of the Wise approach by producing an explicit, parameterized implementation of the iterative stimulus timing adjustment algorithm (ISTAA), simulating the performance of the implementation under various conditions, and optimizing the three parameters associated with this implementation: response filter bandwidth, error sampling delay, and response adjustment gain. The IIFMS response prediction technique described in Chapter 7 and [62] provides the cornerstone of the approach presented here. It enables simulation of arbitrarily long sequences of ISTAA iterations, and hence, measurement the algorithm’s behavior for various parameter values. The ability to simulate algorithm behavior enables a thoroughness of parameter space exploration and testing of the ISTAA performance that would be not practicable in-vivo in a research or clinical setting. Detailed exploration of the parameter space provides a means of identifying parameter values that optimize algorithm performance. Ultimately, the work presented here contributes to the potential utility and effectiveness of this approach in research and clinical FES applications.

## 8.2 Methods

The results presented here employ muscle response data recorded in-vivo during the same series of neuromotor electrophysiology experiments described in Chapter 7. In those experiments, muscle responses were collected from isolated plantar flexor (soleus, medial and lateral gastrocnemius, and plantaris) preparations in two cat (surgical methods are described in detail in Chapter 2 and [62]). To summarize, muscle contractions were evoked via constant-pulse-width, constant-frequency stimulation trains delivered on individual electrodes within a Utah slanted electrode array (USEA) implanted in the sciatic nerve. Re-

sponse waveforms were measured by a single-axis force transducer attached to the achilles tendon and recorded by a commercial data acquisition system.

### 8.2.1 IIFMS Response Modeling

The IIFMS trains used in this study, to simulate algorithm performance, were composed of actual single-electrode trains with known responses—recorded in-vivo (as described in the previous step). The predicted muscle response to an artificially constructed IIFMS train was computed by shifting each of the single-electrode train responses a number of samples corresponding to the time-shift specified in the IIFMS train and then summing the shifted waveforms. The validity of predicting IIFMS response as the linear sum of constituent electrode-train responses was demonstrated in work presented in the previous chapter.

### 8.2.2 Ripple-Reduction Algorithm

The ISTAA was implemented in the following steps (depicted in Figure 8.1):

1. Start with a period-long segment of the IIFMS response waveform corresponding to the most recently completed stimulation cycle.
2. Bandpass filter the segment from frequency band  $f_{low}$  to  $f_{high}$ , where  $f_{low} = f_{constituent} \times (1-\alpha)$  and  $f_{high} = f_{constituent} \times (1+\alpha)$ , and  $\alpha$  is  $1/2$  of the filter width expressed as a fraction of the constituent frequency. (Note: The filter was a 3rd-order Butterworth, applied in both directions for zero phase distortion).
3. Remove any remaining DC offset.
4. Normalize the adjusted segment to the mean of the original segment. The resultant waveform is the error signal.
5. Sample the error signal at  $t_{delay}$  ms after each electrode stimulus.
6. Multiply all of these error-sample values by some gain  $g$ .
7. Adjust each interelectrode time by the corresponding error value. (Limit the minimum time to 0 and the maximum time to the cycle length)
8. Repeat 1-8 after the next stimulation cycle.

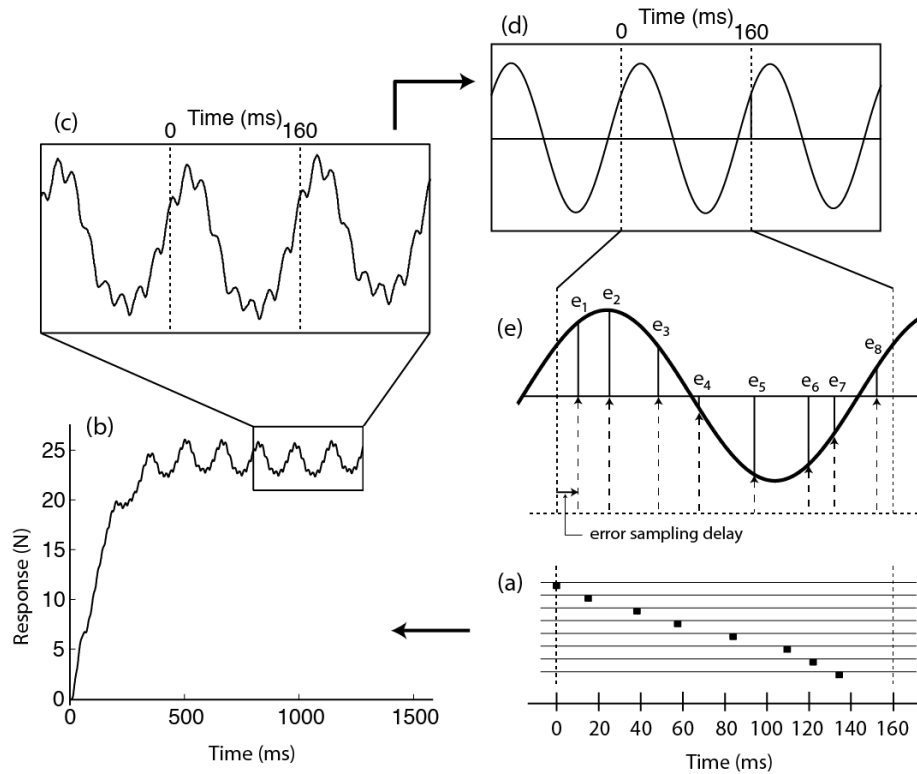


**Figure 8.1:** Diagram of the iterative stimulus timing adjustment algorithm (ISTAA). a) The stimulus timing, within one IIFMS cycle, for each of 8 electrodes (filled squares). b) The predicted IIFMS response. c) The last 3 periods of the response. d) The filtered, demeaned, and normalized response segment. e) The error signals to be used for updating the timings.

### 8.2.3 Simulating Algorithm Behavior

Behavior of the algorithm, over multiple iterations of a long-running IIFMS train, was simulated using a novel approach that employs the response modeling technique described in Chapter 7 combined with previously-recorded responses to short-duration, single-electrode trains. It is important to note that there is no known method to accurately predict actual responses to long-duration IIFMS trains. As a real IIFMS train progresses, forces contributed by constituent electrodes vary over time (increasing and decreasing as a result of secondary factors such as potentiation and fatigue). The approach employed here does not purport to predict these time varying components of IIFMS responses. Rather it attempts to simulate the timing-adjustment algorithm behavior over successive periods of an IIFMS response, where the waveform for each period is generated with the model, using fixed, period-long segments from previously recorded sets of single-electrode train waveforms. In each successive iteration, the same period of the single-electrode responses is used to generate a new period-long segment of IIFMS response for analysis.

During simulation runs, each sequence of iterations started with an IIFMS train with evenly distributed stimulus timing. The predicted response was computed, and the timing adjustment algorithm was executed. Successive algorithm iterations were simulated until the change in response ripple from one iteration to the next converged to below a predetermined threshold (less than 5% of previous value). If convergence was not reached within 200 iterations the simulation was terminated.

### 8.2.4 Optimizing Algorithm Performance

Algorithm performance was measured in two dimensions: number of iterations required to reach convergence, and percent ripple in the steady-state response. The effect of each parameter, on performance, was evaluated by simulating algorithm behavior for various values of the parameter while holding the other two parameters constant. Effects of each parameter were evaluated for multiple electrode set sizes (4, 5, 6) and many unique sets of single electrode responses ( $n = 19,320$ ).

## 8.3 Results

Simulation results demonstrate that the algorithm implementation described above, does, as expected, reduce response ripple (Figure 8.2). Additionally, results suggest that, over a wide range of parameter values, the algorithm converges (Figure 8.3). Each of the parameters exhibited a measurable impact on algorithm performance. Values for the three ISTAA parameters that minimize both steady-state ripple and time to convergence are as follows: 1) response filter band is most effective when set to 80%-120% of constituent stimulation frequency, 2) error-sampling-delay has the greatest effect at 15 ms, 3) a timing-adjustment-gain of 0.5 achieves rapid convergence without overshoot.

## 8.4 Discussion

The results presented here, specifically those displayed in Figure 8.3, demonstrate that there is significant potential for optimizing the ISTAA algorithm as originally presented in [61]. Overall, convergence speed was the performance metric most affected by changes in algorithm parameter values. For example, changing the timing adjustment gain from 1.0 to 0.5 decreased the average number of cycles to convergence from approximately 13 to 4. For IIFMS cycle times of 100 ms (10-Hz constituent frequency), this would yield a reduction in convergence time from 1300 ms to 400 ms—valuable from both a controls perspective and that of improving the FES patients subjective experience.

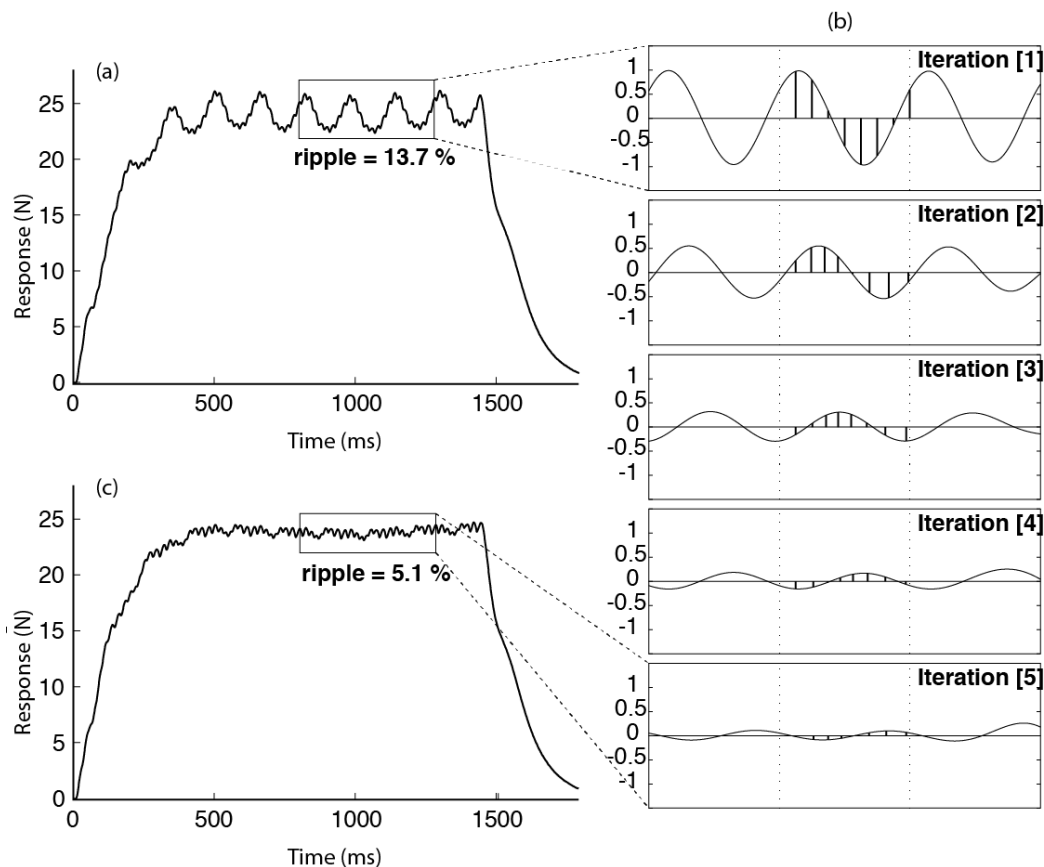


**Figure 8.2:** Five example iterations of the timing-adjustment algorithm. (a) Predicted response to the IIFMS train with evenly-distributed stimulus times. Ripple for this train is 13.7%. (b) Change in error signal over 5 iterations of the algorithm. (c) Predicted response to IIFMS train with optimized stimulus times. Ripple for this train is 5.1%.

Response ripple was also affected by modulation of algorithm parameters (though the effects were not as large as those for convergence). As might be expected, delaying the error sample time decreased the steady-state ripple—though without the ability to simulate algorithm behavior for various delays, it would have been difficult to determine that the most effective delay is 15 ms, and that using this value improves the steady state ripple by approximately 17% as compared with a delay of 0 ms (note: error sampling delay was not specified in the algorithm description, as originally presented in [61]).

One possible criticism of the work presented in this chapter is that the linear summation model may not be sufficiently accurate to allow for realistic simulation of algorithm behavior. This is a possibility, and indeed, the results presented here should, ideally, be confirmed in-vivo. However, although the response modeling technique is not exact, it has been shown to be quite accurate for isometric contractions [58, 61, 62]—which are the very sort targeted by this approach to stimulation control.

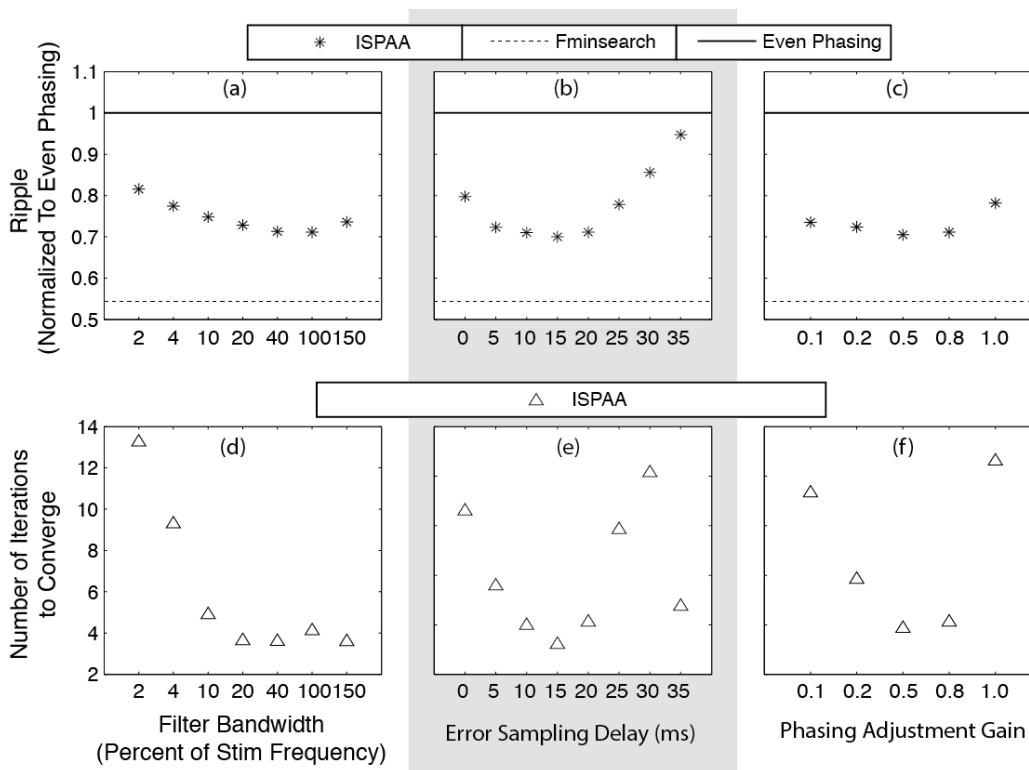


**Figure 8.3:** Performance of the ISTAA algorithm for various parameter values. Top row shows algorithm performance in terms of steady-state response ripple (i.e., after algorithm convergence) normalized to ripple at start of algorithm. Dashed line shows ripple for optimal stimulus timing (as determined by a ripple-reduction algorithm described in [62], that, unlike the present algorithm, uses a prior knowledge of individual response waveforms to search for optimized timing). Bottom row: algorithm performance in terms of iterations to convergence. Left column: change in algorithm performance for various filter bandwidths. Middle column: algorithm performance for various error sampling delays. Right column: algorithm performance for various timing adjustment gains.

Ultimately, the specific optimizations presented here, and more generally, the use of IIFMS response modeling for purposes of parameter optimization, represents valuable contributions to the nascent field of asynchronous multielectrode FES.

## CHAPTER 9

### DISCUSSION

#### 9.1 Summary

For individuals who have lost motor faculties as a result of injury, stroke, or disease, surrogate electrical activation of the nervous system, especially via emerging techniques such as IIFMS, offers the potential for significant improvements to quality of life. This dissertation presents the design and use of a hardware platform and software algorithms that greatly facilitate IIFMS motor-restoration research.

A major motivation for building this platform was to create an environment that provides programmatic control of the electrical-stimulation/muscle-response feedback loop. This seemingly basic ability enables implementation of a variety of software programs to map and explore a virtually unlimited range of physiological responses to stimulation. To demonstrate the value of the platform, three routines were implemented to automate response-mapping tasks (prerequisites to planning sophisticated stimulation patterns) that had previously been accomplished by hand in a time-consuming and painstaking manner. All three software algorithms—one for mapping perithreshold stimulus levels, another for mapping stimulus-response curves, and a third for mapping axonal excitation overlap—were validated in-vivo, in neuro-motor electrophysiology experiments involving 100-electrode USEAs implanted in to lower-limb nerve trunks. All three routines employed well-known software algorithms and principles to accomplish various aspects of the mapping tasks. For example, identifying periasymptote stimulus levels was accomplished with a modified binary search algorithm. Recruitment curve asymptotes were identified by testing successive responses for convergence. Filling recruitment curves was accomplished with a gap bisection algorithm that is, in essence, a modified form of a binary search. Ultimately, for each of these response mapping tasks, application of the appropriate algorithms resulted in an overall routine that executed efficiently, and in a time frame practical for complex neuro-motor, electro-physiology experiments.

Another major motivation for building the platform was to conduct experiments ex-

ploring the impact of the various IIFMS parameters on muscle response characteristics, and to develop an approach for feed-forward control of short-duration muscle contractions. A software routine to explore the influence of stimulus level, stimulus frequency, and stimulus timing on intraperiod response variation (ripple) for IIFMS trains, and for selecting intraperiod stimulus timings that minimize ripple, was implemented, and then executed, using the platform in a series of in-vivo experiments. A major conceptual component of the feedforward, stimulus-timing-selection algorithm is an IIFMS response-prediction model. The model relies on the assumption that the net force (at the tendon) of a set of independent pools of motor units firing at the same time is simply the linear sum of the forces produced by each pool. Though other research has demonstrated the validity, under certain conditions, of this assumption, it was not known if it would prove accurate enough to support the use of a function minimization technique. Ultimately, experimental results proved the model sufficient to allow the stimulus-timing space to be explored *in silico*, thus reliably enabling the identification of stimulus timings that elicit low-ripple responses.

Finally, a technique for modeling the effect of stimulus-timing changes on isometric responses to long-duration IIFMS trains was developed. This technique is based, in part, on the assumption that the efficacy of a timing-adjustment algorithm is not dependent on the specific responses of the constituent motor unit pools (i.e., the algorithm is applicable, at any time, regardless of the constituent response values). The technique employs fixed, single-period segments of single-electrode train responses to simulate successive periods of a long-duration IIFMS train response. This technique was used to provide a novel method for simulating the behavior of a previously published, feedback-based control algorithm for IIFMS response-ripple reduction. An explicit, parameterized version of the control algorithm was implemented, and a series of simulations with varying algorithm parameters was executed. As expected, the results of these simulations indicate that algorithm performance—as measured by cycles to convergence and ripple reduction—is affected, in some cases substantially, by parameter values. Ultimately, the approach provides a practical solution to tuning IIFMS control algorithm parameters that can be used in a research or clinical environment.

## 9.2 Impact

The closed-loop platform and response-mapping algorithms have been successfully used for 5 years in over a hundred neuro-motor physiology experiments spanning two research institutions. Together, they have played a substantial role in facilitating at least two

successful doctoral research projects [40, 63]. Coupled with the work done by Dowden, on the use of noninvasive techniques for response measurement, the work presented here, on platform and mapping algorithms, demonstrates, to the broader FES community, that high-channel-count neural interfaces can be practicable in a clinical setting.

The work on stimulus timing adjustment quantifies, for the first time, the influence of this parameter on response ripple, and highlights its importance in specific conditions—namely varying response kinetics among the activated motor-unit groups. The results presented here should serve to inform current and future research on real-time IIFMS control techniques. As an example, Frankel preferentially employed electrodes with similar response kinetics to minimize, for the purposes of his study, the potentially negative influence of this factor on ripple, in the context of the evenly distributed stimulus times used by his algorithm [64]. Additionally, even in situations where kinetics are the same, it is the case that motor unit groups, recruited by individual electrodes in the IIFMS set, may fatigue differentially (as shown by Wise et al. [61]). In such situations, timing adjustment would allow a controller to maintain a higher mean force output while still preserving low ripple.

Another demonstration of the impact the closed-loop FES platform, and mapping and stimulation-control algorithms, have had on the field of surrogate motor restoration is that they were used by the author, and colleagues, to achieve—for the first time ever with IIFMS—control of coordinated uni-lateral and bi-lateral sit-to-stance movements in a cat model [65]. Given that the sit-to-stance movement involves muscles innervated by three main nerve branches in each leg, this feat necessitated implantation and mapping of 3-6 USEAs (300 to 600 electrodes—for the uni-lateral and bi-lateral cases, respectively) and parameter selection for multiple IIFMS patterns. Furthermore, it required careful orchestration of multiple IIFMS patterns (involving stimulation across 10s of electrodes) to produce the complex, coordinated muscle firing patterns needed to drive the sit-to-stance movement. Accomplishing this goal would not have been possible (especially in a timeframe practical to acute experiments) without the work presented in this dissertation.

### 9.3 Shortcomings

The closed-loop platform, as it was implemented, has a variety of shortcomings, two of which are significant enough that they should be mentioned here. The first is the command-line user interface. Though this type of interface is expedient from a development perspective, it has, ultimately, proven unsatisfactory, from a usability perspective, in an experimental setting. Mapping tasks are characterized by a large enough set of parameters,

that having to enter them by hand (repeatedly for remapping) in a serial manner, was (perhaps a bit ironically) time-consuming and error prone. As evidence of the unsuitability of the command-line interface, other individuals have, over the course of several years, replaced it with a graphical one—though the actual mapping algorithms have remained intact. Another shortcoming of the platform is the lack of real-time capabilities. This deficiency does not limit its ability to support iterative, closed-loop algorithms (such as those for mapping, described in Chapters 4, 5, and 6, or those for parameter exploration, described in Chapter 7); however, it does preclude the ability to execute any real-time control algorithms (such as the one modeled in Chapter 8).

Though this work demonstrates the importance of stimulus timing in IIFMS, the specific technique presented for adjusting this parameter (described in Chapter 7) is of limited utility in clinical practice—that is, only in very specific and controlled FES applications will constituent electrode responses be available before execution of the the target movement goal. Though the algorithm (and optimizations) presented in Chapter 8 does provide a real-time means of adjusting stimulus timing, it has only been shown to work when stimulus levels are held constant. Thus, until this approach can be adapted to nonconstant force trajectories, it is useful in only a limited set of FES applications (i.e., those involving primarily static behaviors, such as postural control).

## 9.4 Future Challenges in IIFMS

It is tempting to believe that what is truly needed, to advance the use of IIFMS in clinical practice, is a control algorithm capable of simultaneously manipulating all IIFMS parameters independently. Though such an achievement might be useful in certain situations, there are several reasons why it may not be worth pursuing at the present time.

One important practical reason is that deployment of a clinical FES system often involves an initial period of muscle conditioning, during which motor units in the target muscles convert from a fast-twitch to slow-twitch phenotype. The main motivation for this process is that it results in muscle forces that last longer under FES control—both because slow-twitch fiber are more fatigue resistant and because tetanus can be achieved at a lower, less fatiguing, rate. This process is relevant to the work, presented here, in that conversion of a muscle’s motor units to a single type results in a single kinetic profile of responses, thus reducing the need for stimulus timing adjustment. However, the possibility of differential fatigue across electrodes during an IIFMS train would still present a situation where time shifting is useful. Ultimately, in clinical IIFMS applications, with appropriately conditioned muscles,

a control algorithm such as Frankel's will likely be largely sufficient.

Another potential development that would obviate the need for an algorithm capable of controlling IIFMS intraperiod timings would be the emergence of neural interface devices with yet higher channel counts than those available today. If very-high channel count access to the peripheral nerve becomes available, IIFMS ripple reduction will cease to be an issue, because asynchronous activation of several dozen small populations of motor units (as compared to the half dozen provided by a typical USEA implant) will produce a low-ripple response naturally. Given such an interface, what would be needed is an algorithm capable of dynamically adding and removing electrodes from the IIFMS set, and controlling stimulus rate. The high-density USEA, a device with 4 times the spatial resolution of the standard USEA, is an example of a newly developed neural interface device that begins to provide this level of specificity.

From a broader perspective, there are other obstacles blocking the path to use of IIFMS in clinical applications that are more deserving of attention from the research community. Among these are poor biocompatibility of existing high-channel-count interfaces, lack of a wireless, high-channel count stimulation platform, lack of a platform for robustly acquiring multiple feedback modalities, and finally, lack of control algorithms that integrate feed-forward and feedback approaches (this applies to all FES systems). As Frankel and others have shown, the response bandwidth of the neuromuscular system limits the size of feedback gains that can be employed and hence the speed of motions that can be accomplished with feedback control alone. Providing a range of movement patterns, similar to natural human abilities, will require FES control techniques with a sophisticated feed-forward component. The advent of clinically approved devices, for wirelessly recording motor intent from the cortex, will enable patients to provide some of these higher-level, feed-forward control signals. However, given that movements like walking are often accomplished with limited direct conscious involvement, feed-forward control algorithms will likely continue to be an important component of clinical FES systems. Such feed-forward control algorithms will need to have the ability to implicitly acquire a model of musculo-skeletal dynamics, tailored to a specific individual, and adapt that model as the patient's functional abilities change (due to conditioning, age, or other ongoing processes). Research involving such feedforward techniques will require a long-term IIFMS model. Some encouraging work has been done on this front; and as more of the technologies mentioned above become available, better, more stable chronic IIFMS models will become possible. Such models will provide an exciting

opportunity for developing and testing integrated feed-forward and feedback IIFMS control techniques.

## REFERENCES

- [1] E. R. Kandel, J. H. Schwartz, T. M. Jessell *et al.*, *Principles of neural science*. McGraw-Hill New York, 2000, vol. 4.
- [2] G. Schalow, “The problem of cauda equina nerve root identification,” *Zentralbl. Neurochir.*, vol. 46, no. 4, pp. 322–330, 1985.
- [3] (2013, June) U.S. census bureau: State and county quickfacts. [Online]. Available: <http://quickfacts.census.gov/qfd/states/00000.html>
- [4] (2012, May) Morbidity and mortality weekly report (mmwr): Prevalence of stroke - united states, 2006-2010. [Online]. Available: <http://www.cdc.gov/mmwr/preview/mmwrhtml/mm6120a5.htm>
- [5] E. Zaloshnja, T. Miller, J. A. Langlois, and A. W. Selassie, “Prevalence of long-term disability from traumatic brain injury in the civilian population of the united states, 2005,” *The Journal of head trauma rehabilitation*, vol. 23, no. 6, pp. 394–400, 2008.
- [6] (2013, March) National spinal cord injury statistical center, facts and figures at a glance. [Online]. Available: [https://www.nscisc.uab.edu/PublicDocuments/fact\\_figures\\_docs/Facts%202013.pdf](https://www.nscisc.uab.edu/PublicDocuments/fact_figures_docs/Facts%202013.pdf)
- [7] C. W. Noonan, S. J. Kathman, and M. C. White, “Prevalence estimates for ms in the united states and evidence of an increasing trend for women,” *Neurology*, vol. 58, no. 1, pp. 136–138, 2002.
- [8] D. R. McNeal, “Analysis of a model for excitation of myelinated nerve,” *Biomedical Engineering, IEEE Transactions on*, no. 4, pp. 329–337, 1976.
- [9] J. Moe and H. Post, “Functional electrical stimulation for ambulation in hemiplegia.” *The Journal-lancet*, vol. 82, p. 285, 1962.
- [10] G. M. Lyons, T. Sinkjær, J. H. Burridge, and D. J. Wilcox, “A review of portable fes-based neural orthoses for the correction of drop foot,” *Neural Systems and Rehabilitation Engineering, IEEE Transactions on*, vol. 10, no. 4, pp. 260–279, 2002.
- [11] P. H. Peckham and J. S. Knutson, “Functional electrical stimulation for neuromuscular applications\*,” *Annu. Rev. Biomed. Eng.*, vol. 7, pp. 327–360, 2005.
- [12] (2013, March) Medical coverage policy: Functional electrical stimulators (fes), diaphragmatic/phrenic nerve stimulation. [Online]. Available: [http://www.synapsebiomedical.com/support/PDFs/ALS\\_Reimbursement/Humana Functional Electrical Stimulators \(FES\), Diaphragmatic\\_Phrenic Nerve Stimulation SCI n ALS 10 25 2012.pdf](http://www.synapsebiomedical.com/support/PDFs/ALS_Reimbursement/Humana_Functional_Electrical_Stimulators_(FES),_Diaphragmatic_Phrenic_Nerve_Stimulation_SCI_n_ALS_10_25_2012.pdf)

- [13] C. Ethier, E. Oby, M. Bauman, and L. Miller, "Restoration of grasp following paralysis through brain-controlled stimulation of muscles," *Nature*, vol. 485, no. 7398, pp. 368–371, 2012.
- [14] S. Harkema, Y. Gerasimenko, J. Hodes, J. Burdick, C. Angeli, Y. Chen, C. Ferreira, A. Willhite, E. Rejc, R. G. Grossman *et al.*, "Effect of epidural stimulation of the lumbosacral spinal cord on voluntary movement, standing, and assisted stepping after motor complete paraplegia: a case study," *The Lancet*, vol. 377, no. 9781, pp. 1938–1947, 2011.
- [15] B. Lau, L. Guevremont, and V. K. Mushahwar, "Strategies for generating prolonged functional standing using intramuscular stimulation or intraspinal microstimulation," *Neural Systems and Rehabilitation Engineering, IEEE Transactions on*, vol. 15, no. 2, pp. 273–285, 2007.
- [16] T. M. Bruns, J. B. Wagenaar, M. J. Bauman, R. A. Gaunt, and D. J. Weber, "Real-time control of hind limb functional electrical stimulation using feedback from dorsal root ganglia recordings," *Journal of neural engineering*, vol. 10, no. 2, p. 026020, 2013.
- [17] W. L. Rutten, H. J. van Wier, and J. H. Put, "Sensitivity and selectivity of intraneural stimulation using a silicon electrode array," *Biomedical Engineering, IEEE Transactions on*, vol. 38, no. 2, pp. 192–198, 1991.
- [18] K. Yoshida and K. Horch, "Selective stimulation of peripheral nerve fibers using dual intrafascicular electrodes," *Biomedical Engineering, IEEE Transactions on*, vol. 40, no. 5, pp. 492–494, 1993.
- [19] A. Branner and R. A. Normann, "A multielectrode array for intrafascicular recording and stimulation in sciatic nerve of cats," *Brain research bulletin*, vol. 51, no. 4, pp. 293–306, 2000.
- [20] D. J. Tyler and D. M. Durand, "Functionally selective peripheral nerve stimulation with a flat interface nerve electrode," *Neural Systems and Rehabilitation Engineering, IEEE Transactions on*, vol. 10, no. 4, pp. 294–303, 2002.
- [21] D. McDonnall, G. A. Clark, and R. A. Normann, "Interleaved, multisite electrical stimulation of cat sciatic nerve produces fatigue-resistant, ripple-free motor responses," *Neural Systems and Rehabilitation Engineering, IEEE Transactions on*, vol. 12, no. 2, pp. 208–215, 2004.
- [22] A. Branner, R. B. Stein, and R. A. Normann, "Selective stimulation of cat sciatic nerve using an array of varying-length microelectrodes," *Journal of Neurophysiology*, vol. 85, no. 4, pp. 1585–1594, 2001.
- [23] A. Branner, R. B. Stein, E. Fernandez, Y. Aoyagi, and R. A. Normann, "Long-term stimulation and recording with a penetrating microelectrode array in cat sciatic nerve," *Biomedical Engineering, IEEE Transactions on*, vol. 51, no. 1, pp. 146–157, 2004.
- [24] D. McDonnall, G. A. Clark, and R. A. Normann, "Selective motor unit recruitment via intrafascicular multielectrode stimulation," *Canadian journal of physiology and pharmacology*, vol. 82, no. 8-9, pp. 599–609, 2004.

- [25] B. R. Dowden, A. M. Wilder, S. D. Hiatt, R. A. Normann, N. Brown, and G. A. Clark, "Selective and graded recruitment of cat hamstring muscles with intrafascicular stimulation," *Neural Systems and Rehabilitation Engineering, IEEE Transactions on*, vol. 17, no. 6, pp. 545–552, 2009.
- [26] B. R. Dowden, H. A. Wark, and R. A. Normann, "Muscle-selective block using intrafascicular high-frequency alternating current," *Muscle & nerve*, vol. 42, no. 3, pp. 339–347, 2010.
- [27] B. Dowden, M. Frankel, R. Normann, and G. Clark, "Non-invasive method for selection of electrodes and stimulus parameters for fes applications with intrafascicular arrays," *Journal of neural engineering*, vol. 9, no. 1, p. 016006, 2012.
- [28] M. A. Frankel, B. R. Dowden, V. Mathews, R. A. Normann, G. A. Clark, and S. G. Meek, "Multiple-input single-output closed-loop isometric force control using asynchronous intrafascicular multi-electrode stimulation," *Neural Systems and Rehabilitation Engineering, IEEE Transactions on*, vol. 19, no. 3, pp. 325–332, 2011.
- [29] A. W. Monster and H. Chan, "Isometric force production by motor units of extensor digitorum communis muscle in man," *Journal of Neurophysiology*, vol. 40, no. 6, pp. 1432–1443, 1977.
- [30] C. De Luca, R. LeFever, M. McCue, and A. Xenakis, "Behaviour of human motor units in different muscles during linearly varying contractions," *The Journal of physiology*, vol. 329, no. 1, pp. 113–128, 1982.
- [31] B. Bigland-Ritchie, D. Jones, and J. Woods, "Excitation frequency and muscle fatigue: electrical responses during human voluntary and stimulated contractions," *Experimental neurology*, vol. 64, no. 2, pp. 414–427, 1979.
- [32] A. R. Kralj and T. Bajd, *Functional electrical stimulation: standing and walking after spinal cord injury*. CRC press, 1989.
- [33] P. M. Rack and D. Westbury, "The effects of length and stimulus rate on tension in the isometric cat soleus muscle," *The Journal of physiology*, vol. 204, no. 2, p. 443, 1969.
- [34] A. R. Lind and J. Scott Petrofsky, "Isometric tension from rotary stimulation of fast and slow cat muscles," *Muscle & nerve*, vol. 1, no. 3, pp. 213–218, 1978.
- [35] J. Petrofsky, "Sequential motor unit stimulation through peripheral motor nerves in the cat," *Medical and Biological Engineering and Computing*, vol. 17, no. 1, pp. 87–93, 1979.
- [36] W. Happak, H. Gruber, J. Holle, W. Mayr, C. Schmutterer, U. Windberger, U. Losert, and H. Thoma, "Multi-channel indirect stimulation reduces muscle fatigue," in *Engineering in Medicine and Biology Society, 1989. Images of the Twenty-First Century., Proceedings of the Annual International Conference of the IEEE Engineering in*. IEEE, 1989, pp. 240–241.
- [37] K. Yoshida and K. Horch, "Reduced fatigue in electrically stimulated muscle using dual channel intrafascicular electrodes with interleaved stimulation," *Annals of biomedical engineering*, vol. 21, no. 6, pp. 709–714, 1993.

- [38] M. A. Frankel, G. A. Clark, S. G. Meek, R. A. Normann, and V. J. Mathews, "Adaptive parameter selection for asynchronous intrafascicular multi-electrode stimulation," in *Acoustics, Speech and Signal Processing (ICASSP), 2012 IEEE International Conference on*. IEEE, 2012, pp. 753–756.
- [39] M. A. Frankel, V. Mathews, G. A. Clark, R. A. Normann, and S. G. Meek, "Closed-loop control of paralyzed limb motion using asynchronous intrafascicular multi-electrode stimulation," *Biomedical Engineering, IEEE Transactions on*, in review.
- [40] B. R. Dowden, "Intrafascicular multielectrode stimulation strategies for neuroprosthetic applications," Ph.D. dissertation, The University of Utah, 2012.
- [41] P. J. Rousche and R. A. Normann, "A method for pneumatically inserting an array of penetrating electrodes into cortical tissue," *Annals of biomedical engineering*, vol. 20, no. 4, pp. 413–422, 1992.
- [42] P. R. Troyk and N. d. e. N. Donaldson, "Implantable FES Stimulation Systems: What is Needed?" *Neuromodulation*, vol. 4, no. 4, pp. 196–204, Oct 2001.
- [43] W. E. Finn and P. G. LoPresti, *Handbook of Neuroprosthetic methods*. CRC Press, 2010.
- [44] W. L. Rutten, "Selective electrical interfaces with the nervous system," *Annual Review of Biomedical Engineering*, vol. 4, no. 1, pp. 407–452, 2002.
- [45] P. T. Bhatti, B. Y. Arcand, J. Wang, N. Butala, C. R. Friedrich, and K. D. Wise, "A high-density electrode array for a cochlear prosthesis," in *TRANSDUCERS, Solid-State Sensors, Actuators and Microsystems, 12th International Conference on, 2003*, vol. 2. IEEE, 2003, pp. 1750–1753.
- [46] K. Wise, D. Anderson, J. Hetke, D. Kipke, and K. Najafi, "Wireless implantable microsystems: high-density electronic interfaces to the nervous system," *Proceedings of the IEEE*, vol. 92, no. 1, pp. 76–97, 2004.
- [47] X. Navarro, T. B. Krueger, N. Lago, S. Micera, T. Stieglitz, and P. Dario, "A critical review of interfaces with the peripheral nervous system for the control of neuroprostheses and hybrid bionic systems," *Journal of the Peripheral Nervous System*, vol. 10, no. 3, pp. 229–258, 2005.
- [48] L. Guevremont, J. A. Norton, and V. K. Mushahwar, "Physiologically based controller for generating overground locomotion using functional electrical stimulation," *Journal of neurophysiology*, vol. 97, no. 3, pp. 2499–2510, 2007.
- [49] K. L. Kilgore, P. Peckham, M. Keith, and G. Thrope, "Electrode characterization for functional application to upper extremity fns," *Biomedical Engineering, IEEE Transactions on*, vol. 37, no. 1, pp. 12–21, 1990.
- [50] C. Lynch and M. Popovic, "Closed-loop control for fes: Past work and future directions," in *10th Annual Conference of the International FES Society*, 2005.
- [51] T. Mandl, J. Martinek, M. Bijak, H. Lanmueller, W. Mayr, and M. Pichler, Eds., *1100-Channel Neural Stimulator for Functional Electrical Stimulation Using High-Electrode-Count Neural Interfaces*. Imperial Riding School, Vienna, Austria: Center for Medical Physics and Biomedical Engineering, Medical University of Vienna, Vienna

- Medical School, AKH 4L, Waehringer Guertel 18-20, A-1090 Vienna, Austria, 09/2012 2010. [Online]. Available: <http://ifess.org/proceedings/IFESS2010/IFESS2010.pdf>
- [52] R. A. Normann, B. R. Dowden, M. A. Frankel, A. M. Wilder, S. D. Hiatt, N. M. Ledbetter, D. J. Warren, and G. A. Clark, "Coordinated, multi-joint, fatigue-resistant feline stance produced by utah slanted electrode arrays in hind limb nerves," *J. Neural Eng*, 2011.
- [53] *Cerebus 128-Channel Data Acquisition System User Manual*, Version 2.00 ed., Cyberkinetics Neurotechnology Inc., 2004.
- [54] D. McDonnall, "Interleaved multielectrode stimulation enhances fatigue resistance," Ph.D. dissertation, Department of Bioengineering, University of Utah, 2005.
- [55] W. K. Durfee and K. E. MACLean, "Methods for estimating isometric recruitment curves of electrically stimulated muscle," *Biomedical Engineering, IEEE Transactions on*, vol. 36, no. 7, pp. 654–667, 1989.
- [56] R. A. Normann and R. A. Normann, *Principles of bioinstrumentation*. Wiley, 1988.
- [57] D. McDonnall, personal communication.
- [58] T. G. Sandercock, "Nonlinear summation of force in cat soleus muscle results primarily from stretch of the common-elastic elements," *Journal of Applied Physiology*, vol. 89, no. 6, pp. 2206–2214, 2000.
- [59] A. M. Wilder, S. D. Hiatt, B. R. Dowden, N. A. Brown, R. A. Normann, and G. A. Clark, "Automated stimulus-response mapping of high-electrode-count neural implants," *Neural Systems and Rehabilitation Engineering, IEEE Transactions on*, vol. 17, no. 5, pp. 504–511, 2009.
- [60] J. C. Lagarias, J. A. Reeds, M. H. Wright, and P. E. Wright, "Convergence properties of the nelder–mead simplex method in low dimensions," *SIAM Journal on Optimization*, vol. 9, no. 1, pp. 112–147, 1998.
- [61] A. Wise, D. Morgan, J. Gregory, and U. Proske, "Fatigue in mammalian skeletal muscle stimulated under computer control," *Journal of Applied Physiology*, vol. 90, no. 1, pp. 189–197, 2001.
- [62] A. M. Wilder, R. A. Normann, and G. A. Clark, "The importance of stimulus timing in multi-electrode functional electrical stimulation," *Neural Systems and Rehabilitation Engineering, IEEE Transactions on*, In Review.
- [63] M. A. Frankel, "Control methods of asynchronous intrafascicular multi-electrode stimulation for neuromuscular prostheses," Ph.D. dissertation, The University of Utah, 2013.
- [64] M. Frankel, personal communication.
- [65] R. Normann, B. Dowden, M. Frankel, A. Wilder, S. Hiatt, N. Ledbetter, D. Warren, and G. Clark, "Coordinated, multi-joint, fatigue-resistant feline stance produced with intrafascicular hind limb nerve stimulation," *Journal of Neural Engineering*, vol. 9, no. 2, p. 026019, 2012.